The formability of corus tubular blanks.

Mullan, H. B

THE FORMABILITY OF CORUS TUBULAR BLANKS™

H B Mullan

Academic Supervisor:
Prof. R.W. Evans

Industrial Supervisors:
B.D. Carleer & Bryan Jones

Summary

Tube hydroforming has already proved successful in sub frame and chassis applications. However, there has been limited uptake of this technology in the production of BIW structural components. Mainly due to the fact that standard tube making methods are restricted to production of tubes with a diameter to thickness ratio of 65:1 at best, where as typical BIW application would be more inline with a ratio of 100:1. The Corus Tubular Blank process enables a greater range of D/t ratio, and therefore a larger scope of manufacture for BIW parts.

The major technical issue concerned with the manufacture of both Corus Tubular Blanks and Corus Tailor Welded Tubes (Corus Tubular Blanks made using LWTB's sheets) is the effect of material elastic recovery after forming has taken place. It has been well documented in previously published literature that the magnitude of elastic recovery (springback) in a component is influenced by the material and forming properties. It is very difficult to have full control of the material properties. However, forming properties are controllable especially if the forming process is simple as in the case of the Corus Tubular Blank. Corus Tailor Welded Tubes introduce a complex combination of springback characteristics inherited from the constituent parent parts of the LWTB.

This thesis provides a method of springback prediction, as well as indication of the important factors associated with springback. Highlighted is the ability of springback to be mitigation via means of increased forming force, in conjunction with the ability to predict the subsequent springback behaviour.
It has been shown in this thesis that springback of an LWTB with the weld line parallel to pressing line can be predicted. Thus instilling tool designers with confidence to produce tooling suited to the formation of Corus Tailor Welded Tubes.

DECLARATION

This work contained in this thesis has not previously been accepted in substances for any degree and is not being currently submitted in candidature for any degree.

Candidate signature.. .....

Date.....25/2/05.....

STATEMENT 1

This thesis is the result of my own investigation, except where otherwise stated. Other sources are acknowledged in the list of references, which is appended.

Candidate signature... .....

Date.....25/2/05.....

STATEMENT 2

I hereby give consent for my thesis, if accepted, to be available for purposes of photocopying and for inter-library loan and for the title and summary to be made available to outside organisations.

Candidate signature.....

Date.....25/2/05.....

Dedication

This Thesis is dedicated to my dear wife Suzanne, and my children Aimee, Alanna and Hollie, to whom I owe a debt of gratitude for their tremendous encouragement and support during the EPSRC Engineering Doctorate programme.

In special remembrance also to a woman who's eternal optimism and support on my early educational journey was inspirational, my late grandmother Margaret Bailie Mullan.

Acknowledgements

The author would like to thank the management, technical and administrative staff of Corus, R, D &T, based at the then Welsh Technology Centre, Port Talbot and the academic staff of the EPSRC Engineering Doctorate Centre and University of Wales, Swansea. In addition, support from the Engineering Physical Sciences and Research Council (EPSRC) is gratefully acknowledged.

Thanks are due to the author's project supervisors, Professor Russell Evans, Dr Bart Carleer, and Bryan Jones who provided technical support and guidance during the term of the research project. Additionally, the author would like to thank the research engineers and technicians based at PAC Ijmuiden (Holland) who provided valuable input into the project.

A special thanks is owed to P&O travel who provided substantial support in terms of travel arrangements on my frequent travel to Holland.

Record of Training

Overview

During the Engineering Doctorate period a broad appreciation of engineering practice within a high tech industrial culture has been gained. This has included experience in health & safety issues, quality assurance and total quality management/principles and techniques, having direct exposure to a strongly customer orientated working environment. In addition, expert knowledge of a specific engineering area has been developed (Tube Hydroforming).

Formal Training

The training was targeted at achieving the technical competencies, professional skills and personal qualities essential for a fulfilling career in industry. The following assessed formal training modules have been successfully completed:

Technical Modules: Steel Process Evolution, Refractories and Steel Structures, Steel Processing, Coated Products, Steel Product Development, Engineering Applications, Environmental Issues, Finite Element Analysis, Statistical Design of Experiments and Training in Windows 95 and Lotus Smartsuite 97.

Professional Development and Management Modules: Development of Personal Skills, Leadership/Teamworking Skills, Investment Appraisal, Business Process Engineering, Graduate Management, Total Quality Management, Effective Management, Employee Relations, Health and Safety Awareness, Financial Awareness and Business Awareness.

Informal Training

In addition to the formal training modules a range of other tasks have been completed facilitating the development of a range of competencies.

Presentations have been made to a range of external groups and senior management within Corus Plc (upto Executive Board level). Presentations have been made to the following groups:

Conferences/Seminars

Presentations have been made at the following conferences/ seminars, resulting in experience in communicating and defending technical issues with a learned audience:

- Preparation of poster presentation at the EngD Annual Seminar, University of Wales, Swansea. Sept. 2000.
- Preparation of poster presentation at the EngD Annual Seminar, University of Wales, Swansea. Sept. 2001.
- Preparation and oral presentation of Publication (1) at the EngD Annual Seminar, University of Wales, Swansea. Sept 2002.
- Preparation and oral presentation of Publication (2) at Shemet 2003, Belfast, N. Ireland
- Preparation and oral presentation of Publication (3) at AMPT 2003, Dublin, Ireland
- Preparation and oral presentation of Publication (4) at IMC 20 2003, Cork, Ireland
- Preparation of a poster presentation at the EngD Annual Seminar, University of Wales, Swansea. Sept. 2003.

Publications

From the research programme carried out the following papers have been produced entailing a number of days planning and preparation in each case.

1. H B Mullan, Influence of springback on final formed component shape . publication to be arranged

2. H B Mullan, Influence of springback on final formed component shape of thin high strength sheet steel, Sheet Metal 2003, Proceedings of the International

Conference, 14-16 April 2003, University of Ulster Jordanstown, ISBN 1 859231713, pg 447-454

3. H B Mullan, Improved prediction of springback on final formed components, AMPT 2003, Dublin City University, 8th-11th July 2003, ISBN 1 872327 397, pg 1056-1060

4. H B Mullan, Influence of Springback on Tailored Blank Components, IMC 20, September 2003, Cork Institute of Technology, ISBN 0-9545736-0-9, pg 706-713

Skills and Competencies

Training has also been received for a variety of test equipment and facilities leading to competence in the following:

- Optical metallography techniques including electronic image capture.
- Wide range of small scale formability tests and mechanical tests
- Circle Strain Analysis
- Operation of Anton Bauer High Pressure Hydroform Press

Contents

1.0 Introduction

Government and consumer pressures have forced the automotive industry to re-look at the method of manufacturing an automobile. With a greener outlook, the automotive industry is beginning to improve fuel economy, reduce emissions and reclaim the vehicle at the end of its useful life.

Tube hydroforming and LWTB's (Laser Welded Tailored Blanks) are two of the new methods, which help to reduce a vehicle's weight. The use of such advanced technologies coupled with holistic design concepts, means that the present-day vehicles are becoming lighter. Such technologies also offer opportunities in terms of developing improved crash performance compared to conventional pressed formed components of the same weight.

The tube hydroforming process utilises forming fluid, under high pressure, to stretch a tube blank into the shape of a die cavity. The application of the internal pressure may be accompanied by axial feeding of the tube ends to push additional tube material into the die cavity. Close control of process parameters and the die design are essential to produce successful, defect-free components.

LWTB's are made up of two or more pieces of steel sheet laser welded together to form a single composite blank. LWTB's offer many benefits, including part consolidation, improved material utilization, and component performance.

Tube hydroforming has already proved successful in sub frame and chassis applications. However, there has been limited uptake of this technology in the production of BIW structural components. This has been mainly due to the fact that standard tube making methods are restricted to production of tubes with a diameter to thickness ratio of 65:1 at best, where as typical BIW application would be more inline with a ratio of 100:1. The Corus Tubular Blank process enables a greater range of D/t ratios, and therefore a larger scope of manufacture for BIW parts.

The Corus Tubular Blank machine receives a flat sheet blank, which undergoes a multiple pressing operation using a circular punch and die profile. The open formed tubular shape is then finally laser welded to form a closed section. The number of pressings required for the blank is dependent on the degree of formability of the sheet blank, and also the amount of forming pressure required to deform the sheet blank.

Both tube hydroforming and tailor blanking have their own individual merits. By combining the two, not only will the automotive manufacturer retain the benefits of both, but also gain the ability to form many other components that were previously impractical to manufacture.

The major technical issue concerned with the manufacture of both Corus Tubular Blanks and Corus Tailor Welded Tubes (Corus Tubular Blanks made using LWTB's sheets) is the effect of material elastic recovery after forming has taken place. It has been well documented in the literature that the magnitude of elastic recovery (springback) in a component is influenced by the material and forming properties. It is very difficult to have full control of the material properties. However, forming properties are controllable especially if the forming process is simple as in the case of the Corus Tubular Blank. Corus Tailor Welded Tubes introduce a complex combination of springback characteristics inherited from the constituent parent parts of the LWTB.

An understanding is needed of both the key material and loading factors that influence springback, to be able to predict springback for a single material, and also composites of several differing types of sheet steel welded together. The methods of springback mitigation will effect the subsequent hydroformability of the formed tubular blank.

2.0 Literature Review

2.1 Automotive manufacturing trends

2.1.1 Globalisation

As with all industries the automotive market has seen an increase in the level of globalisation as the market place has become more open and thus more competitive. Alliances and licensed agreements have increased to ensure that demand is satisfied, and that market share is increased in mutually beneficial agreements. Joint ventures such as the planned cooperation between Suzuki Motors Corporation and Opel for the development of the mini platform for the Suzuki Wagon R+ and Opel Agila is one such agreement. Many others exist within the automotive market, another example is the joint development of a Sports Utility Vehicle (SUV) platform by General Motors (GM) and Isuzu Motors [2.1.1].

One of the effects of globalisation is the reduction in the number of independent automotive manufacturers. Over the last decade the manufactures/groups has decreased to a level where approxiamately 20 exist. These also have undergone a degree of synergy, and a further whittling of numbers has taken place. [2.1.2,2.1.3]

The effect of globalisation on the electronics industry has meant that wild swings between profit and loss now occur. If the product is not seen as cutting edge and blue chip then the degree of profit is greatly reduced, and the competition greatly increased. It may be questioned how this relates to the automotive market place, but consider the fact that the electronics industry has had a head start of about 20 years in true globalisation, the trends are likely to be the same for the automotive market.

Consider the electronics industry and the production of televisions, the first development was the introduction of a common chassis for the cathode ray tube (CRT) dependent on size. This meant that only the exterior of the set was different. Secondly, because of the adoption of common internal parts it was possible to modularise the manufacture, allowing quicker time to market and a more fluid ability to change to customer demands and needs.

Along with the outsourcing of components,agreements and sharing components with other manufacturers, this has meant that the electronics industry has reduced time to market and increased profitability on each unit produced.
From the trends in the automotive market thus far a mirroring effect can be seen.

2.1.2 Vehicle body construction

The requirements of the vehicle body have changed considerably from the initial development of the automotive industry. No longer is the vehicle body just for occupant space and weather protection. Leglislation and consumer pressure has lead to increased passive safety requirements, lower manufacturing costs, reduced vehicle weight, aerodynamic characteristics and also increased ride comfort (low noise, good road handling).
Vehicle bodies today can be classified into two differing groups, monocoque (unibody) or body-on-chassis (space frame).[2.1.4]
The most effective means of protecting the occupants of a vehicle is to maximise the effective utilisation the vehicle body construction. This is possible by the adoption of large closed box like sections in the vehicle for impact absorbtion, distribution and to develop effective crumple zones. These closed sections have also been enhanced to the torsional resistance and bending stiffness of the vehicle body leading to improved road handling characteristics.[2.1.5]
Sheet steel stampings that are subsequently welded into these closed sections have been the traditional means of manufacture for structural sections.

2.1.3 Modularisation

An early form of this type of manufacturing ethos is the pre-fabs built after the second world war. Accomodation was is great demand, and the government had to fulfill this need with cheap rapidly constructed buildings. Introduction of such buildings meant the sacrifice of variability in construction design.

This form of complete modularisation has given way to one in which the interior size is kept constant and the exterior changed to suite the location, customer and local by-laws. The automotive industry has adopted this methodology also, as described in section 2.1.1, with a further additive. Automotive OEM's (original engineering manufacturer) are no longer having to develop, source, stock, inspect, manage and then assemble parts of a component such as a gear box; instead these operations are carried out by tier 1 or 2 suppliers. [2.1.3]This ultimately results in the creation of a 'screw driver plant' where once an intergrated car plant existed. This movement of assembly ethos has realised the OEM's targets of reduced stock, storage, product range and improved time to market. Secondly the financial commitment for the launch of a new product is also greatly reduced as the burden is now spread amonst many suppliers eager to compete for the new business.[2.1.3]

2.1.4 Cost reduction

Year on year price reduction has become the norm in the automotive industry, and is built into all long-term contracts. Suppliers are required to give accurate detailed breakdowns of costings. This however does not give a true indication of the actual costs, as vehicle manufacturers are not privy to the cost of all the component and materials purchased. This type of target pricing system enables a calculation of savings over a notional price.[2.1.3]

Global purchasing results in continued pressure on supplier costs. This means that the pressure is most acute in the second or third tier supplier, which is situated between the material suppliers and vehicle manufacturers.

An increase in raw material costs will be magnified further up the supply chain, resulting in the vehicle manufacturer bearing the brunt of this increase. It is for this reason that vehicle manufacturers enter into supply agreements, and therefore cascade this risk back down the chain. A method adopted to encourage supplier comittment, is the incentive of shared profits for a supplier on cost reductions thus enabling targets to be met, but also rewards given in gratitude.[2.1.3]

2.1.5 Vehicle weight reduction

During the last two decades, environmental issues have played a major part in the directives issued by governments targeted at vehicle producers [2.1.6]. One of the largest concerted international drives is to reduce the amount of CO_2 emissions into the atmosphere. It was recognised early on that one of the determining factors of a vehicle's fuel consumption and resultant CO_2 emission is that of vehicle weight [2.1.7]. This was coupled with the realisation that oil reserves are a finite resource, and the West was dependent on the Middle East for oil (highlighting this dependency was the 1973 OPEC crisis). Consequently, the North American Government, introduced the CAFE (**C**orporate **A**verage **F**uel **E**conomy) Regulations in 1978 that required car manufactures to produce a fleet with an average fuel economy of 13.1 Ltr/100km. This has since been reduced to 8.5 Ltr/100km [2.1.7, 2.1.8]. If these requirements are not met then the producer incurs financial penalties.

The resultant changes in body and power train design realised a weight reduction for the average saloon class car from 1560 kg in 1977 to 1225 kg in 1986. Since then the weight has grown steadily by 1.0% pa; this is accounted for by increased safety standards and customers desire for added extras [2.1.7].

2.1.6 Steel trends in automotive structural members

The overall trend in body weight of Japanese passenger cars (medium and compact) over the last two decades has been an increase of 136.8%. This difference in weight trends could be the reflection of Japanese consumer request for driving comfort, improving safety and the increase in optional extras [2.1.8].

To counteract the trend of increasing weight automotive manufactures have increasingly turned to new lightweight materials [2.1.9]. The material ratio in Japanese passenger cars (medium and compact) over a period from 1973 to 1992 has changed somewhat. Comparison of these figures show that the ratio of iron and steel components present in the car has decreased from 81.1% to 72.3%, the ratio of non-ferrous metals has increased

from 5% to 8% of which aluminium accounted for 6% of this figure in 1992, a rise of 3.2% from 1973. Polymer materials showed an increase of 2.9% to 7.3% [2.1.9].

A recent survey carried out by Mintz [2.1.10] of automotive designers and specifiers, along with researchers on high strength steels, indicated that the trend for the greater use of high strength steels in the automotive sector would continue. Other trends indicated in this survey was that of increased corrosion protection, leading to guarantee of 5-8 yrs for cosmetic and 12-15 yrs for perforation, and the drive for cost reduction in corrosion protection by using cheaper methods. This is evident from the Ford/GM/European trend of EG (Electro galvanised) ⇒GI (Hot Dipped Galvanised) exposed, and Japanese manufactures change from EG ⇒GA (Hot Dipped Galvannealed) and once successful ⇒ GI.[2.1.11]

The survey results of Mintz are almost mirrored in a study by Mathews [2.1.12], which was carried out as a strategic aid for the positioning of Corus in the automotive sector. Automotive components were grouped into steel yield strengths suitable for various applications. Most notable from this report is the foreseen coating methods to be adopted; with a progressive trend towards the use of GI.

Mintz [2.1.10] results regarding coating solution seems to be more plausible, as automotive companies have already begun the transition from Electro galvanised to the cheaper Hot Dipped Galvanising systems. The most noticeable example is Nissan, who over the last year have moved away from NIZEC™ (Zi-Ni Electro deposited) into GA [2.1.11], and have announced that the new Micra, to be built in Sunderland, shall be of a GI protective coating. Interrogation of these two recent surveys, and also work carried out on the ULSAB [2.1.13] and HIBS [2.1.14] projects have indicated the steel grades and coating methods most likely to be adopted for automotive components. Many steel components are prime candidates for hydroforming.

The recent report from the ULSAB-AVC Consortium [2.1.15] has also shown a willingness to push the boundaries of material utilisation in the direction of so called advanced high strength steels (AHSS). Proposed body material listings of hydroformed tube components can be seen in Table 2.1, parts which have been indicated as HFT (Hydroformed tube) or, HFT/TWT (Hydroformed tube/Tailor welded tubes) will be manufactured on a machine similar to the Corus Tubular Blanks machine.

Application of high strength sheet steel and changes in body structure design have been effective methods for combating the rise in vehicle weight. However, the positive influence of high strength steel use is accompanied with a negative aspect that of inferior formability compared to mild steel. A factor of concern in regard to the ULSAB-AVC project is the strength of crash members. These members have been chosen for their ability to absorb energy.

2.1.7 The ULSAB project [2.1.13]

One of the concerns from a steel producers point of view is the increased percentage usage of aluminium in the BIW. To combat this, and also draw attention to new manufacturing technologies, a consortium of 32 prominent sheet steel producers from 18 countries around the world came together in 1994 with the common goal of reducing the weight of an all steel auto body structure whilst still delivering affordability and performance.
The programme was arranged into two phases.

Phase 1 involved the concept design of a medium to large saloon car.
The 'holistic approach' has often been quoted as the key to the success of this programme [2.1.16]. Porsche Engineering Services, who were commissioned by the consortium to design a vehicle utilising the latest component technologies and manufacturing techniques, approached the design with a fresh outlook viewing the **B**ody-**I**n-**W**hite (BIW) not as a series of individual components assembled together, but as a cohesive amalgamation of materials and techniques [2.1.16].
Two preliminary design approaches were investigated, that of the Unibody structure (see fig 2.1) and that of the **H**ydroformed **I**ntensive **B**ody **S**tructure (HIBS later to be developed by British Steel and Rover Group) (see fig 2.2).
The Unibody structure was to become the predominant of the two in this project and the prototype for the final design. HIBS highlighted the difficulty surrounding the joining of other structures or components to the hydroformed sections, but also showed the benefits

of weight saving and greater structural integrity compared to identical structures, which were spot welded [2.1.13, 2.1.14].

The initial unibody ULSAB design incorporated three hydroformed components, these were:

i. Side roof rail
ii. Fender supports
iii. Pass-through beams

However,` only the side roof rail made it through to the final design concept.

The front fender support was replaced by a conventional two-piece stamping. The rationale behind this change was related to the perceived assembly route where the body side outer and inner sub-assemblies were to be loaded after the front-end assembly was in place. A hydroformed component would have made it impossible for the vertical and horizontal adjustment needed in mass production.

The pass-through beam, or A-post, was again replaced by a two-piece design; as the front part of the assembly forms an integral part of the 'front end assembly', whilst the rear part is incorporated into the 'inner assembly'. This part if hydroformed would have had an extra weld between the two parts in a critical area (from a structural aspect) [2.1.13, 2.1.14] .

Phase 2 involved the design detail, analysis and building of the **Body-In-White**

Potentially one of the biggest obstacles for the ULSAB consortium was to waylay fears of automobile manufacturers that the crash simulations were realistic representations of the physical crash tests that would normally be performed. Such practical tests are destructive and often require a fully running vehicle [2.1.14]. However, the CAE results were good indicators of what would happen in practice, and it also showed that reducing the body structure mass, using high strength steel in various grades and applications of tailored blanks, was a viable alternative to traditional components and assemblies. The economic analysis carried out showed that the lightweight structure carried no additional cost penalties. Again it must be recognised that the cost model produced for a competitive type car in the year 2000 had general assumptions attached to it. For example, the study identified part groupings, instead of individual real parts as with

ULSAB, and assumed improved fabrication and assembly techniques [2.1.17, 2.1.13, 2.1.14, 2.1.18].

The knowledge gained in the ULSAB project helped to develop concepts for the ULSAC (Ultra Light Steel Auto Closures), (Ultra Light Steel Auto Suspension) projects, and also contributed to the initial concept for the ULSAB-AVC (Advanced Vehicle Concepts) project.

The ULSAB project sent out a clear message to automotive manufacturers; in an all steel autobody the recycling costs will be reduced and this will go part of the way to satisfying future End of Life Directives. The only downside is that the increased use of coated steels in the autobody will downgrade the quality of scrap produced at end of life. It does seem that the ULSAB project and its various forms will only delay the increased usage of materials other than steel. However, it will go some way to securing steel as a main contender for the major load bearing components within the vehicle for the medium term [2.1.19].

2.1.7a ULSAB-AVC

The ULSAB-AVC (Advanced Vehicle Concepts) consortium which was formed in January 1999 by 33 sheet steel manufacturers, was set up to develop safe, optimised, and affordable steel vehicle structures. Hydroformed tubes are seen as one of the methods to reduce the vehicle's weight.

The ULSAB-AVC program followed the ULSAB Steel Auto Body program, which reported final results worldwide in March 1998. Both are initiatives of the steel industry's to find solutions to the challenge facing automakers, government regulators and environmentalists around the world to improve the automobile's environmental profile through increased fuel efficiency, while improving safety, performance and maintaining affordability.

The ULSAB-AVC holistic approach copied that of ULSAB, to the development of a new architecture for advanced steel vehicles. The program went beyond ULSAB. ULSAB-AVC produced complete design concepts that would meet the perceived vehicle

performance and safety requirements for 2004. Closures, suspensions, engine cradle and all structural and safety-relevant components were chosen to be hydroformed in principle. The major limitation of this project in enabling further acceptance of hydroforming as an alternative forming medium is the fact that this project is merely a concept project with no building of prototype structure. With no actual components being formed and assembled, it is more difficult to convince an OEM or tier 1 manufacturer that this present technology is ready to run as is.

2.1.8 Steels for automotive structural members

Steel remains the major load bearing material for the automotive industry to date. With an array of properties, steel lends itself readily for use as a structural, autobody, chassis or wheel material. This, coupled with the added quality of recyclability, and excellent price to performance ratio, ensures that it stays one step ahead of the competition.

The development of higher strength phosphorus-alloy, micro alloyed and interstitial free steels goes back to the 1970's.

Given the potential of weight saving through the usage of these steels, it seems surprising that they made no real impact until the mid 80's [2.1.20]. However, the main reasons for this was two fold:

i. Production had to adapt to steels with changed properties.
ii. There was only a limited possibility of including modified High Strength Steel parts in current vehicle models.

Due to the constant demand for weight saving and improved performance other steels were created. These steels were 'bake hardenable' (BH), 'dual phase' (DP), 'transformation induced plasticity' (TRIP) and carbon-manganese (CMn); notably TRIP steel could reach a yield beyond 800 MPa.

With new concepts in design philosophy and manufacturing techniques, such as the use of tailor welded blanks and hydroforming, it is possible to downgauge components using higher strength steels. The majority of tube hydroformed sections currently used in the automotive industry are for structural applications.

High strength steels have been recognised as one of the major contributing factors to the weight savings achieved in the ULSAB project [2.1.13]. High strength and Ultra high strength steels are defined by a minimum level of yield strength of 210 MPa and 550MPa respectively [2.1.20].

2.1.8a Precipitation strengthening/grain refined steels [2.1.21]

The term micro-alloyed is used extensively to describe the addition of small amounts of niobium, vanadium or titanium to ferrite-pearlite steels for the development of higher strength. A strengthening action through the refinement of the ferrite grains is possible by the additions of typically 0.05% Nb or up to 0.15% V; further strengthening can occur due to the precipitation of fine particles of NbCN or V_4C_3 .Steels of this type are called High Strength Low Alloy (HSLA) steels.

The micro- alloying elements, particularly niobium and titanium, are only partially soluble at slab reheating temperatures and the fine particles of Nb (CN) or TiC/TiN that remain out of solution will serve to refine the austenite grains. Recrystallization behaviour can be modified by the amount of fine particles that go into solution at the reheating temperature. This will modify the steel to produce a finer austenite structure during rolling. In turn, this produces a fine ferritic grain size. However, the micro-alloying elements dissolved at the reheating stage will also form fine precipitates of carbides or carbonitrides during the transformation from austenite to ferrite, causing a strengthening effect known as precipitation hardening.

In hot rolled strip, the combination of ferrite grain refinement and precipitation strengthening can result in the development of yield strength values of up to 550 N/mm^2.

On subsequent cold rolling and annealing, the fine precipitates coarsen and the precipitation strengthening effect is lost. However, the particles are effective in maintaining a fine grain size and the associated alloy strengthening effect is retained. Yield strength values up to about 350 N/mm^2 are produced in micro-alloyed, cold reduced strip.

2.1.8b Solid solution strengthening/rephosphorised [2.1.21]

Additions of up to 0.1% P are made to strip steel in order to promote high strength through the mechanism of solid solution strengthening. The effect is due to the disturbance and misalignment of the iron atoms, when atoms of a different atomic size are dissolved in the iron lattice. These so called rephosphorised steels have yield strength values of 220-260 Nmm^2. This form of strengthening is also induced by other alloying elements such as silicon and manganese, but to a smaller extent.

2.1.8c Dual phase steels [2.1.21]

In normal heat treatments, steels are generally heated to a temperature where the structure is completely austenitic. However, if steel is heated to a temperature in the two-phase austenite plus ferrite region, below the austenitic area, and held there, carbon diffuses out of the ferrite and into the austenite, where it is more soluble. If the steel also contains a significant alloy content then this factor, coupled with the enriched carbon content, will cause the austenite to transform to martensite as a consequence of rapid cooling, which is extremely strong. Ordinarily a steel of this type, which is given a conventional heat treatment would transform to ferrite and pearlite but the dual phase version of the material has a structure of ferrite and martensite. Such steels are characterised by low yield strengths but with high rates of work hardening. Therefore they develop high tensile strengths (in excess of $800N/mm^2$) and high n (stretch forming) values.
Dual phase steels are normally produced in both hot rolled and cold reduced gauges via continuous annealing furnaces where rapid cooling rates can result in the formation of martensite, without resort to very high alloy contents. Even so, the alloy content needed to promote the formation of martensite tends to make dual phase steels expensive and this has inhibited their utilisation.

2.1.8d Bake hardening steels [2.1.21]

The term bake hardening derives from the paint baking or curing process that is applied to automobiles and typically involves a heat treatment of 170° C for 20 minutes. During

cold forming of an automotive outer body panel, the strip undergoes a strain of the order of 2% and this results in an increase in yield strength of about 40 N/mm^2. Given a suitable composition and prior treatment, carbon that was in solution will precipitate to dislocations (atomic misalignment) in the cold worked structure during the bake hardening treatment to provide a further strengthening increment of about 50 N/mm^2.

2.1.8e TRIP steels [2.1.21]

TRIP is an acronym for Transformation Retained Induced Plasticity steel. This type of steel is obtained through a combination of controlling cooling on the hot mill and also modifying the composition. Within the material microstructure small amounts of untransformed austenite exists. Once this material has undergone a forming process in which it encounters plastic strain, the induced energy allows the untransformed austenite to transform into martensite, resulting in a significant increase in energy absorption.

2.1.9 Recycling

At present no statutory policy exists for the recycling of automotive components in Europe at this present time. However, the threat of a Carbon Tax and End of Life Directive has meant that not only does the weight reduction play a part, but also the manner in which the redundant vehicle can be dismantled and recycled at little additional cost to the manufacturer. Of the material used in present day vehicle body, steel is the one which lends itself more readily to recycling.

2.1.10 End of life directive

This regulation will be in force in the year 2004. Each vehicle producer will be responsible for the recovery and reuse of materials associated with their product [2.1.6, 2.1.7]. It will be necessary that by 2005, 85% of a vehicle will be reusable or recyclable, and that by 2015, 95% will be reusable or recyclable [2.1.7].

This places the car producer in a rather difficult situation. Not only does he need to worry about the weight of the car but also the recyclability of the materials and the ability to reverse the fabrication process that these materials undergo during production.

Recycling of steel is relatively easy in contrast to aluminium where the likely inclusion of tramp elements in the material during recycling make it impractical to manufacture into sheet grade efficiently. Secondly the amount of energy required to do so is not cost effective.

Plastics raise an even greater challenge for producers because of their numerous forms, and difficulties in recycling.

Therefore it is paramount to a vehicle manufacturer to produce not only a lightweight vehicle, but also one which lends itself readily for recycling after its useful life.

2.1.11 Reference

2.1.1 Word Automotive Manufacturing, issue No. 24, April 2000

2.1.2 Engineering Doctorate 'Tube hydroforming of steel for automotive applications', University of Wales Swansea, Roger Darlington, 2003

2.1.3 'Automotive Materials - The Challenge of Globalisation and Technological Change', Financial Times Automotive, 1998, ISBN 1 85334 9127

2.1.4 'Holistic Design – The key to light vehicle structures', Peterson, P.T., Proc, International Symposium on Automotive Technology and Automation, 1996

2.1.5 Handbook of Automotive Body Construction Design Analysis, J. Fenton, Professional Engineering Publishing Ltd., ISBN 1 86058 0734

2.1.6 Dr D Wolsey, Eng.Doc First Year Course Environmental Issues

2.1.7 Internet search http://www.aiada.org/gr/issues/cafe/cafe.htm 'Corporate Average Fuel Economy', 08/02/00

2.1.8 Dr M.J. Wheeler, 'The Drive for Light Weight Vehicles in North America', Materials for Lean Weight Vehicles Conference, November 24-25, 1997

2.1.9 Hayashi, Hisashi, 'Forming Technology and Sheet Materials For Weight Reduction of Automobile, Recent Technical Trends in Japan', 19th IDDRG Biennial Congress, June 1996

2.1.10 Prof. B. Mintz. University of London/British Steel Welsh Laboritories, UK, Project ZCO-33-1, May-December 1999

2.1.11 Conversation with T.B.Jones, C.Chanillor, K.Chivers, CTC Automotive Section, WTC Port Talbot.

2.1.12 Mathews, Austin, 'European competitive position of BSSP High Strength Steels for Automotive Body-in White as a Strategic Aid' Memorandum, 8/11/1999

2.1.13 ULSAB Electronic Report 1.0 CD-ROM

2.1.14 ULSAB 40 Project Report AEG 1075/1 CD-ROM

2.1.15 ULSAB-AVC (Advanced Vehicle Concepts), Project Report

2.1.16 E.F.Walker C.Eng.FIM, M.W.Boyles C.Eng. MIM, K.Lowe C.Eng.,MIM, British Steel Strip Products, 'ULSAB (Ultra Light Steel Auto Body)', Materials for Lean Weight Vehicles Conference, November 24-25, 1997

2.1.17 R.Koehr, Porsche Engineering Services, 'ULSAB Project Overview and Results', JSEA Materials Forum, May 20th, 1998, pg 10-21

2.1.18 M. van Schaik, Hoogovens Steel Strip Mill, 'The Use Of Hydroforming In The ULSAB Project' lib no 9835212

2.1.19 P.Wells, M.Rawlinson, Centre for Automotive Industry Research, 'ULSAB – A Critical Appraisal, IBEC'97, Advanced Body Concept and Development, pg 89-95

2.1.20 Dr R.W. Simon, Thyssen Stahl Ag, 'New Steel Products For The Automotive Industry', Steel Times International, November 1997, pg 44-50

2.1.21 D.T. Llewellyn 'Steel Products and Properties', British Steel Booklet in the series 'Introduction to the Iron and Steel Industry', volume 2

2.1.12 Figures / Tables

Figure 2.1: ULSAB Unibody

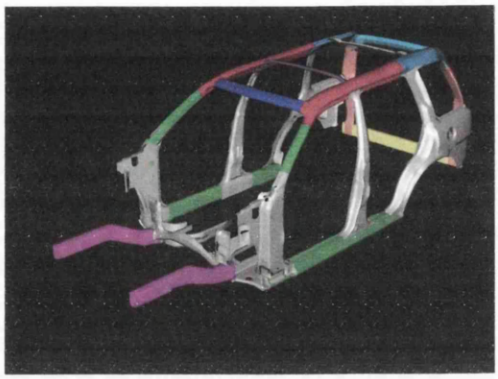

Figure 2.2: ULSAB HIBS

Part Number	Name	Blank No.	Material Thickness (mm)	Material Type	Grade (Mpa)		Manufacturing Process Code	Vehicle Class
					Yield Strength	Tensile Strength		
AVC-2-1050	Member Rail Front RH	1	1.5	DP Tube	500	800	HFT/TWT	C-class
		2	1.3	DP Tube	500	800	HFT/TWT	C-class
AVC-2-1051	Member Rail Front LH	1	1.5	DP Tube	500	800	HFT/TWT	C-class
		2	1.3	DP Tube	500	800	HFT/TWT	C-class
AVC-2-1132	Member Body Side Inner RH		1	DP Tube	500	800	HFT	C-class
AVC-2-1133	Member Body Side Inner LH		1	DP Tube	500	800	HFT	C-class
AVC-3-1050	Member Rail Front RH	1	1.5	DP Tube	500	800	HFT/TWT	D/E-class
		2	1.3	DP Tube	500	800	HFT/TWT	D/E-class
AVC-3-1051	Member Rail Front LH	1	1.5	DP Tube	500	800	HFT/TWT	D/E-class
		2	1.3	DP Tube	500	800	HFT/TWT	D/E-class
AVC-3-1130	Member Body Side Inner RH		1	DP Tube	500	800	HFT	D/E-class
AVC-3-1131	Member Body Side Inner LH		1	DP Tube	500	800	HFT	D/E-class

DP Dual phase steel
HFT Hydroformed Tube
HFT/TWT Hydroformed/Tailor Welded Tubes

Table 2.1: Proposed ULSAB AVC Hydroformed components

2.2 Material formability

The formability of a material is its ability to be plastically deformed, under defined conditions, into a given shape.
Several key areas need to be investigated to be able to draw conclusions on a materials formability and application to a process. These are:

Properties of object being formed. The raw material form i.e. sheet-bar-rod-billet each have differing properties from one another resulting from their complex internal structure i.e. composition, grain size & orientation, texture, void density, inclusions, residual stresses. Other factors such as surface topography, texture and coating also play an important role.

Formability criterion. Factors such as ductile fracture, galling, wrinkling tendency, non-uniform thickness, folding, creasing and earring.

Conditions when forming. These are conditions, which are set by the process engineer and to a certain extent controllable – geometry of punch & die, press set-up, temperature during forming, velocity of working (strain rate) and lubrication type and amount.

Considering these three areas, it is possible, by means of tests, to rank each material and known path of forming. Unlike many other forming processes tube hydroforming is a secondary operation. The tube needs to be firstly formed. It is useful therefore to understand each of the process steps and their resultant changes to the original condition of the material.
It has been stated by Zdziskaw [2.2.1] there is no one critical factor when looking into a materials formability, but an amalgamation of the material properties and the process parameters under which it is to be formed.
However what must remain foremost in the mind of the engineer is the requirements of the customer in respect to the final product.

2.2.1 Simulative tests

A problem, which always arises when trying to carry out tests on material to depict their behaviour, is how to duplicate the actual forming conditions the material will undergo. This aspect can never really be fully tested unless the actual process is used in the experimentation and given today's manufacturing ideology of high process utilisation this would seem highly unlikely.

It is better to find a test, which is indicative of the process and will reflect adequately the conditions the material will encounter.

An example of a well-known simulative test is that of sheet stretchability assessment, better known as the Erichsen test. Such a test provides good indicators of a materials formability under particular constraints, but caution must be shown when trying to relate a new forming process to an already established simulative test [2.2.1].

To try and counteract this unknown it has been suggested by Zdziskaw [2.2.1] that the following steps be followed.

In order to simulate properly the real forming conditions encountered in different operations, the number of different simulative tests should be almost as high as the number of possible forming operations and typical forming conditions.

The range of applications of each of the simulative tests is confined to specific cases, when the maximum deformation that a material can suffer in the test is limited by the same phenomenon as in the real operation.

2.2.2 Formability by means of material properties

Provided that the forming operation is known another means of ranking formability is to look at the plastic properties of the material, these properties are defined by constants [2.2.3]. In cold forming the properties of prime importance are:

Plastic strain ratio	r
Mean Plastic strain ratio	r_m
0.2 % Proof stress/Yield stress	σ_y

Strain hardening index	n
Strain rate sensitivity	m
Surface roughness	Ra
Young's Modulus	E
Coefficient of friction	μ

The majority of these properties can be found by performing a standard tensile test on the material.

2.2.3 Intrinsic properties and theory of plasticity

Mechanical properties of sheet steel are determined from a standard tensile test. The test consists of a specimen continuously subjected to an increasing axial load applied at a specified speed by a tensile testing machine. During the duration of the test the applied load and elongation of gauge length are recorded.
An engineering stress/strain curve resulting from the standard tensile test does not truly represent the characteristics of a material under deformation as all calculations are given in respect to the specimen's original c.s.a. (cross-sectional area). The true representation would be to relate each of these conditions to the instantaneous c.s.a. In normal plastic deformation the strains are frequently large and the gauge length extension is extensive [2.2.2]. Fig. 2.2.1 shows a typical engineering stress/strain curve versus a true stress/strain curve for the same material.
For this problem Ludwik proposed that true strain and true stress is described as follows.

2.2.4 True strain (ε)

$$\varepsilon = \Sigma\, (L_1 - L_o)/L_o + (L_2 - L_1)/L_1 + (L_3 - L_2)/L_2 \ldots \quad \text{eqn. 2.2.1}$$

where
L_o = initial length of test piece
L_1 = first arbitrary length of test piece

L_2 = second arbitrary length of test piece

L_3 = third arbitrary length of test piece

$\varepsilon = \ln L/L_o$ eqn. 2.2.2

2.2.4a Engineering strain (e)

$e = \Delta L/L_o = (L - L_o)/L_o = (L/L_o) - 1$ eqn. 2.2.3

Therefore from equation 2.2.2 and 2.2.3

$e + 1 = L/L_o$ & $\varepsilon = \ln L/L_o = \ln(e+1)$

$\varepsilon = \ln(1+\Delta L/L_o)$ eqn. 2.2.4

ΔL = resultant elongation

2.2.5 True stress (σ)

True stress = $\sigma = p/a$ eqn. 2.2.5

Where

a_o = original cross sectional area

a = cross sectional area

p = force

2.2.5a Engineering stress (s)

Engineering stress = $s = p/a_o$

$\sigma = p/a = (p/a_o)(a_o/a)$ eqn. 2.2.6

keeping volumetric consistency from equation 2.2.5 and 2.2.6

$a_o/a = L/L_o = e + 1$

$\sigma = p/a_o\,(e + 1) = s(e + 1)$ eqn. 2.2.7

If

$\sigma f = \sigma f(\varepsilon)$

and is denoting stress required for plastic deformation under an uniaxal state of stress then the relationship for a multi axial stress state would be of equivalent stress σ_{mean} and equivalent strain ε_{mean}.
Therefore for uniaxial state

$\varepsilon = \varepsilon_{mean}$ eqn. 2.2.8

It is assumed that in the range of uniform deformation the stress is constant over the c.s.a. The range of uniform deformation is limited by the amount of elongation from which the maximum force is obtained. e_u
Above this elongation the deformation becomes unstable and necking occurs.
Disadvantage with tensile testing is that necking occurs at a rather low strain value [2.2.2], see fig. 2.2.2 for schematic of necking region.

$\varepsilon_u = \ln(1+e_u)$ for most metals eqn. 2.2.9
$= 0.2\text{-}0.3$

2.2.6 Holloman /Ludwik

For most unalloyed and low-alloyed steels at room temperature it has been shown by firstly Holloman and ratified by Ludwik that strain will follow a flow curve of the following law

$$\sigma f(\varepsilon) = K\varepsilon^n \qquad \text{eqn. 2.2.10}$$

Where K and n are material constants

n- strain hardening coefficient (log-log plot of true stress –true strain i.e. slope of line see fig. 2.2.3)

K-Strength coefficient

$$K = Su\,(e/n)^n \qquad \text{eqn. 2.2.11}$$

Su= tensile strength

e= elongation

Hot and cold forming is usually defined as deformation regarding elevated temperatures and room temperature respectively. These conditions affect the metals ability to recover and also for recrystallization to take place. Therefore the flow curves will be dependant not only on the temperature but also the speed or rate of strain undergone. This relationship can be expressed by the equation

$$\sigma f = K\varepsilon^n \dot{\varepsilon}^m \qquad \text{eqn. 2.2.12}$$

where m is the strain rate sensitivity index of the material

For most steels this ranges from -0.02 to + 0.05 @ 20 - 450°C, 0.1 to 0.2 @ 880°C and above [2.2.2].

2.2.7 Yield criteria & stress strain relations

Although the flow curve can indicate the yield of the material in one direction, it cannot directly indicate the materials behaviour under a complex state of loading [2.2.2]. In hydroforming, like many other kinds of forming, seldom is there a condition where loading is carried out in one plane. Therefore, to enable the prediction of material behaviour during forming, it is necessary to take into consideration all principle axes under which loading can occur. In a tensile test (one dimensional) yield takes place when

p/a_o reaches σf eqn. 2.2.13

In multi axis stress state yielding is dependant on a combination of stress states.
The work in this field has produced many equations suited to differing conditions but the two most robust are:

1 Distortion energy criterion (von Mises, Hencky)

2 Maximum shear stress criterion (Tresca, Mohr)

2.2.8 Distortion energy criterion

Von Mises postulated that the onset of flow was dependent on a combination of normal and shear stresses the magnitude of which remained constant with a change in co ordinate system

$$\sqrt{\tfrac{1}{2}}\,[(\sigma_1 - \sigma_2)^2 + (\sigma_2 - \sigma_3)^2 + (\sigma_3 - \sigma_1)^2] = \sigma f$$

or

$$\sqrt{3/2}\,[(\sigma_1 - \sigma_m)^2 + (\sigma_2 - \sigma_m)^2 + (\sigma_3 - \sigma_m)^2] = \sigma f \qquad \text{eqn. 2.2.14}$$

where σ_m = mean stress

In a one dimensional state $\sigma_1 = f/a \quad \sigma_2 = \sigma_3 = 0$

$\sqrt{\frac{1}{2}(2\sigma_1^2)} = \sigma f$ eqn. 2.2.15

2.2.9 Maximum shear stress criterion

Mohr postulated that the permanent deformation at a point would occur when the largest shear stress at this point reached critical value

$\tau_{max} = (\sigma 1 - \sigma 3)/2$ eqn. 2.2.16

This is represented by Mohr's circle with radius k
In uniaxial test $\sigma_2 = \sigma_3$

$\sigma_1 = f/a = \sigma f = 2k$

$k = \sigma f/2$

Therefore maximum shear stress criterion

$\sigma_1 - \sigma_3 = \sigma f$

From fig.12 it can be seen that its centre position relevant to σ or τ does not affect onset of yield.

Mean normal stress = $\sigma_m = (\sigma_1 + \sigma_2 + \sigma_3)/2$ eqn. 2.2.17

If we inspect the two criteria for maximum shear stress for Mohr and von Mises

$\tau_{max} = \frac{1}{2}\sigma_1 = 0.5\,\sigma f$

however when we look at pure shear

$\sigma_3 = -\sigma_1$ $\sigma_2 = 0$

Mohr gives $\tau_{max} = \sigma_1 = 0.5\sigma f$ eqn. 2.2.18

von Mises gives $\tau_{max} = \sigma_1 = \sigma f/\sqrt{3}$ eqn. 2.2.19

From experiment, it has been seen that von Mises criterion holds better for actual conditions [2.2.3].

2.2.10 Yield locus

For biaxial plane stress condition $\sigma_2 = 0$ von Mises yield criteria can be expressed as

$\sqrt{}\ ½ [(\sigma_1 - \sigma_2)^2 + (\sigma_2 - \sigma_3)^2 + (\sigma_3 - \sigma_1)^2] = \sigma f$ eqn. 2.2.20

$\sqrt{}\ ½ [(\sigma_1)^2 + (\sigma_3)^2 + (\sigma_3 - \sigma_1)^2] = \sigma f$

expanding $(\sigma_3 - \sigma_1)^2$

$(\sigma_3 - \sigma_1)(\sigma_3 - \sigma_1) = \sigma_1^2 - \sigma_1\sigma_3 + \sigma_3^2$

$\sqrt{}\ ½ [2\sigma_1^2 - 2\sigma_1\sigma_3 + 2\sigma_3^2] = \sigma f$

$\sigma_1^2 - \sigma_1\sigma_3 + \sigma_3^2 = \sigma f^2$ eqn. 2.2.21

Equation 2.2.21 is the equation of an ellipse, the major axis of which is $\sqrt{2}\sigma f$ and minor $\sqrt{2}/3\sigma f$

The plot of this equation gives what is known as the yield locus. Within the bounded areas of the locus, elastic conditions are encountered outside which plastic conditions are assumed.

Tresca locus – conservative condition which is good for design factor of safety

von Mises – better for forming as plastic region is always sought after

2.2.11 Anisotropy

All calculations and equations have assumed that the material being considered is isotropic i.e. same characteristics in all planes. However, this is seldom true in the real world as work of some kind has been carried out on the material and alloys may have been added. We must therefore consider the material to be anisotropic i.e. characteristics change in relation to rolling direction. Initial work in this field was carried out by Hill, who extended von Mises yield criterion to an anisotropic material considered to have three planes lying vertically to one another (orthotropic)

Hill formulated

$$F(\sigma_y - \sigma_z)^2 + G(\sigma_z - \sigma_x)^2 + H(\sigma_x - \sigma_y)^2 + 2L\tau_{yz}^2 + 2M\tau_{zx}^2 + 2N\tau_{xy}^2 = 1$$

F...N are constants looking at principal axis

$$F(\sigma_2 - \sigma_3)^2 + G(\sigma_3 - \sigma_1)^2 + H(\sigma_1 - \sigma_2)^2 = 1 \qquad \text{eqn. 2.2.22}$$

Where

$$G/H = 1/r_0 \qquad F/H = 1/r_{90}$$

r being plastic strain ratio of tensile specimen, subscript 0 & 90 showing tensile specimen origin 0°-rolling direction, 90°-transverse direction. The effect of r on the yield ellipse of a material can be seen in fig. 2.2.5.

Two other relationships that have been developed from Holloman's original power law is that of

Krupkowsky/Swift,

$$\sigma = K (\varepsilon_0 + \varepsilon)^n \qquad \text{eqn. 2.2.23}$$

and

Ludwik proposed

$$\sigma = \sigma_0 + K \varepsilon^n \qquad \text{eqn. 2.2.24}$$

Where ε_0 and σ_0 denote strain hardening prior to tensile test and initial yield stress, respectively.

During the coarse of this engineering doctorate the forming strain conditions are just beyond the 0.2% proof stress of the material, therefore the engineering stress/strain curve data will be used throughout this thesis. The descriptor σ will be adopted as the indicator for engineering stress. This is possible because the material will have only just undergone plastic yielding and the c.s.a. of the sheet metal component will not have varied to any significant level.
Secondly to ensure consistency throughtout the yield point of all materials has been taken as the 0.2% proof stress

2.2.12 References

2.2.1 Zdziskaw, 'Assessment of Material Formability', Advanced Technology of Plasticity, 1984, Vol.1, pg 685-694

2.2.2 G Dieter, Mechanical Metallurgy SI metric edition, Material Science and Metallurgy, Mc Graw-Hill, 1998, ISBN 0-07-100406-8

2.2.3 Sheet Steel Forming Handbook, SSAB TUNNPLÅT, Edition 1, ISBN 91-971592-9-8, sec 5.1-5.5

2.2.13 Figures / Tables

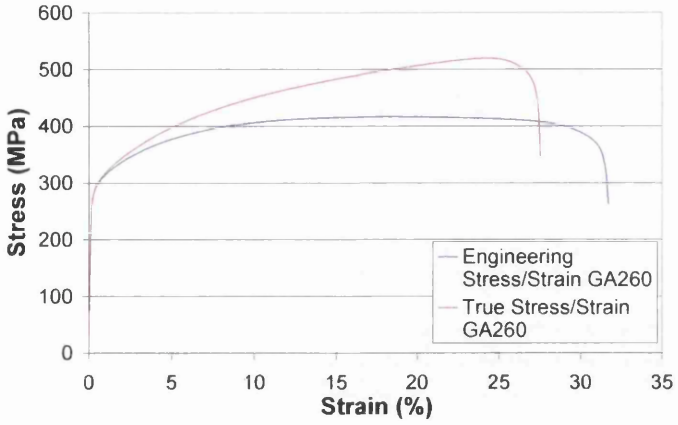

Figure 2.2.1: Engineering stress/strain vs True stress/strain

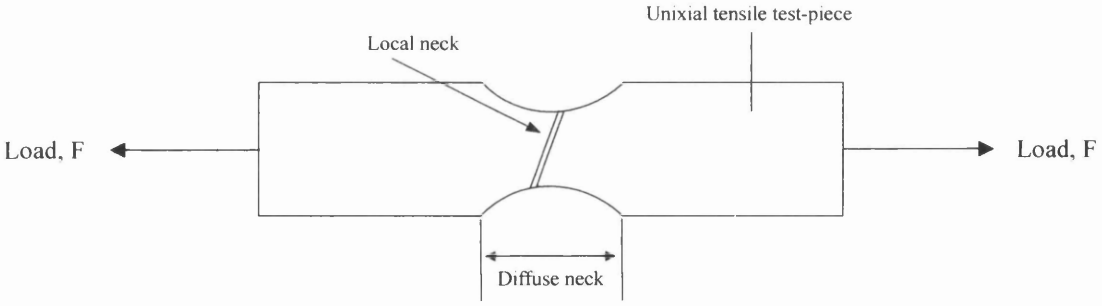

Figure 2.2.2: Schematic illustration of uniaxial tensile necking behaviour

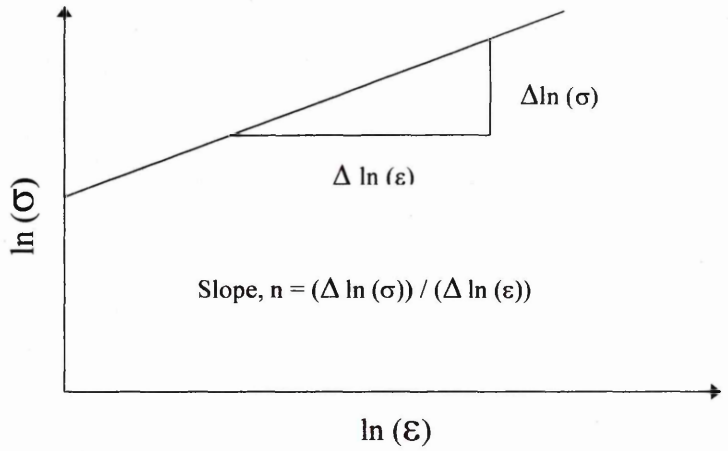

Figure 2.2.3: Schematic illustration of n-value (strain-hardening exponent) determination

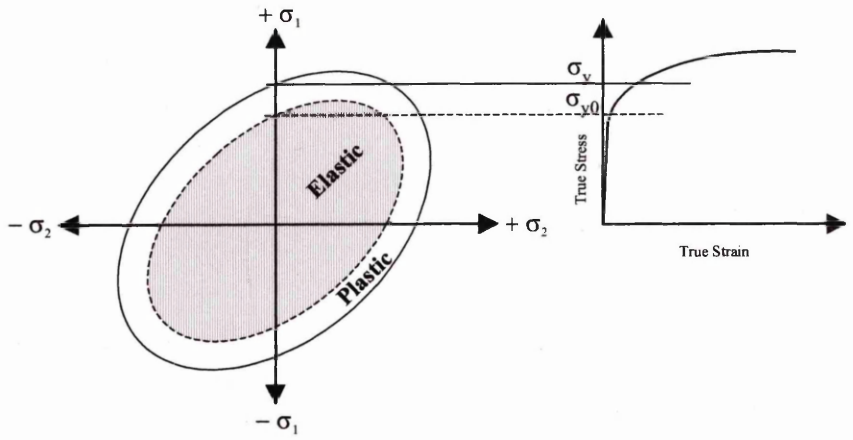

Figure 2.2.4: Schematic illustration of yield ellipse showing elastic and plastic deformation

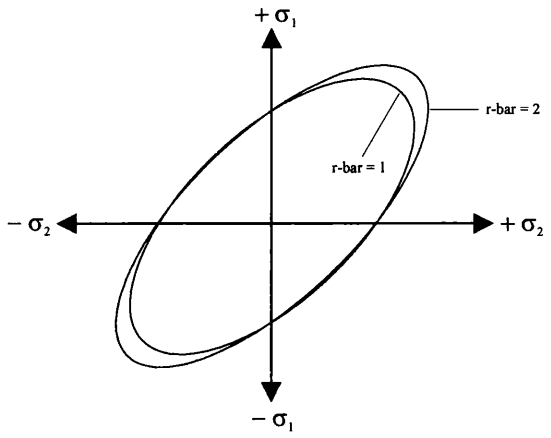

Figure 2.2.5: Schematic of yield ellipse showing influence of average plastic strain ratio

2.3 Hydroforming

Contrary to popular belief hydroforming has been used and researched in industry in one form or another for more than fifty years (bulge forming). Initial investigations centred on the forming of aluminium, copper and brass/aluminium alloys in tubular components with a plan to incorporating this technology into the aerospace industry.

During these investigations, the forming path was studied and related back to theoretical formulae on material behaviour. Work carried out by Limb [2.3.1] laid the foundations on how the process parameters (feasible working region) could be obtained. Limb carried out work using a bulge machine that would expand the test tube into a tee section and also allow for axial feed of material from the end of the tube stock. By alternating the feed of tube into the working area and increasing the pressure until bursting he was able to form the bursting region line, this was then reversed and the pressure was kept the constant at differing stages while feed from both ends was induced until buckling occurred thus giving the buckling line. A typical feasible working region graph can be seen in fig. 2.3.1

2.3.1 Background

Hydroforming is a process in which forming of a work piece is carried out by the transfer of force created by fluid under pressure onto the work piece and forming it around fixed tool geometry. There are two types of forming

1. Tubular
2. Sheet

Of which both have high and low pressure alternatives.

2.3.2 Sheet/flex forming

This type of forming is ideal for small batch components. Utilises the pressure of a fluid, which is enclosed behind a flexible membrane to form sheet metal against die face profile. Cheap tooling costs, lower capital investment, and no need for die/punch match up.

2.3.3 Tubular

Up until recently, tubular hydroforming has been the area of focus for industrial application investigation (interest in sheet forming increasing). A rapid growth was seen during the early eighties when the automotive sector turned its attention to this type of forming. It was seen as an ideal way to reduce not only weight, but also production costs, capital outlay, tooling and at the same time improve part accuracy, integrity of component and fuel economy of vehicle.

2.3.4 Process principles

A tube is placed into the tool cavity, it is the profiling of this cavity which will be the resultant shape / profile of the finished product. The tool is split into upper and lower segments to enable the tube to be inserted and removed. These tool segments are then closed onto the work piece; two axial rams then engage the tube ends and form a pressure tight seal.
The tube is then filled and pressurized by a forming fluid. During this pressurization it is imperative that the axial rams sustain enough pressure at the tube ends to seal and ensure there is no loss of internal forming fluid pressure.
As the forming fluid pressure increases so, the material begins to be forced into the tool cavity. This stages presents two problems,

1. The material will begin to thin as the pressure forces it into a vacant cavity.

2. As the thinning is occurring, the material in the tool cavity is drawing the other tube material, which is already against the tool face. This will result in material around the axial ram (forming the seal) to move, and break the seal.

Both these situations can be counter acted by increasing the axial ram force, thus maintain the seal, and also induce material flow into the cavity. If however the axial feed rate were quicker than that of the material forming speed then the result would be that of material buckling, see fig. 2.3.2 for schematic of tubular hydroforming process.
Once the press has reached the desired pressure and idled to allow for full forming, then the forming fluid pressure is released. The tools and rams are removed, allowing for the finished part to be ejected from tool segment.
Papers dealing with the process parameters of forces, pressure and instabilities were published almost thirty years ago. These concentrated on the theoretical approach to this type of forming. The papers concentrated on the structure of pipe work elements, which were usually rotationally symmetric. Derivations for the solution to these investigations were mainly generated using membrane and shell theories coupled also with theories of plasticity.
As hydroforming becomes more developed the capabilities of producing complex lightweight automotive parts is pushed forward. The days of simple 2D geometry shape forming has long since been left behind, and more complex patterns are being produced, who in themselves have to be preformed in some manner.
With the added advantage of being able to pierce and extrude nodes the hydroforming process can produce work pieces as varied as axle components, engine sub frames and exhaust system components.
Reduced lead-time from design concept to working part, hydroforming has leant itself readily to the ever changing word of consumers wants.

2.3.5 Forming loads for hydroforming [2.3.2]

Forming takes place through the internal pressure Pi inside the work piece and also the axial load Fa as exerted by the axial rams at either stock end.

These forming loads cause stresses in the work piece, which if considering the tube in thin shell theory could be referred to as plane stress.

The analogy of a stress σ_θ acting against the circumference.

$$\sigma_\theta = P_i D/2t = P_i r/t \qquad \text{eq. 2.3.1}$$

and longitudinally

$$\sigma_z = P_i D/4t = P_i r/2t \qquad \text{eq. 2.3.2}$$

where P_i= Applied internal pressure
D= Diameter of tube
r= Radius of tube
t= Tube thickness

note the circumferential stress is twice the longitudinal stress, meaning that the tube will yield in the circumferential direction well before the longitudinal yield occurs.

Expansion would occur when the resultant combination of these stresses σv is equal to the local yield stress of the work piece material but does not give rise to necking. This is von Mises yield criterion of a two dimensional system.

$$\sigma_v = \sqrt{\sigma_\theta^2 + \sigma_z^2 - \sigma_\theta \sigma_z} \qquad \text{eq. 2.3.3}$$

This stress is true up until the elastic limit.

The axial force which is also induced and carries several component factors. If the work piece is long and has several bends (changes of direction) the frictional forces of tool and material begin to play their part. Friction has been shown to be a function of length and

component bends. This leads to a reduction in the useful work done by the axial force. We can therefore say that the axial force is

$F_a = F_u + F_d + F_r$ eq. 2.3.4

F_u force on axial ram maintaing plastic flow of material along with internal pressure

F_d sealing force required to maintain internal pressure

$F_d = P_i A_i$ eq. 2.3.5

Where A_i = area of punch face

F_r = friction between tube and tooling which must be overcome by a force

$F_r = \mu \sigma_n A_r$ eq. 2.3.6

Where σ_n = stress in action area

A_r = area in contact with tool face

μ = Co efficient of friction

2.3.6 Present Applications

Marando [2.3.3] summed up the situation regarding the application of tubular hydroforming in industry when he made analogies to the PC boom in the early nineties and that of the rapid increase in the development of hydroforming. 'The killer application that allowed tubular hydroforming to become truly successful was the automotive chassis, automotive chassis engineers embraced tubular hydroforming because it allowed them to make their designs more effective.' However, success in a manufacturing field is never measured by passed deeds, and with this in mind, tubular hydroforming is making gains into the area of the vehicle space frame. Already this area has seen research carried

out on several fronts ULSAB, ULSAB 40, ULSAB AVC, Volvo, GM (most noticeably '97 corvette) and Audi to mention but a few [2.3.4 - 2.3.10]. Other applications are the steering and suspension system, also engine, and drive line (see table. 2.3.1).

Bollinger and Jutten [2.3.11] highlighted the differing sizes and properties of the components presently in production (see fig. 2.3.3).

Body application	Tube Diameter = 20 – 140 mm	thickness = 0.5 – 2 mm
Sub frame	Tube Diameter = 80 – 130 mm	thickness = 1.5 – 3.5 mm
Suspension parts	Tube Diameter = 25 – 80 mm	thickness = 1.2 – 4 mm
Exhaust parts	Tube Diameter = 30 – 60 mm	thickness = 1 – 3.5 mm

From the listed parts shown above it can be seen that the D/t (Tube diameter/ thickness) ratio on average of parts required for suspension is 20, where for body parts it is around 65.

The range of steel materials used in hydroforming is also growing. However, a major obstacle is that of the inherited mechanical properties of the tube after being formed from sheet. With steels such as dual phase of a yield strength of > 600Mpa it is important to understand the total amount of work carried out on the steel even before hydroforming has taken place.

As the understanding of hydroforming and pre processing effects increases, then so will the range of steel being brought into service.

2.3.7 Tailored Tube Blanks

The concept of tailored tube blanks has been the natural combination of two of the most researched and written subjects about today's automotive structure, that of tailor welded blanks and tubular hydroforming. By prefabricating tubes with differing material properties and thickness it would be possible not only to reap the same benefits as those found with tailored blanks, but also push forward the types of hydroformed component being able to be produced. There are many occasions were it has not been possible for a

part to be hydroformed as the expansion rate in one area of the design is just to great. This could be addressed by increasing the o/d of the tube in this area thus not warranting a large expansion on the tubes behalf. Tubes could have axes in parallel, concentric or even eccentric planes.

The Department of Forming and Cutting Techniques of the Institute for Manufacturing Technology and Quality Management (IFQ) University Magdeburg [2.3.12] have carried out simple experiments on tailored tubes. These tubes have been laser welded in the circumferential direction and then in a separate batch in the longitudinal direction. The material tested was X6CrTi12 in two differing thickness of 1mm and 1.5mm.

A series of forming test were carried out, where the internal pressure was differed in each experiment. A variation of widths from the centre segments being 1.5mm thick, and a 1mm material at either side, the results are not unlike those of tailored sheet blanks.

The findings were as follows:

1. Welded seams should be positioned in areas of low expansion
2. Material properties and thickness of the highest strength material govern the forming process pressure
3. Springback begins to become an issue in high strength materials
4. The amount of axial feed and load is governed by the lowest strength material

These results are not groundbreaking observations. However concerns must be raised as to the lack of detailed experimental data available to substantiate these results.

GM [2.3.13] have patented several ideas regarding tailor welded tubes. However, it would appear that these are not specific enough to hinder research and development in this field.

Investigations were also carried out by Darlington [2.3.14] on the formability of HR and stainless steel tube during the course of an Engineering Doctorate, the component was a three-piece tailor welded tube (TWT) manufactured using a rotary manipulator in conjunction with the 5kW $C0_2$ Laser Ecosse laser welding facility at the CTC. Initial results were promising regarding the ability to produce and hydroform the component,

but further work was needed to push forward the conceptual ideas. See fig 2.3.4 for component design.

2.3.8 Steel Tube Manufacture

Tube manufacturing is a process of two extremes. This dictates the requirements of the raw material and the final qualities of the finished product [2.3.15]. In the welded tube manufacture not only is the material either hot or cold rolled, but also material cleanliness composition and homogeneity play their part in the finished product's ability to be made and the resultant quality [2.3.16].

Customer requirements such as corrosion resistance, ability to withstand internal or external pressure, heat transfer, resistance to creep and cold embrittlement, along with good surface finish, dimensional accuracy, formability and the ability to be further fabricated, gives direction to the manufacturer on the most appropriate process, material and finishing to be undertaken [2.3.7].

2.3.9 Tube Manufacture Suitable For Automotive Tube Hydroforming

Hydroforming is a process in which forming of a work piece is carried out by the transfer of force, created by fluid under pressure, onto the work piece to form it around a fixed tool geometry. The material will begin to thin as the pressure forces it into the vacant tool cavity. This thinning may be offset by introducing an axial displacement of the material towards the cavity; this would force more material into the area and thus reduce the amount of material thinning taking place. Consistant wall thickness is therefore necessary for a stable production process.

Seamless tube does not akin to this as the finished materials wall thickness is of low tolerance in comparison to welded tube. BIW parts have a high D/t ratio, and also require good surface finish of parts visible in the final product. Two processes lend themselves readily to this, they are Welded tube (most notably ERW) and also Corus Tailored Blanks. Although ERW tube is readily available off the shelf, it has limitations with

regard to the D/t ratio range which is likely to reduce its applicability to hydroforming application.

Corus Tailored Blanks are less cost effective than ERW tube. However, as the trend of the automotive producer begins to cater for the individual, the need for production flexibility increases. An area where both hydroforming and Corus Tailored Blanks can make an impact.

2.3.10 ERW Tube (Electric Resistance Welded)

ERW tube (Continuous Upset welding) process utilises both heat and deformation to form a weld. The heat source originates through the resistance of the material to the flow of electrical current at the edge interface. Deformation occurs because of the force generated to squeeze the edges together to form the enclosed tube, and also because of the resultant material softening is caused by material heating. The process begins by feeding a coil strip into a set of forming rolls, then resistance heating the edges with wheel electrodes, and applying a force to upset the edges together, see fig. 2.3.5. This results in a solid state weld (no melting at joint is evident as all molten metal has been pushed out during deformation), resulting in a strong metallurgical bond.

There are a few key variables in the process, they are :

- Force required to bring the two edges together
- Current/Voltage required for heating
- Motion of weld head during welding

ERW tube, is capable of being produced to D/t ratio of up to 65. The finished tube surface quality is similar to that of sheet material suitable for pressing. With a tighter wall thickness tolerance band to that of seamless, a more reliable process window is possible. However, a major short fall in ERW tube, is that the D/t ratios possible only satisfy part of the total tube requirement in the automotive industry. The hydroformed tube components being used in the automotive vehicle is tending towards D/t ratios over 80 (see fig 2.3.3).This was evident in the HIBS project undertaken by British Steel and

Rover Group, of the nine components to be manufactured by hydroforming only four could be manufactured using standard ERW production methods. Two other components although manufactured on a ERW mill, and having a D/t ratio of approximately 80, had to have subsequent heat treatment to enable manufacture. The remaining components were produced using the Corus Tailored Blank Method [2.3.15]

2.3.11 Corus Tailored Blanks

The Corus Tailored Blank machine was developed by Soudronic Manufacturing, with initial conceptual ideas coming from the research and development centre at the then Hoogovens Strip Steel in Ijmuiden, Holland. Its purpose was to answer the call of researchers and manufacturers who foresaw the possibilities of combining tailor blank technology with that of hydroforming [2.3.17].

The basic principle of the machine is to receive a flat sheet blank, which is then pressed using a circular punch and die profile used in conjunction with a hydraulic press. The open formed tubular shape is then finally laser welded to form a closed section (see fig 2.3.6). Pressing of the sheet is done in an uneven number of steps, with the sheet extremities pressed first and the unformed sheet progressively pressed towards the centre of the blank until the final pressing is carried out in the centre of the blank. The number of pressings required for the blank is dependant on the degree of formability of the blank and also the amount of forming pressure required to form the blank.

The resultant weld is not identical to that of a laser weld, as some degree of upsetting takes place. This level of upsetting varies with differing kinds of thickness and material strength (hence springback). As the open formed tube approaches the laser it will pass between two sizing rollers to ensure correct dimensional tolerances. The process makes use of Soudronic Souvis 1,2 and 3 [2.7.17] (as described over leaf) to ensure the process parameters are correct.

2.3.12 Corus Tailored Blank capabilities

Presently the machine has only been tested on several geometries and materials, as listed below.

Tube Dimensions

Diameter	60 – 250 mm
Thickness	0.6 – 2.75 mm
Length	900 – 4750 mm

Material

Steel (IF, mild steel)

Welding speed

8 – 12 m/mm

Souvis 1 enables high quality welding by detecting and monitoring edge and laser focus position. Additional to this is the ability to detect the incoming edge position and thus allowing the process to compensate. Protocol for the process is measured in the following manner.

- Lateral edge position
- Width of remaining gap
- Mismatch
- Large edge defects
- Blank position (height)

Souvis 2 is a method of checking quality of the seam profile, on upper and lower seam. Integrated into this is a direct feed back loop recording and adjusting welding parameters, by means of investigating the following.

- Seam Concavity
- Seam Convexity
- Mismatch
- Bead width
- Lack of penetration
- Lateral bead position

Souvis 3 is a method of continuously checking for seam perfections using the following criteria.

- Seam discontinuities
- Seam imperfections
- Seam holes / pores

All of the Souvis systems have ISO accreditation, as accuracy is directly related to ISO 13919 – 1 quality B criterion.

2.3.13 Competitive alternatives to Corus Tubular Blanks

Thyssen-Krupp Stahl presented their capability to produce prototype tube blanks at their Application Technology Centre [2.3.13], using a similar process to the Soudronic process. The Thyssen-Krupp facility was claimed to have the capability of producing tubes of 3m in length, with diameters in the range of 60-160mm and wall thickness values in the range of 0.6-2.5mm, thereby meeting most potential hydroforming B-I-W requirements [2.3.18].

To achieve higher output and further cost savings, Voest-Alpine Industrieanlagenbau (VAI) have developed the CTA (Cost Saving, Time reducing, Availability increasing) technology for welded tube production [2.3.13]. The CTA tube production lines utilise the computer-controlled, motorized adjustment of the roll-forming tools [2.3.19]. CTA technology allows production of a wide range of tube and pipe diameters using the same

production tooling. Additionally, the standard CTA tube mill facilitates production of much higher D/t ratio tubes, having outside diameters of 127mm with a wall thickness of 1.5mm [2.3.19].

2.3.14 References

2.3.1. M.E.Limb et al, 'Hydraulic Forming of Tubes and Feasible Working Region', International Congress on Material Eng., Sheet Forming 15th-16th September 1981, University of Aston in Birmingham

2.3.2. Dr.-Ing.C.H.Hartl, 'Theoretical Fundamentals of Hydroforming', Siempel Kamp Pressen Systeme GmbH&Co, Krefeld, International Conference on Hydroforming, Fellebach/Stuttgart – Germany, Oct. 12th-13th 1999, ISBN 3-88355-285-2

2.3.3. R.A.Marando, 'Tubular Hydroforming: The Enabling Technology', Dana Corp. Parish Division, Reading PA, USA, International Conference on Hydroforming, Fellebach/Stuttgart – Germany, Oct. 12th-13th 1999, ISBN 3-88355-285-2

2.3.4. E.F.Walker C.Eng.FIM, M.W.Boyles C.Eng. MIM, K.Lowe C.Eng.,MIM, British Steel Strip Products, 'ULSAB (Ultra Light Steel Auto Body)', Materials for Lean Weight Vehicles Conference, November 24-25, 1997

2.3.5. R.Koehr, Porsche Engineering Services, 'ULSAB Project Overview and Results', JSEA Materials Forum, May 20th, 1998, pg 10-21

2.3.6. ULSAB Project' lib no 9835212

2.3.7. ULSAB Electronic Report 1.0 CD-ROM

2.3.8. ULSAB 40 Project Report AEG 1075/1 CD-ROM

2.3.9. P.Wells, M.Rawlinson, Centre for Automotive Industry Research, 'ULSAB – A Critical Appraisal, IBEC'97, Advanced Body Concept and Development, pg 89-95

2.3.10. C.J.Buggeman PhD, 'Hydroforming of Structure Parts For Personal Cars', GM Body Structure Centre, Warren MI, USA, International Conference on Hydroforming, Fellebach/Stuttgart – Germany, Oct. 12th-13th 1999, ISBN 3-88355-285-2

2.3.11. E.Bollinger et al, 'Tubes for Hydroforming', Usinor Tubes, Montataire, France, International Conference on Hydroforming, Fellebach/Stuttgart – Germany, Oct. 12th-13th 1999, ISBN 3-88355-285-2

2.3.12. Dr.Ing.A.Eichorn, 'Innovative Developments Concerning Hydroforming of Tubes', The Department of Forming and Cutting Techniques of the Institute for Manufacturing Technology and Quality Management (IFQ) University Magdeburg, International Conference on Hydroforming, Fellebach/Stuttgart – Germany, Oct. 12th-13th 1999, ISBN 3-88355-285-2

2.3.13. Gerlach, J., Kneiphoff, U., and Wonneberger, I., 'Thin-Walled Tailored Tubes for Body Structures – Production, Testing and Application', ERC / NSM International Conference and Exhibits on Tube and Sheet Hydroforming Technology, Manufacturing of Lightweight components. Detroit, MI, USA, June 2000.

2.3.14. Darlington R. 'Tube Hydroforming of Steel for Automotive Applications' Doctorate Thesis 2002, University of Wales Swansea.

2.3.15. Corus Tube sales literature

2.3.16. M.W.Boyles C.Eng MIM, British Steel Products, G.M. Davies, Rover Group, Through Process Chacterisation of Steel For Hydroforming Body Structure Components, IBEC, 01/1999

2.3.17. Soudronic sales literature

2.3.18. Anon, 'VAI Tube and Pipe Mill Technology Receives an Order for a Tube Welding Line in Russia', VAI press release, Linz, March 23rd 2001.

2.3.19. Anon, VOEST-ALPINE Industrieanlangenbau GmbH & co Homepage : www.vai.at

2.3.15 Figures / Tables

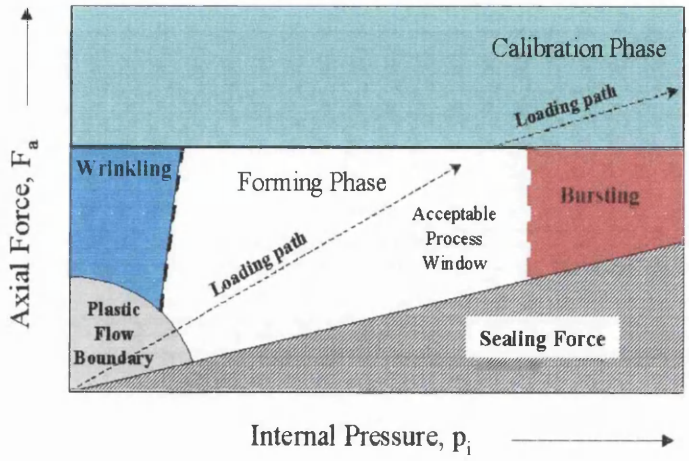

Figure 2.3.1: Feasible working region graph

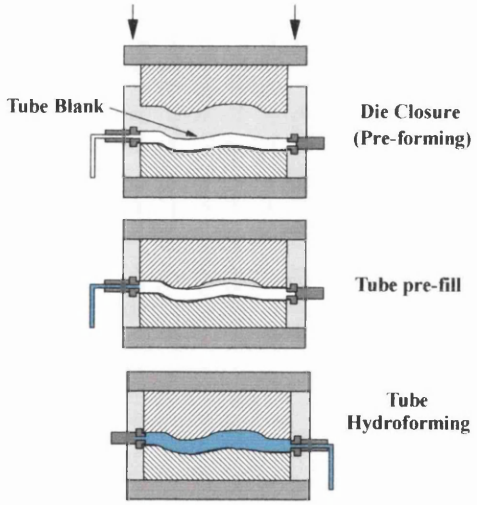

Figure 2.3.2: Schematic of tubular hydroforming process

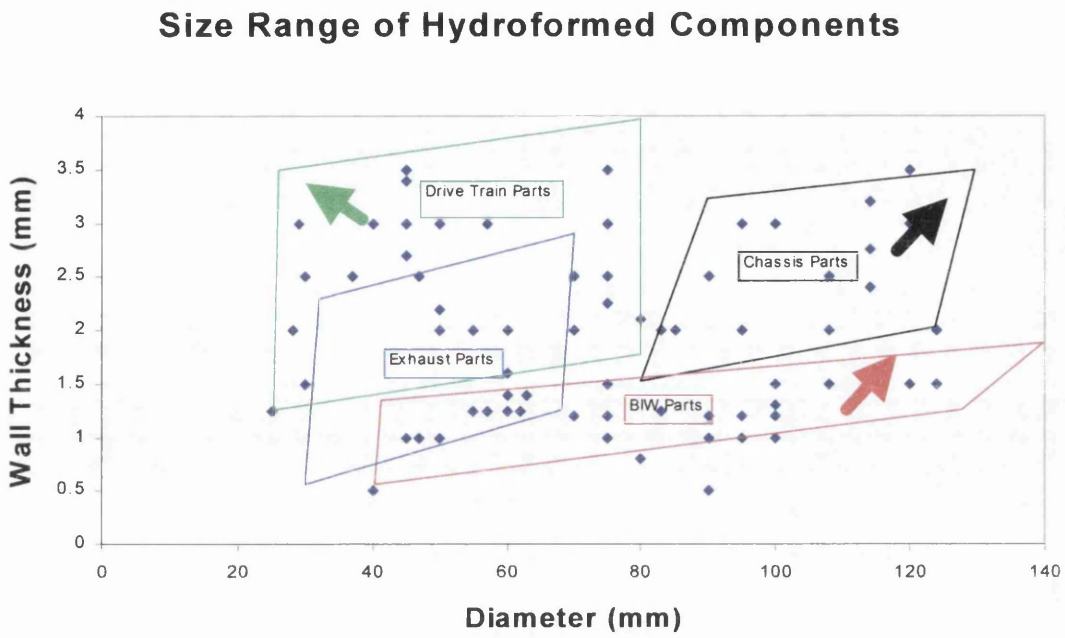

Figure 2.3.3: Tubular hydroformed components presently in production

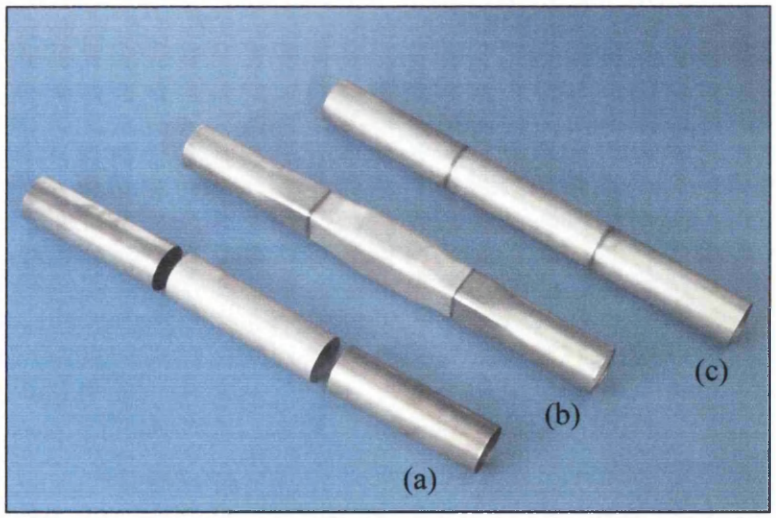

Photograph of FeP04 (70x1.5mm) : SS 304 (70x1.5mm) : FeP04 (70x1.2mm) Tailored Welded Tube (TWT) (a) sub-assembly, (b) Hydroformed TWT (c) TWT

*Figure 2.3.4:*TWT used in Darlington Engineering Doctorate investigation

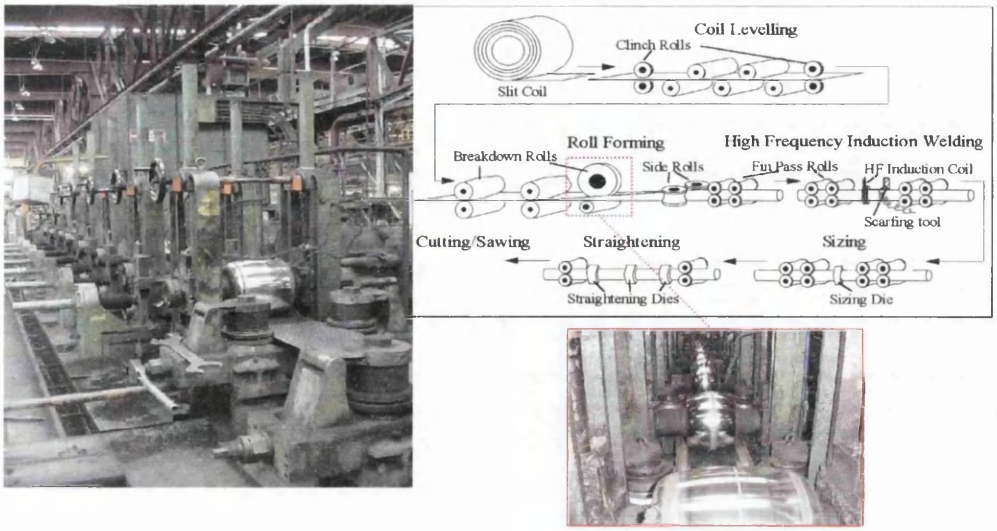

Figure 2.3.5: ERW tube manufacturing schematic

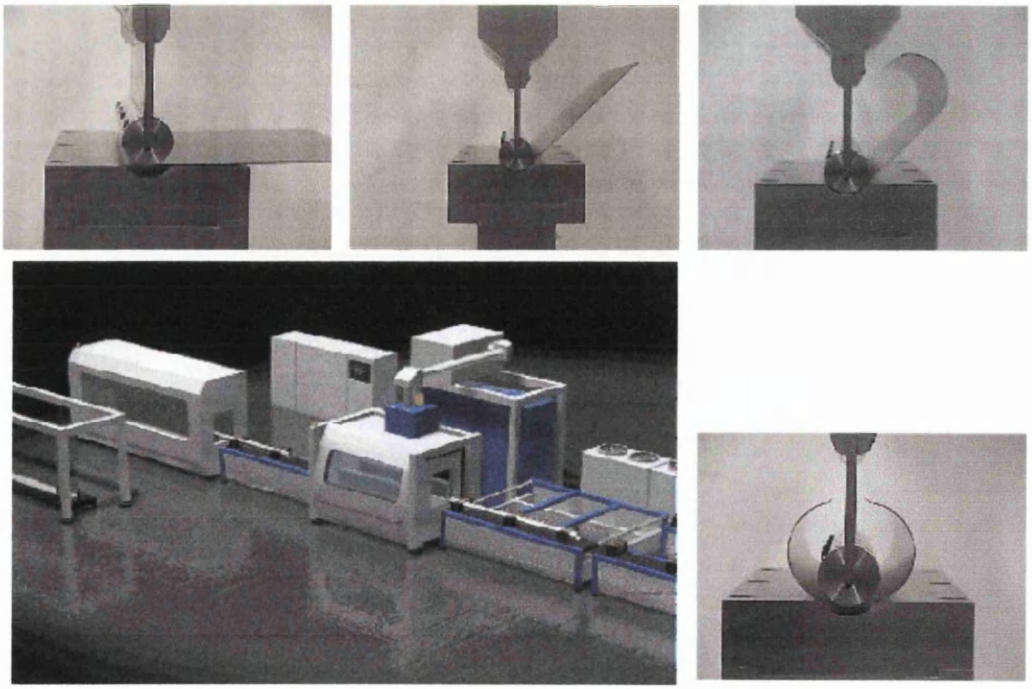

Figure 2.3.6: Corus Tubular Blank manufacturing route

Body Systems	**Chassis Systems/Sub frame**	**Steering and Suspension**	**Engine and Drive line**
Instrument Panel Beams	Front Engine Cradle	Control Arms	Exhaust Manifolds
Radiator Enclosures	Rear Cradle	Trailing Links	Cam Shaft
Seat Frames	Ladder Frames	Steering Columns	Driven Axle Housing
Side Roof Rails	Hitch Bars		
Roof Bows	Bumper Beams		
Body Side Rails			
Roll Over Bars			

Table 2.3.1: Automotive tubular hydrofomed components

2.4 Bending

Bending is one of the most common metalworking operations. Parts are made either by simple bending of sheet metal, or can be manufactured as a component through a combination of more complex sheet metal forming operations. Bending is the plastic deformation of metals about a linear axis called the bending axis with little or no change in the surface area. When multiple bends are made simultaneously using a punch and die, the process is sometimes called forming. What distinguishes bending from generalised forming is that the bend axis is linear and independent. Independence means that bending about one axis has no effect on the bending about the other axis. If the axes of deformation are not linear or are not independent, the process becomes drawing and/or stretching, not bending.

2.4.1 Deformation in the bending process

The tooling used in bending operations results in the sheet metal being deformed in the areas of contact between punch and die. The localized stresses occur only in the bend radius. The remaining unformed part of the blank is not stressed during bending. The stresses acting in bending are illustrated in fig. 2.4.1. The metal on the outside of the bend radius is elongated; where the metal on the inside is compressed. In small bend radii it is common for fracturing to occur at the outside bend surface.

Any wrinkling will occur on the inside surface of the bend. This wrinkling also has to be taken into account when designing parts and processes, but is usually less of a concern than is outside bend fracture.

During bending the blank is held stationary by the punch and die. This region of the blank is bent, and the unformed areas move up or down to create the change in contour. This free metal movement is often called swinging and is a characteristic common only to bending operations. In design of a bending die, the swinging action must be accommodated.

2.4.2 Shifting of the neutral axis

During bending the outer surface of the sheet metal is increased in length and the inside surface of the sheet metal is decreased in length. Because the sheet metal is stressed in tension on one surface and in compression on the other, a reversal of stresses must occur somewhere in the sheet. This position or line is of zero stress, and is called the neutral axis. There is no change of length along the neutral axis, which is a zone where the stress is nil. This fundamental idea is used to define strain in bending. See fig. 2.4.1.
The neutral axis length is used in many bending calculations. However, in cases of large deformation (small bend radius) the stress becomes asymmetric about the geometric centre of the blank thickness, and so the location of the zero stress point or the neutral axis location shifts. When the blank is first being bent, the neutral axis is near the centre of the sheet thickness. As bending progresses, the neutral axis shifts towards the inside, or compression side, of the bend.

2.4.3 Strain in bending

Predicting the bending strain is important in bending process design and operation. Successful bending processes require producing plastic strain so that the workpiece is permanently deformed, strain to be less than the materials failure strain (usually fracture on outer surface, but inside radius wrinkling may be of concern). The amount of springback is dependent on the strain imposed.
The amount of deformation imposed in bending varies across the blank thickness. For a given blank thickness, t, the strain is expected to vary with bend radius ρ. For a given ρ it is anticipated that the strain is larger with larger workpiece thickness.
The strain on the outer surface of the bend is given by

$\varepsilon = t/2\rho$ eqn. 2.4.1

2.4.4 Description of stress/strain in bent sheet

Fig. 2.4.1 shows the stresses acting through the thickness of the sheet as it is being bent. The largest tensile stress occurs in the outside surface region of the sheet. The tensile stress decreases toward the center of the sheet thickness and becomes zero at the neutral axis. Compressive stress increases from the neutral axis toward the inside of the bend. The maximum stress should be less than the tensile strength of the material to avoid localization of deformation and fracture.

Even with large plastic deformation in bending, the center region of the sheet remains elastic and so on unloading elastic recovery occurs. When the sheet is released from the punch and die, the elastically deformed section tries to return to its original flat condition. The plastic zones prevent full recovery but elastic recovery does occur. This movement of the part is known as springback. There is also some elastic recovery in the plastically deformed material.

2.4.5 Compensation

Springback must be compensated for in bending operations, otherwise the operation will yield parts of undesired dimensions and shape. Several methods are used to overcome or counteract the effects of springback:

2.4.5a Overbending

Overbending is a method to compensate for springback. In situations of small bend radii, a 2% addition to the angle of the bend is sufficient allowance for springback in steel parts [2.4.1]. Care must be exercised in applying this allowance, as a thin sheet steel tends to springback more than thicker sheet steel. Bending process models including such effects are complex, and there are so many specific cases that generally useful results are not available from these very specific cases. Knowledge and experience gained through

trial and error seem to be the best guides for estimating needed overbends and thus resulting in a black art mentality to this type of compensation.

2.4.5b Bottoming or setting

Large, short-time loading or impact type loading applied at the bottom of the bend produces high compressive stresses that set or hold the bend. A problem with this form of handling springback is that the deformation is not well controlled when using a press break type of press. Secondly, the effect on the post formed material characteristics is unclear [2.4.1].

2.4.5c Stretch bending

Stretch bending is a method of springback control which introduces additional plastic deformation into the blank. The addition of plastic deformation is usually undertaken when a small strain is to be produced in the formed sheet.
In stretch bending the sheet is first stretched so that the blank is stressed past the yield strength. The sheet is then forced over the punch to obtain the desired contour.
This pre stressing before bending results in reduced springback. Only relatively large radii are bent by this method, since the imposition of a small strain is a problem and because the stress added in bending to sharp radii would take the pre stressed metal beyond its tensile strength. This type of bending is common in the aircraft industry for producing outer body panels, having very large radii [2.4.2].

2.4.6 Forming stage pure bending analogy

The theory of pure-moment bending of sheet using linear-elastic laws, has been the subject of many theoretical investigations [2.4.1]. A multitude of textbooks have been written with regard to this subject[2.4.1-2]. The application of plasticity theory to sheet bending is often simplified, so that solutions can be obtained. The tubular blank process

in itself can be looked upon as a pure bending process, which is ideally suited to a material model reflecting elastic perfectly plastic behaviour.

2.4.7 Review of elastic bending mathematical modelling [2.4.1]

It is often the case that when mathematical models are postulated, they do not represent bending completely. This reflects on the complexity, and number of variables that are present for any given bend.

Therefore, the models that are presented contain assumptions that are logical, and more importantly, simplify the overall model.

In pure bending calculations, the assumptions are as follows

Assumptions

1. The uniformly thick and uniformly wide sheet is bent by a pure moment; the bending line is therefore a circular arc.
2. The sheet is infinitely wide in relation to its thickness, so that edge deformations do not occur and a plane state of strain exists (no deformation normal to the bending plane).
3. The work material is homogeneous and isotropic; there are no residual stresses prior to bending.
4. Plane sections normal to the sheet surface and parallel to the bend axis remain plane.
5. The sheet consists of many thin layers independent of one another. Existing compressive stresses perpendicular to the sheet surface, which are necessary for the creation of curvature, are neglected. Stresses parallel to the bend axis are neglected as well
6. The stress-strain curves of the work piece in the tensile and compressive regions are symmetric with respect to the origin.
7. Sheet thickness remains constant during the bending process. This follows from volume consistency when assumptions 1-6 are satisfied.

These assumptions were the result of Ludwik's work on the study of sheet bending, which helped to simplify the analysis of strains and stresses

2.4.8 Material model

In bending calculations σ is a function of ε. The function, is dictated by the magnitude of strain, and the type of material behaviour under consideration.
Material models will usually fall into one of four types, see fig. 2.4.2.

2.4.8a Rigid, perfectly plastic

This model is used when the type of bending is severe; the elastic section may be neglected and a rigid proportion substituted into its place.

2.4.8b Elastic, perfectly plastic

Improved representation of the behaviour of real materials, in that it exhibits elastic behaviour prior to yielding. Once yielding has occurred it is assumed that the plastic part of the curve is constant.

2.4.8c Elastic, linear hardening

Improved representation of the behaviour of real materials, in that it exhibits elastic behaviour prior to yielding. Once yielding has occurred it is assumed that the plastic part is a function of a constant, which reflects a linear hardening law.

2.4.8d Non linear hardening

With larger bending strains, strain hardening may need to be accommodated. This is done by use of Ludwick's empirical law.

$\sigma_1 = k\varepsilon^n$ eqn. 2.4.2

2.4.9 Tubular blank bend modelling

Consider the bending operation of the Tubular Blank process. It is possible to say with a significant amount of confidence that the most representative model is that of an elastic, perfectly plastic type. There are several indicators to this statement, as follows:

- The Tubular Blank is capable of a finite range of manufactured tube configurations. Therefore the range of strain induced by bending without coining is also finite. The maximum level of strain induced in a tubular blank would be under conditions of smallest radius and maximum thickness. See fig. 2.4.3 for a graphical representation of manufactured tube configuration capable of production on Corus Tubular Blank.

Strain being

$$\varepsilon = t/2\rho \quad = 0.75/50 \quad = 0.015 \qquad \text{eqn. 2.4.3}$$

t is sheet thickness

ρ is bend radius neutral axis

from which it can be seen that the maximum level of strain is 1.5%. This would indicate that low levels of strain are produced in the most extreme forming conditions in the tubular blank capability. Material law's best reflecting this bending operation are those that include the elastic proportion of the stress strain curve, and one's in which little or no importance is given to the strain hardening of a material.

- As mentioned previously the Tubular Blank process is only an intermediate step in the final product. It is therefore the aim to produce a product which transfers as much of the original sheet properties to the tube product. This indicates that high

strain bends are not in line with the Tubular Blank manufacturing ideology. This would indicate that a material law, which enables the calculation of high levels of strain, is not necessarily wrong but model simplification would be constrained as the effect of the elastic proportion is reduced.

Taking account of the above points a mathematical model can be chosen for the prediction of springback.

2.4.10 Elastic, perfectly plastic bending [2.4.3]

As previously described, this material model obey's a linear law up until the point of yield. Subsequent deformation will yield a condition where strain hardening has no effect. This allows the behaviour of the material to be analysed in two differing regimes, elastic and plastic. It is this differentiation that makes possible the ability to predict the level of likely elastic recovery of a material.

Fig. 2.4.5 depicts the bending moment versus the inverse bend radius for a typical bend. It can be seen that in the initial stages of the curve i.e. from origin to yield point position (position 2), the moment remains linear (no plastic deformation). After this the linearity is lost as plastic deformation is induced into the sheet. Point 4 depicts the point of full plastic deformation. When analytical models are created to depict this behaviour a simplification of the curve occurs. The elastic region as shown by the prefix Me and the plastic region is given the prefix Mp. This results in the exclusion of the curve from positions 2-4. A graphical representation of the stress distribution through the thickness of the sheet during bending can be seen in fig. 2.4.5 also.

2.4.11 Residual stress/springback in an elastic, perfectly plastic sheet [2.4.3-4]

During a bending operation, which introduces a proportion of plasticity into a sheet being bent, on removal of the bending force a degree of elastic recovery will occur, this is known as springback, see fig. 2.4.4b.The analogy of this can be seen in fig 2.4.6. This

elastic change, which is negative, can be written in terms of a change in curvature, this can be seen in fig 2.4.6.

This change in curvature can be related to the differential between the elastic and plastic moments Me and Mp, see fig 2.4.7. It is possible to see that the springback of the sheet is a ratio of elastic to plastic deformation. This ratio is often known by the springback K value, and can be written as:

$$K = {}^{\alpha_r}\!/_{\alpha} = {}^{\rho}\!/_{\rho+\Delta\rho} = 1-3({}^{\rho}\!/_{t})({}^{S}\!/_{E_1}) \qquad \text{eqn. 2.4.4}$$

where:

K = springback value

α_r = bend angle after springback

α = bend angle during forming

ρ = neutral axis bend radius

$\rho + \Delta\rho$ = neutral axis bend radius after springback

t = material thickness

S = plane strain yield stress

E_1 = modified Young's modulus

2.4.12 Predictive Springback Models

Current predictive models all retain the assumptions laid down by Ludwik for pure moment sheet bending. The following are condensed reviews of published papers dealing with mathematical models for the prediction of springback.

Leu [2.4.5].dealt with incorporating normal anisotropic value R, and the strain hardening exponent n, to develop a model capable of predicting springback. Bending resistance and maximum bending moment in pure bending were also investigated.

The main emphasis of the model postulated was a reflection on the work that Hill carried out on the theory of plasticity, and the effects of anisotropy on material performance. Comparisons were made between calculated values, using the model developed, with previously published experimental results. The agreement between the two sets of results was good; the maximum error was 0.66° on a pressed angle of 90°, with a measured springback of 4.00° and calculated value of 3.34°.
The conclusions drawn were that a greater r-value would result in reduced bending resistance. An increase in r-value would result in a greater springback ratio, but the reverse occurs when considering the strain hardening n-values or sheet thickness.

Zhang et al [2.4.6] investigated springback using three differing methods of material and solid mechanic laws. Comparisons were made against one another in this study, Hill's formula for pure bending, shell theory for both bending and stretching, and membrane theory were the three differing laws used.
It was found that both the membrane and shell theory models were not suitable for the prediction of stress and strain distributions through the thickness, except for bending of very small curvatures. Results from the postulated models showed that tangential strain increases as the original middle surface curvature increases. It was also shown that as the bend radius increased so the tangential stress through the sheet mid surface would be at a stress of zero.
Material data for the models were supplied but no comparisons were made to actual experimental results. Allowances were also made for a modified Young's Modulus to compensate for the relationship of plane strain and plane stress in the elastic region, but this did not transfer through to the final predictive formula.
This paper does appear to have an error within one of its principle equations, namely that of the bending moment in Hills pure bending model for non-hardening materials. It is quoted as

$$M = \sigma_y \big/ 2\, t_0^2$$

when in fact it is

$$M = \sigma_y \big/ 4\, t_0^2$$

As with the majority of papers Vegter [2.4.7] has followed the assumptions laid down by Hill in his theory of plasticity. The material model used is one of elastic perfectly plastic. The range of material yield strength was from 180-460 N/mm^2. Sheet steel was bent in a three point bending rig (whose punch radius was 15mm) into 30^o angles while punch force was still being applied. Correlation between predicted results and those gained through experimentation were satisfactory. The greatest inaccuracy being 49%(stray point?), the least, which also reflects the majority of the results being 4%.

A factor, which has been neglected by Vegter when postulating the Elastic Moment, is that of a modified Young's Modulus. This factor was not ignored in the Plastic Moment calculations.

2.4.13 References

2.4.1Prof Lange, K, Handbook of Metal Forming McGrall-Hill, Inc, 1985. ISBN 0-87263-457-4, pg19.7

2.4.2Z.Marciniak & J.L. Duncan, Mechanics of Sheet Metal Forming, 1992, ISBN 0-340-56405-9, Pg 69-79

2.4.3http://www.menet.umn.edu/~klamecki/Forming/bending.html

2.4.4G. E. Dieter, Mechanical Metallurgy, McGrall-Hill, Inc, 1988. ISBN 0-07-100406-8, pg19.7

2.4.5Leu,Daw-Kwie, 'A simplified approach for evaluating bendability and springback in plastic bending of anisotropic sheet metals',Journal of Materials Processing Technology 66,1997/9/7

2.4.6Z.T.Zhang & S.J.Hu, 'Mathematical Modelling in Plane Strain Bending', Journal of Materials and Manufacturing, 106, 1997 Pg458-471

2.4.7H.Vegter,'A Model for the Prediction of Springback Under Pure Bending Forming Conditions with Validation Using Experimental Results', Internal Document from PAC Hoogovens, Ijmuiden, Holland, 16 July 1986 Arch. Lab. Nr. 58.455

2.4.14 Figures / Tables

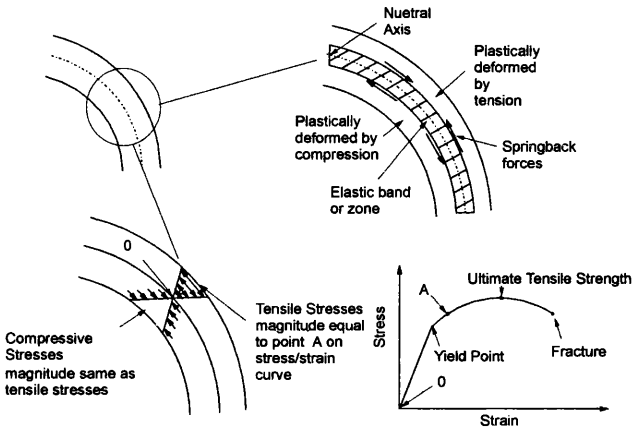

Figure 2.4.1: The stresses acting during bending

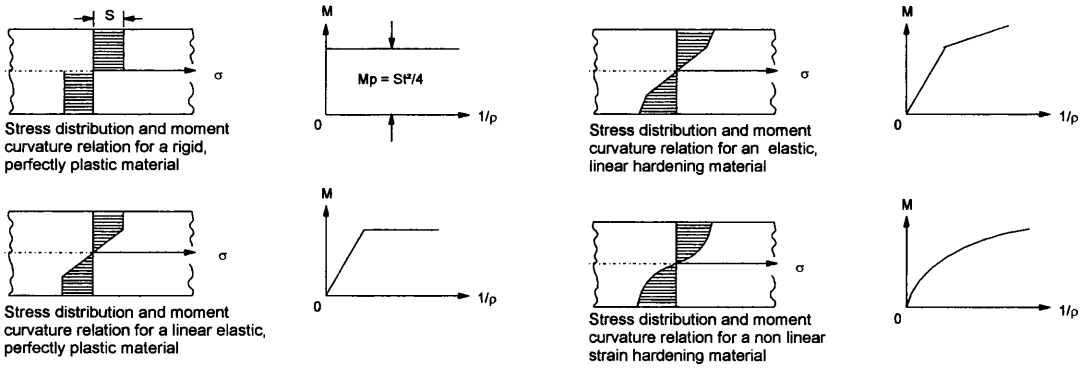

Figure 2.4.2: Material model types

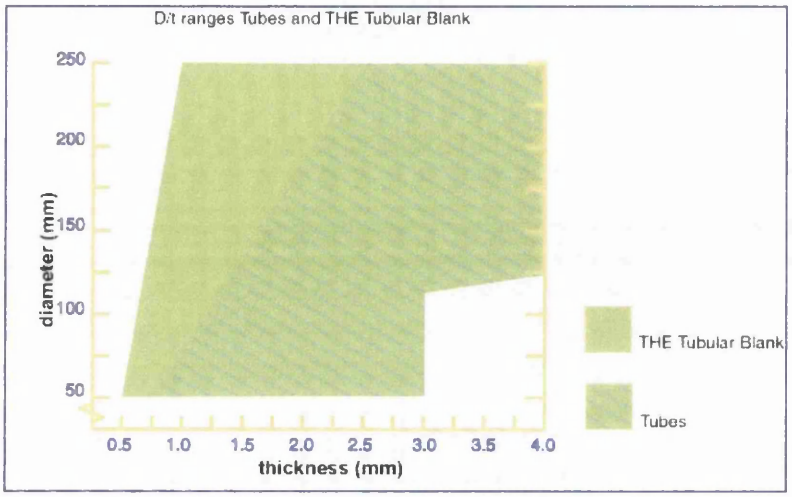

Figure 2.4.3: Manufactured tube configuration capablity of Corus Tubular Blank

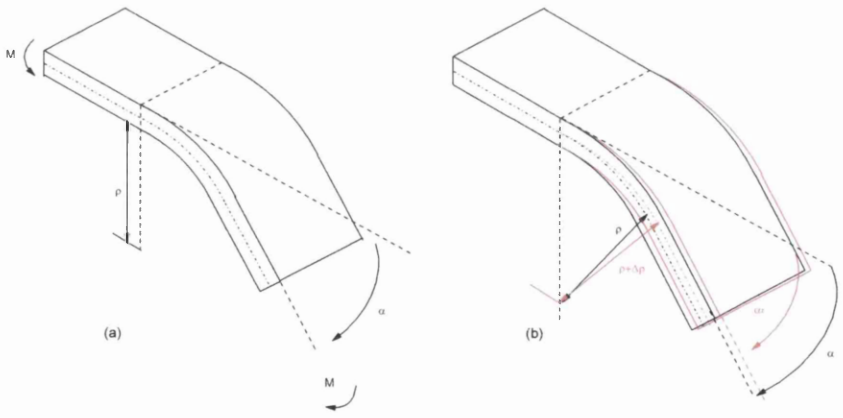

Figure 2.4.4: Beam in pure bending conditions with moments still applied (a), Beam in pure bending conditions with moments removed (b),

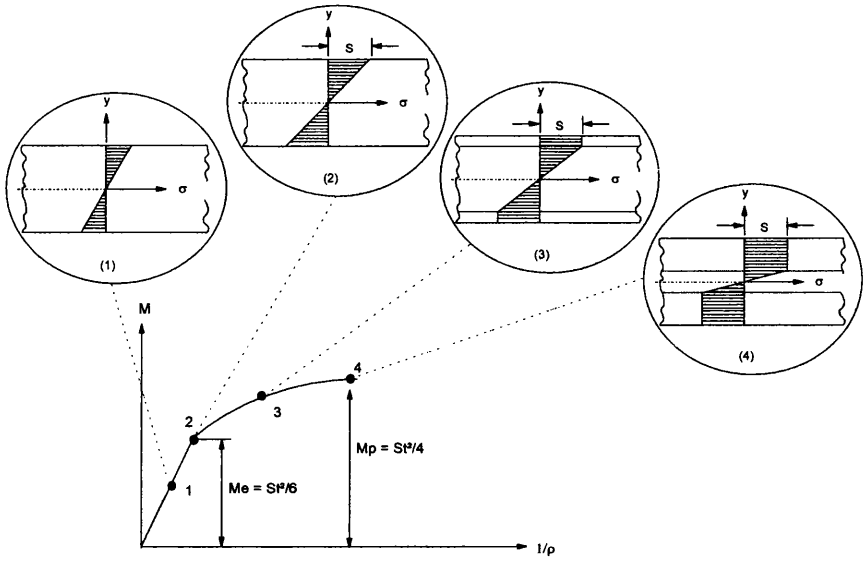

Figure 2.4.5: Stress distribution through thickness of sheet during bending assuming elastic, perfectly plastic material laws

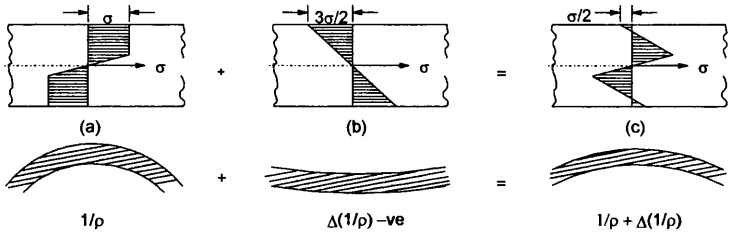

Figure 2.4.6: Analogy of springback in term of an elastic, perfectly plastic material

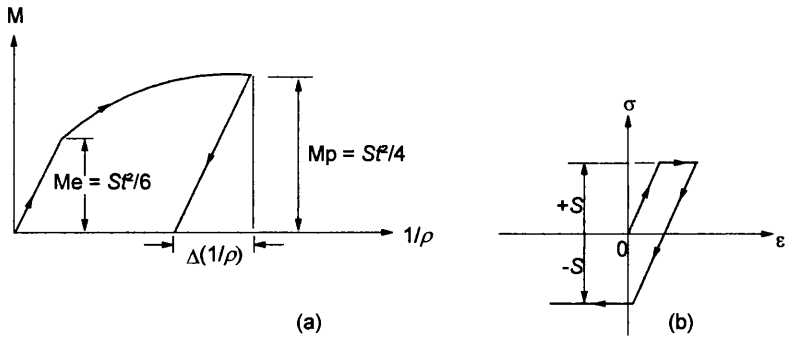

Figure 2.4.7: The strain relation (a) for elastic material and moment curvature relation (b) showing the unloading path

3.0 Definition of research project

The Engineering Doctorate Research project, in conjunction with 26 weeks of taught courses, was completed, and a thesis examination within 4 years of its start date, October 1999. The following sections, 3.1 and 3.2 outline the project descriptor and provide the base for the literature review and a guide to the project work undertaken.

3.1 General project objectives

The general project objective was to examine the behaviour of sheet steel during the forming process associated with the Corus Tubular Blank production facility. Within the scope of the project, a critical assessment of predictive springback models was carried out. The key influencing factors affecting springback are highlighted in the literature review and assessed as to their relative importance.
The effects of the forming process on the homogeneity of the finished tube with respect to mechanical properties was also carried out.
By carrying out such investigations it was possible to correctly identify tooling geometry for given sheet steel types and grades, and also indicate the likely formability of the finished tube.

3.2 Project Description

It is the aim of this project to understand the issues, particularly the process and material parameters affecting Corus Tubular Blanks manufacture.
A selection of sheet steels has been chosen that represent present, and future materials to be used in BIW construction. The pressing result of these steels, formed the base to which predictive springback models were measured against. A limited selection of these materials were used to investigate the effects of springback mitigation by means of increasing punch pressure during forming.
A refined selection of the original materials whose properties are at the two extremes of material mechanical behaviour were used as the constituent parts of the investigation into the effects of springback on tailored blanks.

4.0 Experimental methodology and programme

4.1 Methodology

4.1.1 Tensile mechanical properties

4.1.1a Standard tensile test

Mechanical properties were determined from a standard tensile test, in which an axial load was applied to produce an uniaxial deformation until failure of the specimen, in accordance with BS EN 10 002-1. The tests were carried out on accurately machined specimens of length 240mm and width 20mm, and results were calculated over a gauge length of 80mm, see fig. 4.1.1.

4.1.1b Mini tensile tests

To enable tensile characterisation of pressed blanks it was necessary to produce tensile coupons small enough for testing, as the pressing blanks were too small to enable a standard test specimen to be taken from the finished formed blank.
The tests were carried out on accurately machined specimens, of length 120mm and width 2mm. Results were calculated over a gauge length of 20mm, see fig. 4.1.2.

4.1.2 Chemical Characterisation

Chemical analysis of the base materials were carried out by technicians at the Central laboratory, Ijmuiden integrated plant, Holland. The samples were made up of 3cm x 3cm square samples and approximately 5g of nibblings for each.

4.1.3 Sheet Steel Microhardness

Hardness is defined as the ability of a material to resist indentation from a concentrated load applied by a specific indenter. Most commonly used methods of determining hardness are the Brinell, Rockwell and Vickers tests. These are all comparative type of tests, i.e. the results are expressed relative to other materials, and tables are also available so that conversion from one type of test result to another is possible. These tests can be used as indicators to material formability as an increase in material hardness will generally result in a low material formability.
During the course of this investigation, the Vickers method of hardness testing was carried out using a load of 200 grammes.

4.1.4 Springback measurement

Springback K value is calculated by eqn. 2.4.4 in section 2, measurement of variables was as follows:

4.1.4a Protractor Method

The sample press angle is measured firstly at the bottom of the pressing stroke, i.e. with force still applied. Secondly, after removal of pressing force, the sample was placed on an engineered flat and surface the press angle measured again. The springback value is then calculated from the two measurements shown in fig. 2.4.4. The accuracy of the protractor used is to within increments of 5' of a degree. In instances were it is not possible to align the flats of the protractor to the surfaces of the sample (sample has a slight curvature due to residual stresses remaining in the sample) a best fit line by eye is adopted.

4.1.4b 3D Profiler Method

This method of measurement is by means of a 3D profilometer situated in the PAC Ijmuiden Holland. This machine is a Mitutoyo 3D profiler accurate to 0.001mm.

Configured to this machine is pc-based software, which enables interrogation of the results see fig. 4.1.3. Utilisation of this software enables an accurate profiled picture of the pressed sample to be generated. It is also possible within this package to measure from data point to data point, thus enabling measurement of the pressed sample's projected inner circumference and radius. Comparisons between the sample radius and that of the punch tool enable a springback value to be calculated. Radii were tested in respect to the tube standard BS EN 10305-3:2002(E). This was done by fixing the 3D profilometer software package tolerance to a recognition level of 0.1mm deviation for circles and 0.5mm deviation for lines. In doing so the software is set below the tube standard for roundness. See fig. 4.1.4 for output file.

4.1.5 Sheet Thickness Measurement

4.1.5a Flat faced micrometer

The measurement of thickness both in the formed component and the parent material was carried out using a flat-faced micrometer accurate to 0.001mm. An average of three measurements was taken for each point.

4.1.5b Round faced micrometer

The measurement of thickness both in the formed component and the parent material was carried out using a rounded-faced micrometer accurate to 0.001mm. An average of three measurements was taken for each point.

4.1.5c Microscope

Thickness measurement by this means, was carried out on the formed and unformed material by technicians at the Central laboratory, Ijmuiden integrated plant, Holland. Formed and unformed specimens were cold mounted, and the substrate thickness of the sample was measured by means of calibrated measurement software attached to the microscope.

4.1.5d 3D profilometer

This type of thickness measurement was carried out so that a picture of profile in relation to the position of blank could be carried out. Software attached to the 3D profiler allowed traced measurements of the inner radius plus average sheet thickness (measured from unformed sample) then subtracted the outer traced profile. The difference is the change in profile due to forming plus errors.

Profile change + Error = (Inner radius + sheet thickness) – outer radius eqn 4. 1. 1

4.1.6 Forming

4.1.6a Sample preparation

Unless stated, all material samples for MTS bend testing were cut to a standard specimen size of 312 mm L x 125 mm W. Prior to pressing, samples were degreased using an ethanol solution, and then wiped clean using lint free cloth, eliminating the interaction of lubrication. Pressing orientation labelling was carried out as shown in fig. 4.1.5.

4.1.6b MTS press machine

The test machine used during forming experimentation of large radius tooling (prototype tooling for Corus tubular blank) was a modified INSTRON ™ MTS 8580. It is a 300 kN servo-hydraulic testing machine, having a single force measuring system, provided by a load cell/ weigh beam. The system incorporates force scale settings giving a single range of 0-300 kN in tension and compression (standard calibration BS EN 10002-2), coupled with programmable input and output hardware/software (INSTRON™ Wavemaker), see fig. 4.1.6.
This made it possible to control all suitable inputs for the pressing and the data acquisition during the pressing operation.

4.1.6c Instron waveform

INSTRON™ Wavemaker is a computer software program, which enables control of the test machinery working parameters, and the acquisition of data from an array of sensors on the INSTRON ™ MTS 8580.
The input interface is a windows based program and the output files are *.csv files which are easily transferred to Excel.
During bending operations in this project, only the punch force (forming pressure) was varied, all other conditions remained the same.

4.1.6d MTS tooling

The experimental pressing tools, which were used in conjunction with the MTS test rig are made of machine tool steel. The surfaces, which are in contact with the material sample, were case hardened. Prior to pressing, the tooling was degreased using an ethanol solution, and then wiped clean using lint free cloth, eliminating the effects of lubrication. The machine can be fitted with a variety of differing punch and die combinations, Table 4.1.1 shows a nominal material thickness and the associated tooling available. The type of tooling fitted is similar to that shown in fig. 4.1.7, which reflects the installation punch tooling on the Corus tubular blank prototype production machine, see fig. 4.1.8. During all trials except those investigating the influence of forming pressure, the minimum forming pressure required for full tool closure was adopted (minimising coining).

4.1.6e V bend experimentation

The test machine used during this experimental programme was a stroke, and pressure controllable hydraulic ram, fitted with V bend tooling of 7mm radius, ensuring a three point bend analogy. The experimental press capacity was set to 30 kN, with the ram stroke set at 1mm/s. see fig 4.1.9. Die tooling of the V bend was also modified so that a channel section at the bottom of the tool existed thus eliminating coining, see fig 4.1.10.

Four of the primary steel materials were tested, in conjunction with material data obtained from a similar springback trial being carried out at the Corus Automotive Application group by Merkle [4.1.1].

The materials to be tested were cut into coupons 80 x 40 mm. All coupons and punch tooling were degreased using an ethanol solution.

4.1.7 Analytical Models [4.1.2-6]

Use was made of a selection of presently published analytical models for the prediction of springback K value, the listing of which is shown below.

Marciniak

$$K = 1 - 3\left(\frac{\rho}{t}\right)\left(\frac{\sigma_1}{E}\right)$$ eqn 4.1.2

Leu

$$K = \left(\frac{T}{e^{-n} n^n}\right)\left(1 + \frac{r}{\sqrt{1+2r}}\right)^{1+n} \times \frac{3(1-\upsilon^2)}{2E(1+n)}\left(\frac{t}{2\rho}\right)^{n-1}$$ eqn 4.1.3

Zhang

$$K = 1 - \left(\frac{3\sigma_1(1-\upsilon^2)\rho}{Et}\right)$$ eqn 4.1.4

Vegter

$$K = 1 - \left(\frac{3S\rho}{Et}\right) + 4\left(\frac{E}{E_1}\right)^2\left(\frac{S\rho}{Et}\right)^3$$ eqn 4.1.5

Klamecki

$$K = -\left(\frac{3\sigma_1\rho}{Et}\right) + 4\left(\frac{\sigma_1\rho}{Et}\right)^3 + 1$$ eqn 4.1.6

Modulus modified

$$K = 1 - \left(\frac{3S\rho}{E_1 t}\right)$$ eqn 4.1.7

4.1.8 Numerical analysis [4.1.7]

4.1.8a Response Surface Method (RSM)

The approach of RSM is to perform a series of experiments, or numerical analyses, for a prescribed set of design points, and to construct a response surface of the measured quantity over the design space. Response surface models may involve just main effects and interactions or they may also have quadratic and possibly cubic terms to account for curvature. Quadratic models are almost always sufficient for industrial applications, such as forming or material processing applications. Response surface method has been shown in the past to be an effective method in both cost and time for solving interactions in the production environment were experimental data is limited and input parameters are few.

4.1.8b Neural Network

Neural networks (NN) have received much attention in engineering applications in the last decade because they are highly flexible and have the ability to be trained, using user-supplied data, to map complex surfaces. The NN can be trained with data from any source-empirical, experimental or analytical. Training is accomplished by adjusting weights on the internal connections of the network through defined training algorithms. The training is a cyclic process in which the weights and biases are repeatedly adjusted until an accurate mapping of the response data is obtained. Once trained, the NN is then able to predict the responses for other points in the design space.
Neural networks require large amounts of data to enable accurate mapping and subsequent predictions to occur.

The purposed use of numerical analyses in this study is not to find the significant factors in a forming environment, but a method to highlight were the analytically derived equations for springback are lacking. Therefore there is no need to carry out investigations into the significance of input parameters. The key parameters in springback have been known for some time. There interactions are known to an extent. It is the

furthering of this knowledge that is required. Therefore the use of response surface method would be better suited to this application.

4.1.8c Numerical algorithms

A method of result interrogation and subsequent formulation of parameter interaction is the study of a response surface with differing parameter inputs. This is possible when large numbers of results with differing parameters are developed as in this investigation. The principle behind the formulation of such interrogations is as follows:
If a set of parameters is considered, say X_1, X_2, ...X_i, ..., X_n, any one set of these will yield a value for springback (K), through the numerical algorithm process from which a model exclusive to these parameters is calculated. A general model however, is only possible if a continuous function R_K is defined that relates the springback behaviour to general changes in Xi.
Thus

$$R_K = f(K, X_1, X_2, \ldots X_i, \ldots\ldots, X_n) + e_K \qquad \text{eqn 4.1.8}$$

The exact nature of f can be found by data fitting the results of computer simulations over a carefully chosen set of values of X_i. e_K is an error term representing the difference between the calculated value by means of numerical algorithm, and that of the actual results. This error may arise from various sources including the method of sampling, from the numerical algorithm simulations, and also by miss-specification of the original parameters. It is acceptable to use R_K as an interpolation function within the levels of the parameters set out previously and investigated by means of gradient or search methods, so long as e_K is acceptably small. The resultant function of springback behaviour consists of linear terms for the main variables together with first order interaction terms. This is presented in the manner of a matrix, from which an expression can be derived.
Consider a set of three variables, X_1, X_2, and X_3. The resultant matrix is set out as shown in fig. 4.1.11. From this matrix it is possible to construct the function that describes springback in a general form.

$$R_K = 1+2X_1+3X_2+4X_3+5X_1X_1+6X_2X_1+7X_3X_1+8X_2X_2+9X_3X_2+10X_3X_3 \qquad \text{eqn 4.1.9}$$

The programme for this is shown in Appendix A.

4.1.9 Normalisation of variables

To indicate the effect of a variable in both analytical and numerical algorithm models it was necessary to range all variables within the same magnitude. This was achieved by calculating the range of all the variables and then individually ranking the variables between 0-1 by the following process.

(Value under consideration - min value in range) / (max – min) values in range
eqn 4.1.10

A number of variable interactions were plotted against one another to highlight the areas where differing mechanisms were at play. This was done by adjusting the chosen variables between the upper and lower ranges of the investigated material normalized parameters, and leaving all other variables at a constant normalized mid point value.

4.1.10 T test [4.1.8, 4.1.9]

T test is a method of calculating the difference between the mean results of two differing sets of samples, thus indicating whether or not the samples come from the same population.
Shown below is an illustration of how a t test is carried out. Consider the two sets of data below from differing samples.

	Sample A		Sample B
Mean	28.0	Mean	29.5
Standard deviation	1.6	Standard deviation	1.2
No. of Observations	5	No. of Observations	8
Standard error of mean	$1.6/\sqrt{5}$	Standard error of mean	$1.2/\sqrt{8}$

Firstly the standard error of difference is calculated for the two samples

Standard error of difference between means = $\sqrt{[(1.6)^2/5 + (1.2)^2/8]} = \sqrt{0.692} = 0.834$

This is then used to calculate the standardized deviate t

$$t=(29.5-28.0)/0.834 = 1.8$$

For small sample sizes it is necessary to introduce a bias in the calculation of the standard deviation, this is done by dividing by one less than the number of observations in a sample. This divisor is called the 'degrees of freedom' of the sample. Thus in this example, the number of degrees of freedom in each sample is 4 for sample A and 7 for sample B. The total 'degrees of freedom' is therefore.

$$\phi \text{ degrees of freedom } = (5-1) + (8-1) = 11$$

Interrogation of Table 4.1.2 with 11 degrees of freedom indicates that the probability levels for a t value of 1.8 is 10%. Therefore it is not too unlikely that the two samples come from the same population.

4.1.11 Prediction / actual graph to interrogate model usefulness

To enable an assessment of predictive models all graphs were made consistent in structure, to create a methodology for interpretation. Graphs were constructed by plotting the actual measured results against the predictive results, allowing interrogation by use of the trend line and R^2 value. The ideal graph would be represented by a trend line who's equation would be y=x and R^2=1. Further investigation is possible to establish the degree to which models over and under predict (points above, over prediction of springback / points below, under prediction of springback). The band or range of the plots along the x-axis would also show the model's ability to cope with varying degrees of springback, see fig. 4.1.12. Secondly, by considering the equation of the trend line, where

$$y = mx+c$$

y denoting the actual springback K value

m the factor of springback over or underprediction (slope of trendline)

c the constant predictive offset value (intercept)

it is possible to rank the models on their degree of predictability at both the upper and lower ranges of springback.

4.1.12 Manufacture of LWTB's

A Trumpf 6kW CO_2 laser situated at the Corus Product Application Centre in Ijmuiden Holland was used to produce the laser welded samples. All samples were precision guillotined and degreased before fabrication. In all cases the butt to butt fit up was no greater that 0.05mm of a gap. Laser power, shield gas type/flow rate and focal length were all held at constant levels, the only variable thus being speed. The method for determination of weld speed acceptance was firstly by visual means, (the narrowest and best formed weld bead being the preferred choice [4.1.10,4.1.11,4.1.12] see fig. 4.1.13). Secondly if two speeds gave similar results, a further test involving a 25mm Erichsen punch height test was adopted (were the sample gaining the greatest height and therefore greatest amount of formability was selected [4.1.10,4.1.11,4.1.12] see fig. 4.1.14).

4.1.13 Pressing of LWTB's

The material to be tested was cut into varying size coupons, dependent on the test carried out. All coupons together with the punch / die tooling were degreased using ethanol to eliminate the influence of lubrication on the experimental results.

Shims were adopted for differing material thicknesses for initial experiments (eliminating differences in tooling tolerance). These were manufactured by means of guillotining copper sheet of 0.3mm thickness to the exact profile of the area required. Soft copper sheet was adopted as the yield strength of this material was less that of the thinner material and would therefore not contribute to the forming operation.

Adhesion of the shims to the work piece was by means of sellotape around the edges. It was felt that this method again would not interact with the pressing, and therefore a more reliable result would be forthcoming.

4.2 Program

4.2.1 Material characterisation

Aim

The aim of this investigation was to characterise the materials involved in this project.

Standard tensile tests and chemical compositions were carried out to characterise the primary steels selected for evaluation. See Table 4.2.1.
Characterisation of the remaining steels chosen for springback evaluation (see Table 4.2.2) was by means of standard tensile tests.
To try to ensure uniformity of material properties, those steels that were classed primary i.e. run through the entirety of the project were obtained in quantity from a single coil.
To assess the degree of anisotropy in the sheet steels, samples were taken in two differing axes relative to the rolling direction of the sheet, longitudinally (0°), and transversely (90°).

4.2.2 Tube forming trials

Aims

A tube forming trial (bending using experimental tooling described in section 4.1.6) was carried out to gain a basic understanding of the experimental project tool forming process, it's influences on the sheet steel (and visa versa), and provide a comparison with the prototype production machine shown in fig. 4.1.8.
One of the major concerns with all manufacturing processes is that of repeatability, without which a manufacturing process is uneconomical to run. It was necessary to demonstrate that the experimental tool provided a stable platform to carry out experiments. In addition, results from the formed tube bends, also needed to be capable

of being translated into production guidelines, to ensure a quality repeatable product was produced.

4.2.2a Formed component springback measurement

Springback was measured from a single source pressing. Measurement was taken at the centre of the pressing, and six consecutive measurements were taken by each method. The best performer of the two was then used as a benchmark to investigate the variation in a series of six individual pressings, all of which were measured 3 times in the centre of the formed component and the average taken. The two methods of measurement adopted were by protractor and 3D profilometer.
Comparison of standard deviation for both types of measurement was also carried out.
The tooling adopted for this trial was a 49.3mm radius punch, and a 50mm radius die with a forming angle of 90°. The forming pressure used was 10kN, and sample preparation was carried out as stated.

4.2.2b Formed component thickness measurement

Measurements of thickness both in the formed component and the parent material were carried out. Parent material thickness measurement was carried out using a flat-faced micrometer. Measurement of formed component thickness was carried out using both a flat-faced micrometer and also a rounded micrometer.
Comparison of standard deviation for both types of measurement was also carried out.
The tooling adopted for this trial was above in section 4.2.2a.

4.2.2c Blank position in tooling

The Corus Tubular Blank machine is capable of pressing tube forms of varying length. It is able to do this is by means of a 4m long pressing punch. This raises the concern of the interaction of the punch when small components are pressed and the positioning of these components on the 4m tooling. In this investigation the experimental pressing tooling had

blanks placed at two different regions in the tooling, see fig. 4.2.1 and 4.2.2 for a schematic drawing of the locations. Fig. 4.2.1 depicts the worst perceived position of a blank, where misalignment has taken place and the blank is now over hanging the outer face of the forming tool. Fig. 4.2.2 depicts the best position, directly under the punch ram position.
The measurements of the resultant formed profiles was by means of the 3D profilometer using tooling described in section 4.2.2a.

4.2.2d Material orientation influence

One of the major advantages of the Corus Tubular Blank is that it is able to form tubes from any orientation within a steel coil (restricted in length by coil width). It is therefore necessary to quantify whether an influence exists of blank orientation w.r.t. rolling direction. Two differing sample directions were tested as shown in fig. 4.1.5.
The measurements of the resultant formed profiles was by means of the 3D profilometer using tooling described in section 4.2.2a. Comparison of standard deviation for both types of orientation was also carried out, along with T tests.

4.2.2e Tooling geometry influence

This investigation adopted two distinctive types of tooling, one was a 49.3mm radius punch, and a 50mm radius die with a forming angle of 90°. The second was a 49.3mm radius punch, and a 50mm radius die with a forming angle of 140°.
Both types of tooling will result in a tube of similar form, the difference is the number of forming steps (tooling with a forming angle of 140° has fewer forming steps than that of 90° to produce a complete tubular shape). A comparison of standard deviation for both types of tooling was also carried out, along with T tests.

4.2.2f Forming force influence

As described previously the Corus Tubular Blank machine is capable of forming differing lengths of blanks. The automated control method on the pressing stage of the machine can be controlled both by force and displacement. It would therefore be beneficial to understand the consequence of reduced blank sizes resulting in increased forming pressure.

The aim of this investigation therefore was to quantify the degree of formed component variation due to increase forming force and secondly, to see if this is a worthwhile avenue for further investigation.

Two types of tool sets were adopted one was a 49.3mm radius punch, and a 50mm radius die with a forming angle of 90°. The second was a 49.3mm radius punch, and a 50mm radius die with a forming angle of 140°. The forming force was increased incrementally from an initial value of 10kN – 300kN. The measurements of the resultant formed profiles were measured by means of the 3D profilometer using the centreline of the sample and taking the average of three measurements. Sample preparation was carried out as stated in section 4.1.6.

4.2.2g Forming effect on material properties

The Corus Tubular Blank machine produces blanks that will undergo a further deformation process in the form of hydroforming. It is therefore necessary to be able to quantify the reduction in material formability due to the tubular blank process.

This investigation set out to attain these goals by means of carrying out mini tensile tests of the formed component in areas that were likely to introduce inconsistencies into the material. The areas selected are highlighted in fig. 4.2.3, and represent the two areas of material that come into contact with the edge of the forming tool and also the material mid point span. These mini tensile tests were then compared to hardness measurements from the same region to quantify whether or not it was possible to use hardness measurement as a means of formability measurement.

The tooling adopted for this trial was a 49.3mm radius punch, and a 50mm radius die with a forming angle of 90°. The forming pressure used was 10kN. Sample preparation was carried out as stated previously.

4.2.3 Tool tolerance

Aims

The aim of this investigation is to understand the influence of tooling tolerance, its effects on roundness of tube, and the springback value K.

The general experimental procedure for pressing of components on the MTS machine was followed, as described in section 4.1.6. During this investigation a matrix of differing tooling was used in conjunction with the primary steels selected. Table 4.1.1 shows the differing tooling, the areas that are highlighted red are the sections were the material is the nominal thickness for the tooling. Roundness was tested in respect to the tube standard BS EN 10305-3:2002(E). This was done by fixing the 3D profilometer software package tolerance to a recognition level of 0.1mm deviation for circles and 0.5mm deviation for lines. In doing so the software was set below the tube standard for roundness. The tooling adopted for this trial was a 49.3mm radius punch, and a 50mm radius die with a forming angle of 90°. The forming pressure used was 10kN. Sample preparation was carried out as stated in section 4.1.6. The measurements of the resultant formed profiles were determined by use of the 3D profilometer.

4.2.4 Springback characterisation

4.2.4a MTS experimentation

Aim

The aim of this investigation was to press a range of mild steel, CMn, IF, and DP steels by means of the experimental tooling available, and quantify the results from the general trends obtained.

Tooling was made to fit the materials nominal thickness so that any ill fitting tooling interaction could be neglected.

All steels selected for this investigation were formed using the MTS machine. Tooling was selected with respect to the nominal thickness of steel selected. The measurements of the resultant formed profiles were measured by means of the 3D profilometer. The minimum forming pressure was used for all steel grades, thus reducing the possibility of coining. Sample preparation was carried out as stated in section 4.1.6.

Comparisons were then made between the prediction of springback from differing analytical models using the methodology outlined in section 4.1.11.

4.2.4b V bend experimentation

Aims

The aim of this investigation was to build on the initial characterisation trials which concentrated on large radius bends using the MTS experimental tooling, using a V bend test rig to enable the study of smaller bend radii bends.

Four of the primary steel materials were tested in conjunction with material data obtained from a similar springback trial carried out at the Corus Automotive Application group by Merkle [4.1.1].

This was then expanded further so that data from both sets of results were analysed together to see if any further trend other that those previously seen could be extracted.

Comparisons were then made between the effective prediction of springback by differing analytical models using the methodology outlined in section 4.1.11.

4.2.5 Coining Investigation

Aims

The aim of this investigation was to study the effect of increasing forming pressure on the final formed component profile, and to quantify the consequential loss in formability.

The initial investigation was carried out on the 0.7mm GA IF 240 material. A subsequent investigation included those materials indicated as primary steels see Table 4.2.1.
Initial forming force trials indicated that an increase in forming force would reduce the amount of springback in a materials final form. This investigation was carried out to further this understanding.
The punch compressive force was set to a maximum of 300 kN on the MTS machine. The tooling adopted for this trial was a 49.3mm radius punch, and a 50mm radius die with a forming angle of 90°.
The material to be tested was cut into coupons that ranged from 5-100 mm in width x 312mm in length. All coupons and punch tooling were degreased using an ethanol solution. The measurements of the resultant formed profiles were measured by means of the 3D profilometer.
Springback K value, thickness, and hardness effects were used as indicators of formability of the final formed components.

4.2.6 Analytical Model Investigation

Aims

The aim of this investigation was to see if a selection of the currently published analytical predictive models were capable of satisfactorily predicting springback, of a range of materials under differing bending and loading conditions, as described in section 4.1.8.

A selection of the presently published analytical predictive models was chosen (see table 4.2.3) to investigate the capability of satisfactorily predicting springback, of a range of material under differing bending and loading conditions. Data from the results of section 5.4 were used for this assessment.

The level of confidence set for a satisfactory prediction was ±5% of the actual measured value. Comparisons were then made between the effective prediction of springback by differing analytical models using the methodology outlined in section 4.1.11.

Comparisons were also made between the MTS experimental results and a combination of the MTS and V bend results.

4.2.7 Numerical algorithm investigation

Aims

The aims of this investigation was firstly to see if it was possible, by the use of a numerical algorithm, to interrogate the mechanical tensile and springback data to highlight the important parameter interactions. The second objective was to ascertain if it was possible to use the numerical algorithm as an accurate means for predicting springback.

The analytical models in section 5.6 highlighted the important parameters affecting springback, and also showed the level of predictability to be surpassed by the numerical algorithm to be considered as a viable alternative to analytical models. Comparisons were then made between the effective prediction of springback by differing numerical input parameter models using the methodology outlined in section 4.1.11.

The interaction of differing parameters on springback K value was also investigated.

4.2.8 Numerical algorithm / analytical model comparison

Aims

The aim of this investigation was to study the areas of differing behaviour for a selection of the models previously interrogated.

Zhang's model was chosen from the group of analytical models considered because whilst it was not the best overall performer it did give relatively good results with a consistent degree of data scatter. The four variable numerical algorithm was also chosen as it used the same input parameters as the Zhang analytical model. In addition to these models the results of the six variable input model was also incorporated into the study to investigate the changing parameter sensativity of the numerical algorithm.
A number of variable interactions were plotted against one another (mapped) to highlight the areas where differing mechanisms were at play.

As in the previous experimental procedure 4.1.9, a number of variable interactions were plotted against one another to highlight the areas where differing mechanisms were at play. This was done by adjusting the chosen variables between the upper and lower ranges of the materials investigated normalized parameters, and leaving all other variables at a constant normalized mid point value.
A comparison between the six, four variable numerical algorithms and of the Zhang analytical predictive model was carried out.

4.2.8a Numerical algorithm / analytical model comparison (excluding outlying points)

Aims

The aim of this mini investigation was to identify the difference between the numerical algorithm models, when out lying points were neglected.
Comparisons were made between the plotted variable interactions.

4.2.9 Initial Tailored Blank Investigation

Aims

The aim of this investigation was to understand the effect of springback on final component geometry in low strain forming modes for tailored blanks.

An understanding of the key material, and loading factors that influence springback is needed to be able to predict springback for a single type material, and also those which are composites of several differing types of sheet steel. Development is needed to accommodate the mismatch in material strength and therefore differing springback behaviour of the different sheet steels used. Thickness changes will produce areas of differing springback, high stress concentration, and variable formability due to weld properties.

This investigation dealt with the interaction between a 0.7mm GA140 and 1.0mm DP800 tailored blank. These blanks were pressed in the configuration shown in fig. 4.2.4. All samples for this investigation were shimmed as described in section 4.1.13.

Differing methods of springback K value prediction of the LWTB was also carried out.

4.2.10 Further Tailored Blank Investigation

Aims

The aim of this investigation was to build on from the initial LWTB experiments increasing the material matrix, and adding to the forming conditions previously observed.

A further investigation was carried out into the effects of shims on the behaviour of the LWTB in terms of both springback and the predictability of the final component shape, using a 0.7mm GA140 and 1.0mm DP800 steel combination.

This was then extended to a 0.7mm GA140 and 1.5mm DP 350 YP LWTB combination.

A small experimental investigation on the behaviour of a 0.7mm GA140 and 1.5mm DP 350 YP LWTB welded at 45° to the pressing direction was also carried out.

An investigation looking into weldline offset from punch centre using 1.0mm DP 800 and 1.5mm DP 350 YP LWTB was carried out to see if the displacement of the weld line relative to the tooling affected the springback characteristics of the final component, see fig. 4.2.5.

Finally a 0.7mm GA140, 1.0mm DP 800 and 0.7mm GA140 triple LWTB was pressed to investigate the behaviour of complex LWTB's.

4.3 References

4.1.1 H. Merkle, High Strength Steel Project, Automotive Applications, Customer Technical Centre, Welsh Technology Centre, Port Talbot, Internal Report

4.1.2 Z.Marciniak & J.L. Duncan, Mechanics of Sheet Metal Forming, 1992, ISBN 0-340-56405-9, Pg 69-79

4.1.3 http://www.menet.umn.edu/~klamecki/Forming/bending.html

4.1.4 Leu,Daw-Kwie, 'A simplified approach for evaluating bendability and springback in plastic bending of anisotropic sheet metals',Journal of Materials Processing Technology 66,1997/9/7

4.1.5 Z.T.Zhang & S.J.Hu, 'Mathematical Modelling in Plane Strain Bending', Journal of Materials and Manufacturing, 106, 1997 Pg458-471

4.1.6 H.Vegter,'A Model for the Prediction of Springback Under Pure Bending Forming Conditions with Validation Using Experimental Results', Internal Document from PAC Hoogovens, Ijmuiden, Holland, 16 July 1986 Arch. Lab. Nr. 58.455

4.1.7 R.W. Evans, Shot peening process: modelling, verification and optimisation, Materials Science and Technology, August 2002, Vol 18, pg 831-839

4.1.8 W.E. Duckworth, 'Statistical Techniques in Technological Research, An aid to Research Productivity', Methuen and Company Ltd, 1968, pg 31-33

4.1.9 M. Rouncefield & P. Holmes, 'Pratical Statistics' Macmillan Press, ISBN 0-333-47344-2, 1989, pg 193-196

4.1.10 Phillip Scriven, Doctorate Thesis, Formability and processing of welded blanks for automotive application, Engineering Doctorate Centre, University of Wales Swansea, October 1997

4.1.11 Damian Dry, Doctorate Thesis, The processing and formability of laser welded tailored blanks for automotive applications, Engineering Doctorate Centre, University of Wales Swansea, January 2001

4.1.12 Craig Bratt, Private correspondance, Corus Welding Research Department CTC Port Talbot, Wales

4.4. Figures / Tables

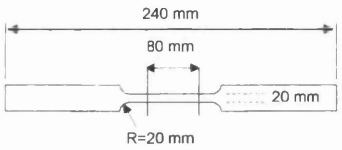

Figure 4.1.1: Standard tensile dimensions

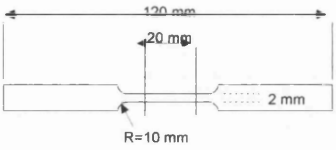

Figure 4.1.2: Mini tensile specimen dimensions

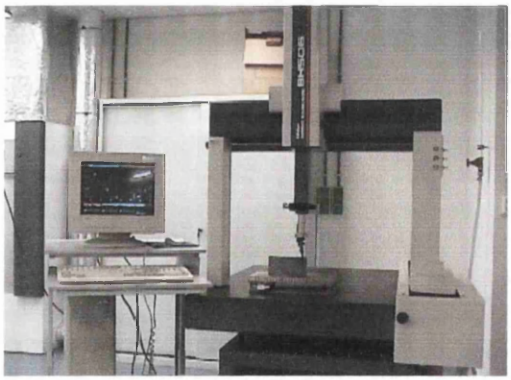

Figure 4.1.3: 3D profilometer machine Mitutoyo BH 506

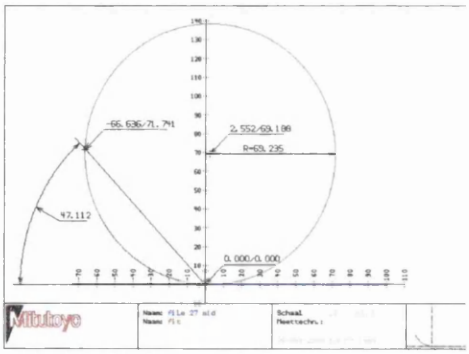

Figure 4.1.4: 3D profilometer output file

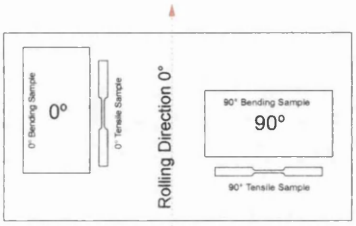

Figure 4.1.5: Tensile and pressing orientation

Figure 4.1.6: MTS test machine

Figure 4.1.7: Tooling used during experimentation

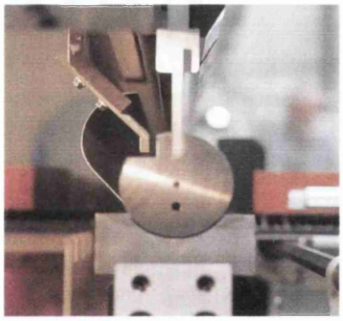

Figure 4.1.8: Actual tooling used on production machine

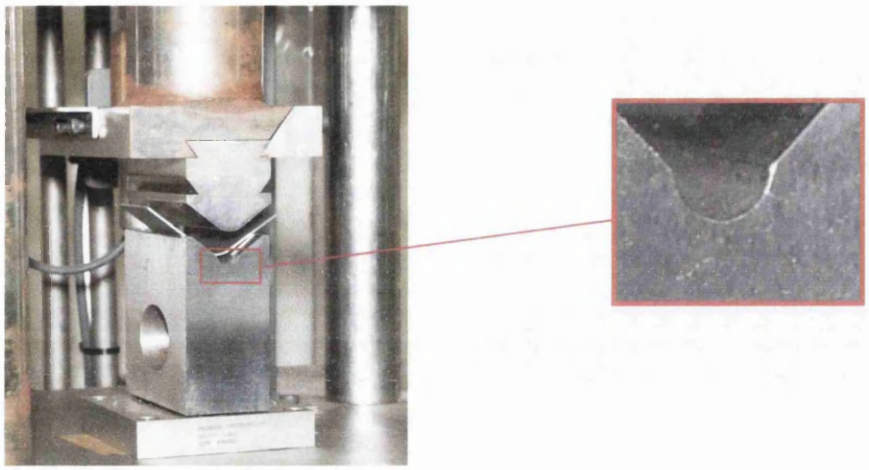

Figure 4.1.9: V bend test machine and tooling

Figure 4.1.10: V bend test machine tooling cut out channel to eliminate coining

	1	X_1	X_2	X_3
1	1	2	3	4
X_1		5	6	7
X_2			8	9
X_3				10

$R_K=1+2X_1+3X_2+4X_3+5X_1X_1+6X_2X_1+7X_3X_1+8X_2X_2+9X_3X_2+10X_3X_3$

Figure 4.1.11: Numerical algorithm result matrix and resultant equation

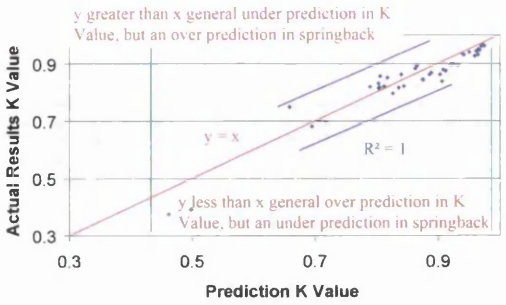

Figure 4.1.12: Graph criterion for predictive models

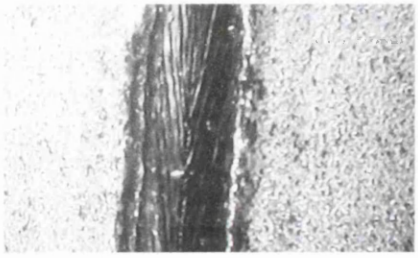

Figure 4.1.13: Image of a well formed laser weld

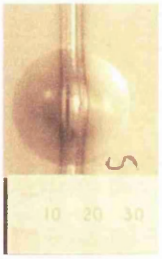

Figure 4.1.14: Typical 25mm Erichsen punch height test result

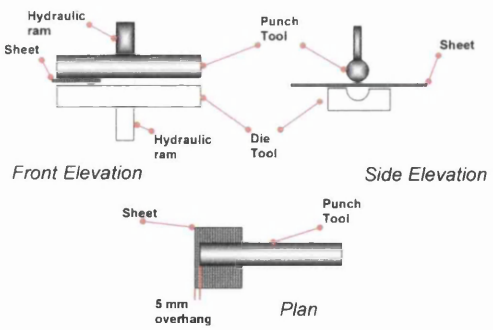

Figure 4.2.1: Overhang positioned blank

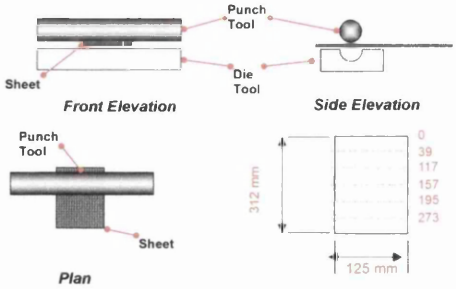

Figure 4.2.2: Centrally positioned blank

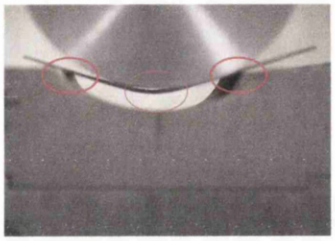

Figure 4.2.3: Areas under investigation during the effects of forming on material properties

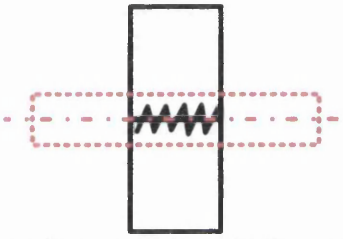

(a) Pressing layout with weld line running traverse to pressing centreline

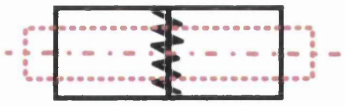

(b) Pressing layout with weld line running parallel to pressing centreline

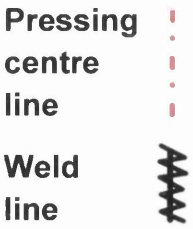

Figure 4.2.4: Experimental LWTB configuration

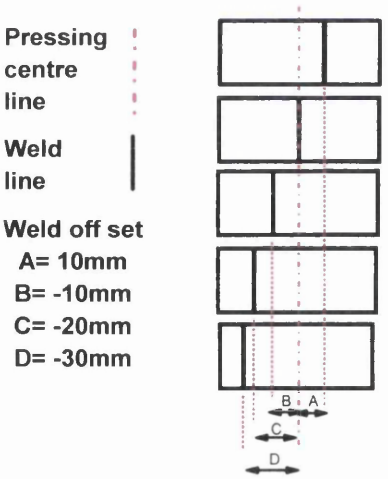

Figure 4.2.5 : Schematic of weld line in relation to the punch centre line

Material	Punch Radius 49.3mm Die Radius 50mm/90°	Punch Radius 42.5mm Die Radius 43.5mm/90°	Punch Radius 48.5mm Die Radius 50mm/90°	Punch Radius 48mm Die Radius 50mm/90°
	Measured Radius of Pressing mm	Measured Radius of Pressing mm	Measured Radius of Pressing mm	Measured Radius of Pressing mm
0.7mm GA 140				
0.7mm GI IF 240				
0.7mm Nizec 260				
1mm DP 800				
1.5mm DP 350YP				

Table 4.1.1: MTS experimental tooling for nominal thickness

Percentage Points of the t*-Distribution*

	Probability %								
ϕ	50	25	10	5	2·5	1	0·5	0·1	ϕ
1	1·00	2·41	6·31	12·7	25·5	63·7	127	637	1
2	0·816	1·60	2·92	4·30	6·21	9·92	14·1	31·6	2
3	0·765	1·42	2·35	3·18	4·18	5·84	7·45	12·9	3
4	0·741	1·34	2·13	2·78	3·50	4·60	5·60	8·61	4
5	0·727	1·30	2·01	2·57	3·16	4·03	4·77	6·86	5
6	0·718	1·27	1·94	2·45	2·97	3·71	4·32	5·96	6
7	0·711	1·25	1·89	2·36	2·84	3·50	4·03	5·40	7
8	0·706	1·24	1·86	2·31	2·75	3·36	3·83	5·04	8
9	0·703	1·23	1·83	2·26	2·68	3·25	3·69	4·78	9
10	0·700	1·22	1·81	2·23	2·63	3·17	3·58	4·59	10
11	0·697	1·21	1·80	2·20	2·59	3·11	3·50	4·44	11
12	0·695	1·21	1·78	2·18	2·56	3·06	3·43	4·32	12
13	0·694	1·20	1·77	2·16	2·53	3·01	3·37	4·22	13
14	0·692	1·20	1·76	2·14	2·51	2·98	3·33	4·14	14
15	0·691	1·20	1·75	2·13	2·49	2·95	3·29	4·07	15
16	0·690	1·19	1·75	2·12	2·47	2·92	3·25	4·01	16
17	0·689	1·19	1·74	2·11	2·46	2·90	3·22	3·96	17
18	0·688	1·19	1·73	2·10	2·44	2·88	3·20	3·92	18
19	0·688	1·19	1·73	2·09	2·43	2·86	3·17	3·88	19
20	0·687	1·18	1·72	2·09	2·42	2·85	3·15	3·85	20
21	0·686	1·18	1·72	2·08	2·41	2·83	3·14	3·82	21
22	0·686	1·18	1·72	2·07	2·41	2·82	3·12	3·79	22
23	0·685	1·18	1·71	2·07	2·40	2·81	3·10	3·77	23
24	0·685	1·18	1·71	2·06	2·39	2·80	3·09	3·74	24
25	0·684	1·18	1·71	2·06	2·38	2·79	3·08	3·72	25
26	0·684	1·18	1·71	2·06	2·38	2·78	3·07	3·71	26
27	0·684	1·18	1·70	2·05	2·37	2·77	3·06	3·69	27
28	0·683	1·17	1·70	2·05	2·37	2·76	3·05	3·67	28
29	0·683	1·17	1·70	2·05	2·36	2·76	3·04	3·66	29
30	0·683	1·17	1·70	2·04	2·36	2·75	3·03	3·65	30
40	0·681	1·17	1·68	2·02	2·33	2·70	2·97	3·55	40
60	0·679	1·16	1·67	2·00	2·30	2·66	2·91	3·46	60
120	0·677	1·16	1·66	1·98	2·27	2·62	2·86	3·37	120
∞	0·674	1·15	1·64	1·96	2·24	2·58	2·81	3·29	∞

ϕ is the number of degrees of freedom.

Source Ref 4.1.8

*Table 4.1.2:*T test probability table of ϕ degrees of freedom

Primary Steel Material ID	Nominal Thickness (mm)
GA 140	0.7
GI IF 240	0.7
Nizec 260	0.7
DP 800	1.0
DP 350YP	1.5

Table 4.2.1: Primary steels

Springback evaluation Material ID	Nominal Thickness (mm)
GA 140	0.8
GA 260	0.8
GA300	0.8
GA 140	1.0
GA260	1.0
DP 350	1.5
GA 200	2.0
GA 300	2.0
CMn 500	2.0

Table 4.2.2: Springback evaluation steels

Marciniak

$$K = 1 - 3(\rho/t)(\sigma_1/E)$$

Leu

$$K = (T/e^{-n}n^n)(1 + r/\sqrt{1+2r})^{1+n} \times 3(1-\upsilon^2)/2E(1+n)(t/2\rho)^{n-1}$$

Zhang

$$K = 1 - \left(3\sigma_1(1-\upsilon^2)\rho/Et\right)$$

Vegter

$$K = 1 - \left(3S\rho/Et\right) + 4\left(\frac{E}{E_1}\right)^2\left(\frac{S\rho}{Et}\right)^3$$

Klamecki

$$K = -\left(3\sigma_1\rho/Et\right) + 4\left(\frac{\sigma_1\rho}{Et}\right)^3 + 1$$

Modulus modified

$$K = 1 - \left(3S\rho/E_1 t\right)$$

Table 4.2.3: Predictive models

5.0 Results

5.1 Material characterisation

5.1.1 Aim

In this section the materials involved in the project are characterised in terms of both mechanical properties and chemical composition.

5.1.2 Tensile mechanical properties

Fig. 5.1.1a – 5.1.5d show the engineering stress/strain graphs for the materials involved in this investigation, and Tables 5.1.1 – 5.1.5 show the corresponding mechanical data for these materials. Materials of similar thickness have been grouped together. Materials have been tested in both the 0° (rolling direction) and 90° (traverse to rolling direction).

Other than the 1.5mm DP 350YP, 2.0mm GA 300 and 2.0mm CMn 500 material which show discontinous yielding, all other steels tested showed continous yielding. Variations in material properties were evident in differing directions, indicating anisotropic behaviour. Thickness variations in the steel were within those prescribed by EN 10142 and 10147 for their nominal thicknesses.

5.1.3 Chemical Composition

Interstitial Free Steel GA 140 and GI IF 240

Interstitial free steels are produced by adding small amounts of titanium and or niobium to reduce the carbon and nitrogen solute contents to very low concentrations, thus improving the cold forming properties [5.1.1]. From table 5.1.6 it can be seen that the chemical composition of the GA 140 adheres very closely to that of an interstitial free steel [5.1.2], though originally labelled as an aluminium killed cold reduced steel. The low amount of carbon, and high amount of titanium and niobium composition, in conjunction with the mechanical properties shown in table 5.1.1, would suggesting a continuous annealed interstitial free steel.

From table 5.1.6 it can be seen that in this instance the preferred method for the reduction of residual elements in solution is by means of both niobium and titanium for both of the interstitial free steels identified

Table 5.1.7 shows that the GA 140 has been galvannealled, this is evident from the chemical composition of both the top and bottom layers. The percentage of aluminium and iron is low, indicating diffusion between the coating and substrate has taken place[5.1.3]. It can also be seen from table 5.1.7 that the GI IF 240 interstitial free steel has been coated by means of hot dip galvanised production methods. The high levels of aluminium and lower levels of iron show this, as a greater amount of diffusion between the two elements would have been the result of a galvannealled process[5.1.3].

Aluminium Killed Cold Rolled Steel-Nizec 260

From the chemical composition shown in table 5.1.7 it would suggest that the Nizec 260 substrate is an aluminium killed cold rolled FeP01, this is further enhanced with the mechanical properties shown in table 5.1.1 which are common to FeP01 type steels. Table 5.1.7 indicates that the coating classification is a NZ40/40, which would have a nominal coating mass per side of 29g/m^2[5.1.4].

Dual Phase Steels DP 350 YP and DP 800

Table 5.1.6 shows the chemical composition of the two dual phase labelled materials that were researched. The table shows that both of the dual phase materials have a large amount of niobium present, compared to the other steels, as well as manganese, chromium, carbon and molybdenum. This would be expected with a dual phase steel, as manganese, chromium, and molybdenum are added to suppress pearlite formation during cooling. It could also be said that manganese is the preferred base element for suppressing pearlite formation, as both molybdenum and chromium are an expensive addition in regards to cost, chromium also increase the likelihood of oxide formation on the surface, which would effect the wettability of the steel for subsequent hot dip galvanising[5.1.5]. The amount of carbon content in the DP 350 YP is significantly lower than expected to ensure a dual phase steel, evidence of which from the tensile test would indicate that the DP 350 YP is not in fact a dual phase steel but, more so a high carbon steel with it's associated

discontinuous yield point (fig. 5.1.4b)[5.1.5]. A large amount of carbon is required so that a sufficient amount of austenite is formed during the annealing cycle. This steel has approximately a third the level of carbon of that in the DP 800 grade steel.
Both dual phase steels have niobium present, this is added as a grain refiner, in which it is envisaged that grain refinement of austenite during the hot rolling process will result in smaller ferritic grain size, and a better stability of austenite in the final cold rolled state. However the DP 800 grade has an amount which is on par with the other single phase steels, given the amount of carbon present in this steel, it would be expected that the resultant steel would be considerably less formable than that of the DP 350 YP, which has a higher niobium content.
Noticeable from the chemical composition in table 5.1.6 is the high level of nickel in both the dual phase steels. As a graphitising agent, (non-carbide and ferrite forming) nickel inhibits grain growth; therefore, carbon will be retained, giving better austenite stabilisation. This effect can also be attributed to silicon, of which DP 800 has a large amount.

5.1.4 Discussion

Table 5.1.8 shows the inherent traits for each of the steels considered in this experimental program, it can be said that in general regardless of yield strength or type of engineering stress/strain curve depicted 90° direction will yield the largest value for Young's modulus, yield strength, and r value. Where as the 0° direction will have the largest values of n and percentage engineering strain before fracture. These results are an indication that the materials being investigated have undergone an amount of cold rolling, as the results show that anisotropic conditions exist in all of the steels investigated.
It can be said that the spread of values for the steels Young's modulus is greater than that often published in engineering text books (210 GPa)[5.1.6]. A difference of 20% between the smallest and largest value of Young's modulus exists. The value and accuracy of Young's modulus for steel is often debated by both academics and industrialists [5.1.8].
The variation and confusion in such an important parameter when considering forming and modelling complicates an already difficult area. It would appear that

Young's modulus variation concern has increased as material manufactures have introduced higher strength sheet steel materials, and the complexity of material ingredients and processing has been pushed forward [5.1.7]. Variations could be the result of tensile testing equipment flexure or jaw slippage, moment movement of test piece resulting in a force not applied axially, inaccuracy of extensometer and automated calculation error. Some of these points have been raised in previous studies [5.1.7], in which large deviations have been noted in the Young's modulus of sheet steel. In one of the investigations carried out into through coil variation it was found that the Young's modulus for a 2.0mm CMn 350 varied from 126 (GPa) to 205 (GPa) in the 0° direction [5.1.7]. In a separate investigation looking at the springback behaviour of high strength steel it was seen that the Young's modulus for the high strength materials ranged between 171 (GPa) and 188 (GPa), where the Young's modulus was calculated from the load extension plot(as shown in BS EN 10 002-1 : 1990 Tensile testing of metallic materials part 1), and not by an automated program within the tensile testing machine [5.1.9]. This evidence suggests that it is in the interest of both academics and industrialists to try and regain a method of Young's modulus determination, which has better accuracy than the present, so that the introduction of newer more complex steels does not compound the situation further.

Fig. 5.1.6 and 5.1.7 shown the plot of r and n value versus the yield strength respectively. It can be seen that a general trend of increased yield strength results in a decrease of the r and n value. Both these trends appear to be very slight in appearance. The r-value of a sheet steel is derived from the cold rolling operation which aligns the grains along the direction of rolling, thus introducing directionality into the sheet. This can be thought of as the ability of the material to resist thickness change. A large r value would imply the material flow comes more from in the plane of the sheet, rather from the thickness direction (higher resistance to thinning). Hall-Petch showed that a relationship between grain size and yield strength of a material existed, this relationship may also be used to explain the r value and yield strength relationship. Consider a high strength steel with a refined grain structure, when under going cold rolling the anisotropic effect in comparison to that of a mild steel would be less as the grain size is smaller in comparison. The n value of a material can be viewed as the ductility and it's ability to resist necking (distribute deformation uniformly). In fig. 5.1.8 it can be seen that a general trend of increasing r value results in increasing n

value, exists for these sheet steels. As mentioned previously this is likely to be the result of grain size effect on the two parameters.

From the material characterisation it has been shown that the colded rolled sheet steel tested in this investigation all exhibited anisotropic behaviour. These results indicate that the degree of springback of the materials will differ dependant on orientation of the sheet being formed. This in turn will complicate the forming machines operations window flexibility, as sheets are to be pressed from varying orientations from the coil.

It is also evident that as r value increases so the n value increases. When considering hydroforming a material with both high r and n value is desired.

The initial stages of tool cavity filling by the tube material will need a high r value, and for corner radius filling a high n value is desired.

5.1.5 Conclusion

1. All cold rolled sheet steel in this investigation exhibit anisotropic behaviour
2. As r value increases so n value increases

5.1.6 References

5.1.1 D. Llewelyn, An Intriduction to Iron and Steel Industry, Volume 2, University of Wales Swansea, 1990 lecture notes

5.1.2 R. Alderdice, E. A. Campbell, Process Plant Implications of ULSAB and High Strength Autobody Steels, Iron and Steel Making 1998, Vol 25 No. 6 pg. 435-442

5.1.3 I. Mc Murray, Coated Steels, Engineering Doctorate year 1 course notes, University of Wales Swansea

5.1.4 Nizec sales literature, British Steel, Port Talbot

5.1.5 G. Lodwig, L. Gavard, Annealing cycles for the Production of Dual Phase Steels, to be published in Iron and Steel making Journal late 2003

5.1.6 Norman E. Dowling, Mechanical Behaviour of Metals, Engineering Methods for Deformation, Fracture and Fatigue, Second Edition, Prentice Hill, 1998, ISBN 013 905 720 x, pg 212

5.1.7 Baljesh Mehmi, Engineering Doctorate Thesis, the Factors Influencing the Final Shape of Formed Components, University of Wales Swansea, 2002

5.1.8 M. Boyles, Manager, Customer Technical Centre, Welsh Technology Centre, Port Talbot, Private correspondence

5.1.9 H. Merkle, High Strength Steel Project, Automotive Applications, Customer Technical Centre, Welsh Technology Centre, Port Talbot, Internal Report

5.1.7 Figures / Tables

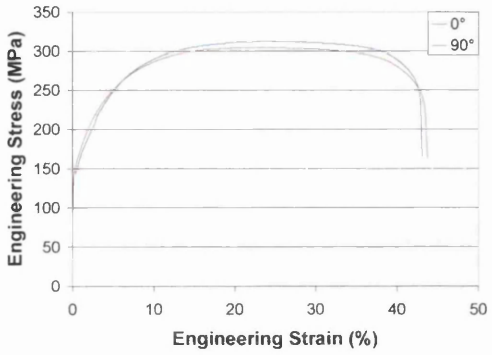

Figure 5.1.1a: Engineering stress/strain curve for 0.7mm GA 140

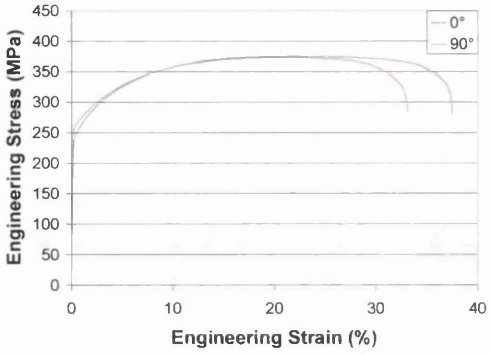

Figure 5.1.1b: Engineering stress/strain curve for 0.7mm GI IF 240

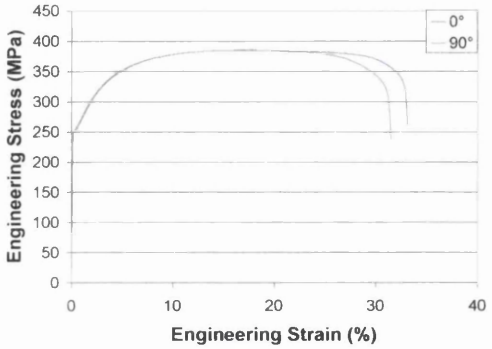

Figure 5.1.1c: Engineering stress/strain curve for 0.7mm Nizec 260

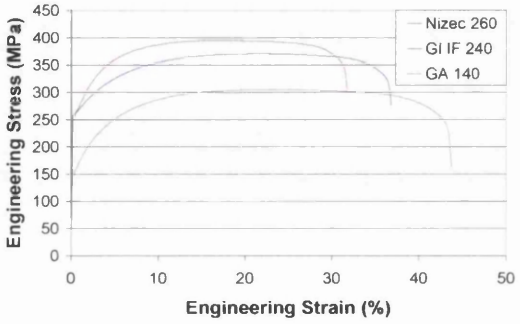

Figure 5.1.1d: Engineering stress/strain curve for 0.7mm material

Material ID	GA140	GA140	GI IF240	GI IF240	Nizec 260	Nizec 260
Rolling Orientation	90	0	90	0	90	0
Thickness(mm)	0.747	0.744	0.653	0.653	0.703	0.693
E(MPa)	194382	210802	212187	206901	215713	214026
Rp(MPa)	149	139	261	242	254	259
Rm(MPa)	305	308	373	376	385	395
r Average	2.322	1.928	1.966	1.532	1.739	1.211
n Average	0.224	0.232	0.198	0.206	0.16	0.163

Table 5.1.1: Mechanical data for 0.7mm material

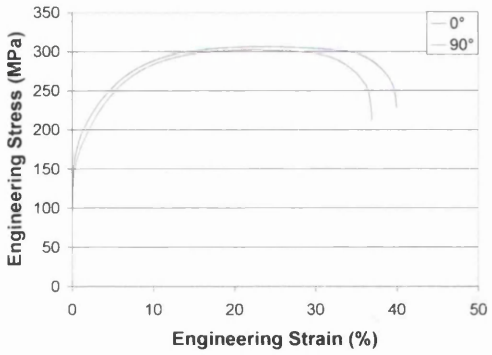

Figure 5.1.2a: Engineering stress/strain curve for 0.8mm GA 140

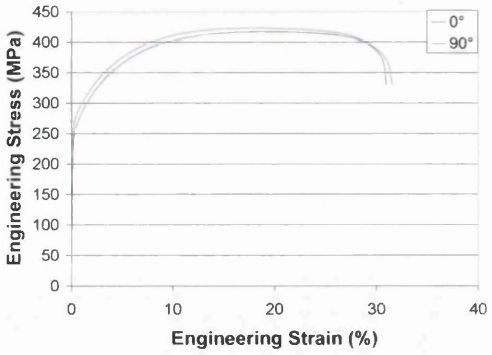

Figure 5.1.2b: Engineering stress/strain curve for 0.8mm GA 260

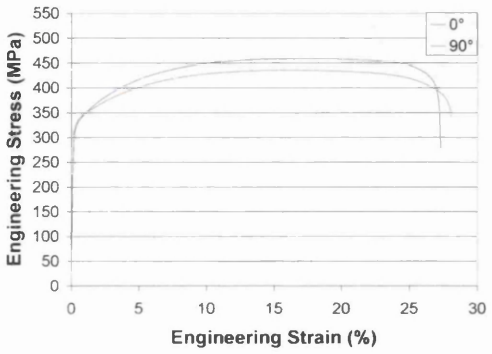

Figure 5.1.2c: Engineering stress/strain curve for 0.8mm GA 300

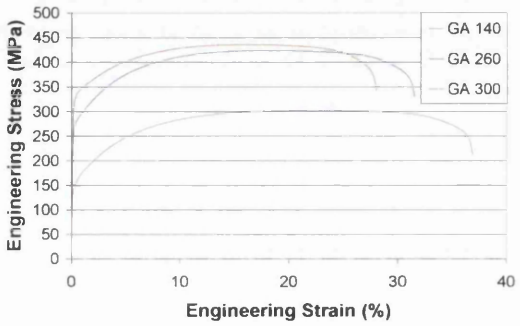

Figure 5.1.2d: Engineering stress/strain curve for 0.8mm material

Material ID	GA140	GA140	GA260	GA260	GA300	GA300
Rolling Orientation	90	0	90	0	90	0
Thickness(mm)	0.812	0.811	0.813	0.814	0.838	0.787
E(MPa)	197000	201000	229000	202000	215000	204000
Rp(MPa)	145	159	274	253	330	322
Rm(MPa)	303	307	423	417	436	459
r Average	1.897	1.526	1.568	1.006	1.388	0.972
n Average	0.227	0.223	0.178	0.188	0.157	0.166

Table 5.1.2: Mechanical data for 0.8mm material

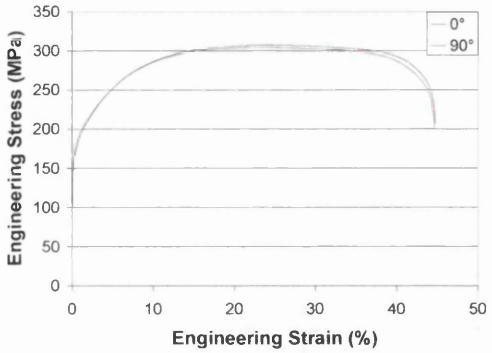

Figure 5.1.3a: Engineering stress/strain curve for 1.0mm GA 140

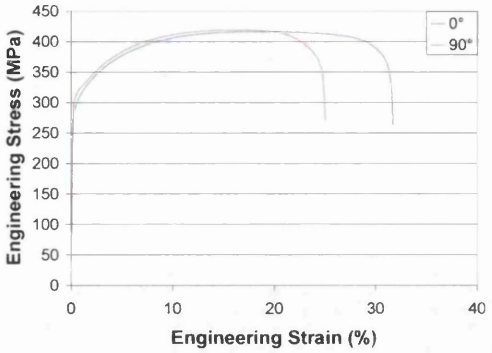

Figure 5.1.3b: Engineering stress/strain curve for 1.0mm GA 260

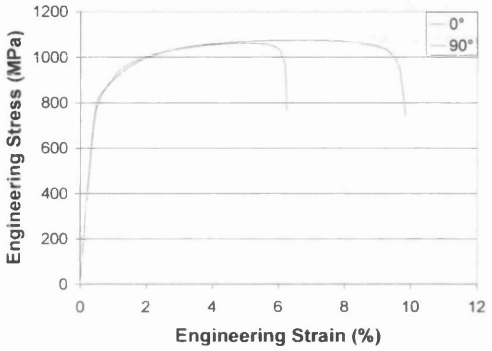

Figure 5.1.3c: Engineering stress/strain curve for 1.0mm DP 800

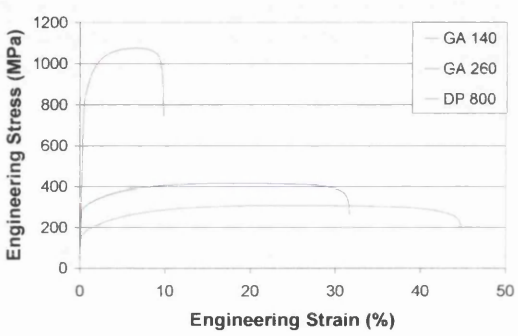

Figure 5.1.3d: Engineering stress/strain curve for 1.0mm material

Material ID	GA 140	GA 140	GA260	GA260	DP 800	DP 800
Rolling Orientation	90	0	90	0	90	0
Thickness(mm)	1.007	1.005	0.991	0.997	0.991	0.998
E(MPa)	201000	184000	214000	199000	206000	196000
Rp(MPa)	168	161	312	286	812	836
Rm(MPa)	305	308	419	417	1062	1076
r Average	2.361	1.853	1.341	1.042	0.99	0.99
n Average	0.229	0.236	0.155	0.172	0.141	0.141

Table 5.1.3: Mechanical data for 1.0mm material

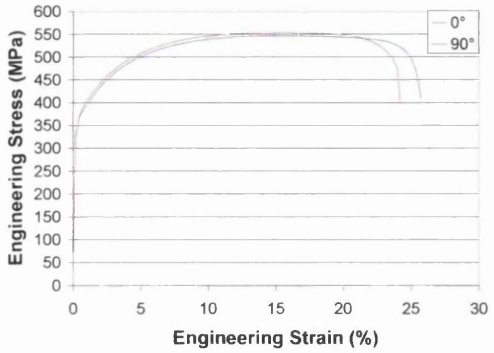

Figure 5.1.4a: Engineering stress/strain curve for 1.5mm DP 350

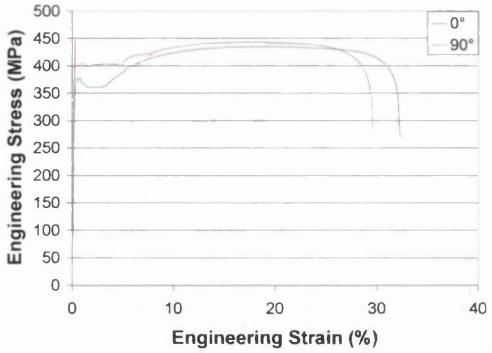

Figure 5.1.4b: Engineering stress/strain curve for 1.5mm DP 350 YP

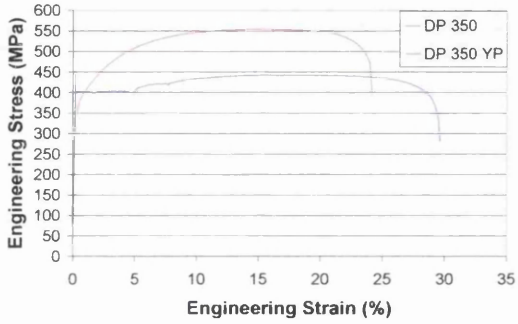

Figure 5.1.4c: Engineering stress/strain curve for 1.5mm material

Material ID	DP 350	DP 350	DP 350 YP	DP 350 YP
Rolling Orientation	90	0	90	0
Thickness(mm)	1.594	1.532	1.49	1.484
E(MPa)	219000	208000	215000	202000
Rp(MPa)	362	361	403	369
Rm(MPa)	554	547	443	435
r Average	0.801	0.581	1.053	0.725
n Average	0.15	0.151	0.164	0.173

Table 5.1.4: Mechanical data for 1.5mm material

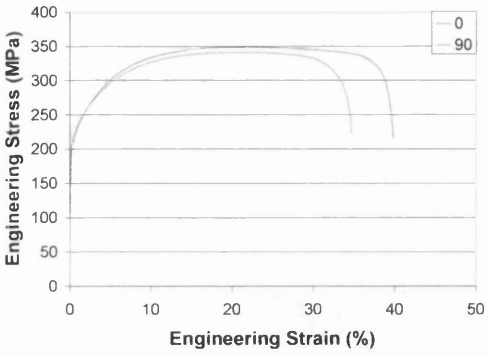

Figure 5.1.5a: Engineering stress/strain curve for 2.0mm GA 200

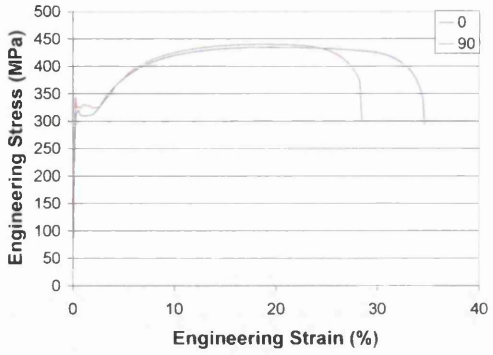

Figure 5.1.5b: Engineering stress/strain curve for 2.0mm GA 300

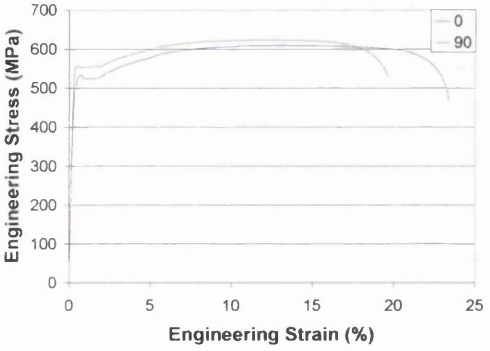

Figure 5.1.5c: Engineering stress/strain curve for 2.0mm CMn 500

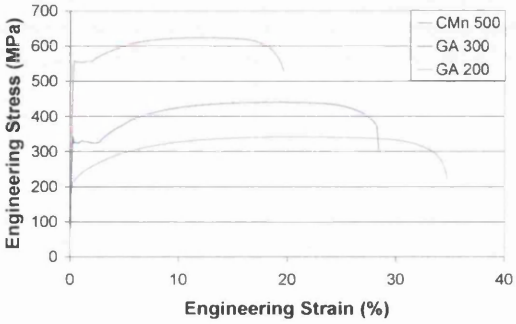

Figure 5.1.5d: Engineering stress/strain curve for 2.0mm material

Material ID	GA 200	GA 200	GA 300	GA 300	CMn 500	CMn 500
Rolling Orientation	90	0	90	0	90	0
Thickness(mm)	2.07	2.047	2.02	2.012	2.001	2.015
E(MPa)	194000	184000	198000	192000	213000	199000
Rp(MPa)	207	201	322	317	555	517
Rm(MPa)	332	340	442	436	624	610
r Average	0.876	0.769	1.052	0.867	0.833	0.666
n Average	0.199	0.196	0.187	0.188	0.117	0.125

Table 5.1.5: Mechanical data for 2.0mm material

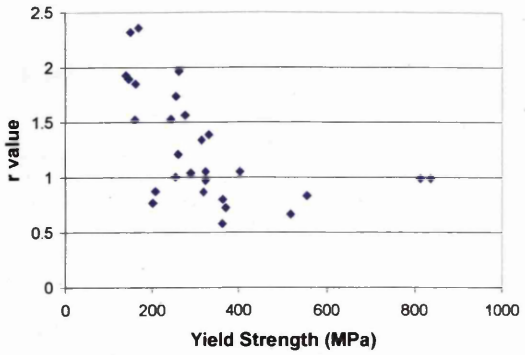

Figure 5.1.6: Selected steels r value vs yield strength

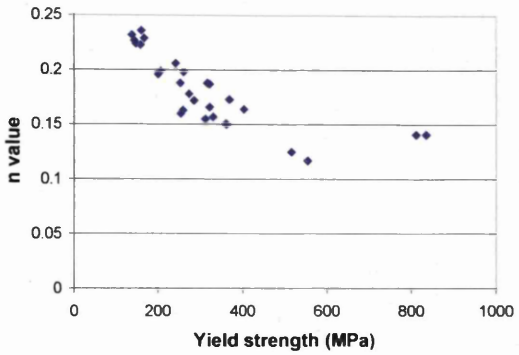

Figure 5.1.7: Selected steel n value vs yield strength

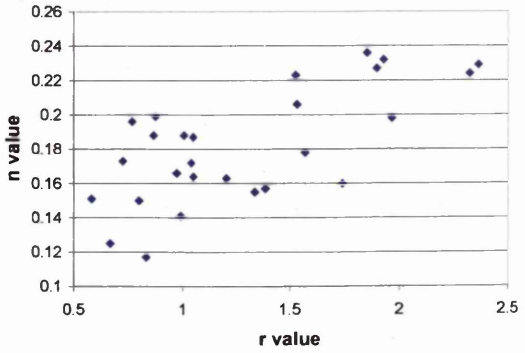

Figure 5.1.8: Selected steel n value vs r value

Material ID					
Element	**GA 140**	**GI IF 240**	**Nizec 260**	**DP 800**	**DP 350 YP**
Al-total (%)	0.04	0.039	0.072	0.042	0.04
Si (%)	0.007	0.007	0.005	0.522	0.005
P (%)	0.014	0.061	0.069	0.008	0.005
Cr(%)	0.012	0.018	0.014	0.03	0.02
Mn (%)	0.167	0.415	0.151	1.49	0.397
Ni (%)	0.015	0.025	0.02	0.044	0.042
Cu (%)	0.007	0.014	0.009	0.006	0.004
Mo (%)	<0.001	0.002	<0.001	0.01	0.012
Sn (%)	<0.001	<0.001	0.005	<0.001	<0.001
Ti (%)	0.03	0.019	0.002	0.004	<0.001
V (%)	<0.001	<0.001	<0.001	0.004	0.004
Nb (%)	0.017	0.019	0.002	0.016	0.026
C (%)	0.002	0.002	0.018	0.152	0.051
S (%)	0.009	0.01	0.01	0.002	0.005
N (ppm)	22	20	20	40	27
B (ppm)	<1	2	<1	<1	<1
Carbon Equivalent	0.0119	0.0252	0.0274	0.2475	0.0741

Table 5.1.6: Primary steels chemical analysis

Material ID			
	GA 140	GI IF 240	NIZEC 260
Al-bottom layer (%)	0.47	0.54	0.02
Al-upper layer (%)	0.4	0.52	0.02
Fe-bottom layer (%)	11.9	0.27	2.03/1.40
Fe-upper layer (%)	11.9	0.23	2.52/1.94
g LL bottom (g/m^2)	39.5	70	32
g LL upper (g/m^2)	40	75.5	30

Table 5.1.7: Coated primary steels coating analysis

Material ID	Yielding type	Largest Young's modulus	Largest Yield strength	Largest r value	Largest n value	Largest strain level
0.7mm GA140	continuous	0°		90°	0°	
0.7mm GI IF240	continuous	90°	90°	90°	0°	0°
0.7mm Nizec 260	continuous			90°		0°
0.8mm GA 140	continuous	0°	0°	90°		0°
0.8mm GA 260	continuous	90°	90°	90°	0°	90°
0.8mm GA300	continuous	90°	90°	90°	0°	90°
1.0mm GA 140	continuous	90°	90°	90°	0°	
1.0mm GA260	continuous	90°	90°	90°	0°	0°
1.0mm DP 800	continuous	90°	0°			0°
1.5mm DP 350	continuous	90°		0°		0°
1.5mm DP 350 YP	discontinuous	90°	90°	90°	0°	0°
2.0mm GA 200	continuous	90°		90°		0°
2.0mm GA 300	discontinuous	90°	90°	90°		0°
2.0mm CMn 500	discontinuous	90°	90°	90°	0°	0°

Table 5.1.8: Tensile samples general characterisation

5.2 Tube forming trials

5.2.1 Aims

The tube forming trials were carried out to gain a basic understanding of the tool forming process, it's influences on the sheet steel, and provide a comparison with the prototype production machine.

One of the major concerns with all manufacturing processes is that of repeatability, without which a manufacturing process is uneconomical to run. It is necessary to demonstrate both that the experimental project tool provided a stable platform to carry out experiments, and that the results from the formed tube bends, also needed to be translated into production guidelines, to ensure that a quality repeatable product was produced.

5.2.2 Results

5.2.2a Formed component measurements

Table 5.2.1 shows the results of this study. It can be seen that on average the 3D profilometer gave the lowest measurement of springback for the same sample. This would in fact relate to a higher amount of elastic recovery. Table 5.2.1 also shows the standard deviation for the two differing measurement methods investigated. It can be seen that the lower measurements of the two were on the 3D profilometer.

Further investigation of a series of pressings using the same tooling and process parameters can be seen in Table 5.2.1. The results for the mid point pressings were generated by the 3D profilometer. Comparison between the standard deviation of the 3D profilometer and of the mid pressings, show that the pressings are two orders of magnitude greater. If 3 standard deviations are considered on the 3D profilometer, then this would account for 99.7% of the readings, and this would still not be greater than the standard deviation shown during the mid pressing trial.

5.2.2b Formed component thickness measurement

From Table 5.2.2 it can be seen that the variation between the two average measurements is small at only 6μm. However, the standard deviation for the rounded micrometer is smaller by almost a half, at 6.578μm. Fig. 5.2.1 shows the plot for these results in conjunction with the measurement of an unformed sample and the BS EN 10305-3:2002 tube standard [5.2.1], which is required for these tubes. It is evident that both of the measured values for the formed component show a slight increase in material thickness compared to that of the unformed sample. Material thickening as a result of the forming operation is unlikely, as the bend radius is large, leaving the probable cause of variation to errors in the method of measurement.

5.2.2c Influence of blank position in tooling

From the results shown in Table 5.2.3 it can be seen that the two differing blank positions yield different results. It can be seen that the 5mm overhang position results in a smaller springback K value than for the sample placed directly beneath the hydraulic ram position. As a consequence the overhang sample would therefore have a greater amount of springback. The cause of this is likely to be the poor tool closure on the sample, as a result of an out of plane bending moment in the tooling, caused by the position of the actual blank.

5.2.2d Influence of material orientation

From Table 5.2.4 it can be seen that on average the blanks that were oriented at 0° direction gave the largest springback K value, which would translate to a smaller amount of springback. This result agrees with previous studies [5.2.2,5.3.3], of which is attributed to the higher yield strength in the 90° direction in comparison to that of the 0° direction

with respect to the rolling direction of the strip. It is also evident that the standard deviation for the 0° direction is smaller.
The resulting T test does however indicate that the mean of the two sets of samples are in fact likely to be from the same population.

5.2.2e Influence of tooling geometry influence

Table 5.2.5 shows the results of the investigation. It is evident that both the tools sets used gave good correlation to one another. There is a degree of difference in the amount of scatter in the result seen from an examination of variation in the standard deviation. This may be attributed to the method of forming (three point bend, greater plastic hinge) or the method of measurement, as the 3 step tooling is a more stable form to measure than a 5 step form. This scatter is within the standard deviation of the initial measurement trial data seen in Table 5.2.1 for the standard deviation of the mid point pressing.
The resulting T test does however indicate that the mean of the two sets of samples are in fact likely to be from the same population.

5.2.2f Influence of forming force

The results shown in fig. 5.2.2 suggest it would be useful to carry out further investigations into the cause and effect on the component of increasing the forming force. This type of springback mitigation tool is often used in situations where small bend radii are required. The process is known as coining [5.3.4]. The reported down side to this is the increased strain in the bend region. However, if coining can be used as a springback mitigation tool, and no ill effects are seen in a large diameter bend, then this would enable greater flexibility in the production process.
A secondary factor investigated during this trial was the effect that increased forming force had on the tool set displacement. Fig. 5.2.3 shows the relative displacement of the toolset when forming force is increased. It is evident that as forming force increases so the relative displacement of the tool set increases. This would be a point of concern when

controlling the forming process by means of displacement; program changes within the microprocessor would have to take account of this.
The likely cause of this displacement is the compressibility of the machine hydraulic fluid.

5.2.2g Influence of forming effects on material properties

One of the first observations during this investigation was that of material movement away from the front face of the punch tooling as the punch descended into the die tool. This can be seen in the highlighted portion of the material at the mid point span in fig. 5.2.4. This type of movement is the result of the initial yielding of the material at the mid point before any other section of material yields. Yield occurs at the mid point before other areas as the bending moment is highest at this point. This type of yield is seen in U bending operations, and also V bending operations where the V bend radius is large, and results in the bending operation turning from a three point bend to a four point bend [5.2.3]. In subsequent investigation this plastic yielding will be denoted as a plastic hinge effect.
The result of the mini tensile trials can be seen in fig. 5.2.5. From the results it is evident that an increase in the yield strength of the material does occur in the highlighted areas, see fig. 5.2.4. This would suggest that there is a detrimental effect on the overall formability of the material in these areas. The average yield strength measured in the unformed samples is 244.8 MPa, edge samples 247 MPa, and the plastic hinge samples 258.3 MPa. This relates to an increase of approximately 5% in the yield strength from unformed to hinge samples. If this is related back to the production of the tubular blank, it would suggest that in the formation of the tube, areas of localised greater yield strength would exist. This type of 'fingerprint' is also seen in ERW tubes, and is the result of the influence of the closure rollers. However, the ERW tube process leaves a 'fingerprint' that is of greater magnitude than that for the tubular blank. On average the yield strength from coil to tube for an aluminium killed mild steel increases from 171.6 MPa average yield in the coil to 213 MPa average for the tube. The variation in yield strength around

the tube would be approximately 51.3 MPa. In comparison from sheet to finished tube the tubular blank has seen an increase of 5% for this material tested, compared to which the ERW tube sees an increase of 20% for the more formable aluminium killed mild steel, with a further variation around the tube circumference. This variation from coil to tube would change dependent on the initial coil properties. It has been shown that as the yield strength of the coil increases so the disparity between coil and finished tube yield strength decreases [5.2.5].

The initial results from the hardness investigation are shown in fig. 5.2.6 which shows the Vicker's hardness for the plastic hinge and unformed areas, against the corresponding yield strength as measured from the mini tensile samples from the same area. It is evident from the results that the scatter encountered in the hardness results is greater than that seen from the mini tensile results as a consequence of which no trend is evident. It would appear that a 5% difference in yield strength as seen from the mini tensile results is to small a range to allow comparisons with the hardness of the material. Results obtained from the through thickness hardness traverse, fig. 5.2.7, 5.2.8 and 5.2.9 show that no trend emerges to indicate a difference at differing points of the formed component. This however does not mean that there is no variation, only that the method of investigation used was unable to distinguish any trend.

5.2.3 Discussion

From the result shown in this section it is possible to answer some of the original set of questions posed.

Of the methods investigated, for final formed component geometry measurement the 3D profilometer has been shown to return the most consistent results.

Thickness measurement is best carried out with a rounded face micrometer as this gives the smallest amount of deviation, although measurement scatter will still exist due to improper measurement techniques. This may be reduced further by increasing the sample rate.

Positioning of the blank in the tooling set is critical as this can led to irregularities in the formed component geometry, and therefore complications in production further downstream of the forming stage. This area of work needs to be investigated further, so that the production machine may be refined. i.e.at present the production machine has a degree of slack built into each of the stages. As the input material changes to more complex higher strength steels this slack will be used up, resulting in production blockages.

Material orientation

From the results shown it can be seen that material orientation influences the final formed component profile, although with an Interstitial Free steel a low degree of anisotropic behaviour is expected. As described previously the slack that is built into the production machine could at some stage be overwhelmed by a material which is strongly anisotropic. That is the machine may be capable of forming a sheet steel in the 0° rolling direction, but should this steel be strongly anisotropic then the forming parameters that are used in the 0° direction may be unsuitable for a forming process using the 90° orientation.

Tooling geometry influence

When considering the influence of tooling geometry on the finished component, from the results shown with the tooling remaining the same radius, and only the angle subtended by the blank during formation changing, there appears to be no influence on the final formed component geometry. However, it is likely that the plastic hinge effect would be greater, as the depth of die tooling for a 3-step forming tool is larger than that of a 5-step tool and therefore the angle subtended at the point of the plastic hinge would be greater for the 3-step tooling.
The effect of springback on tooling geometry can be seen in fig. 5.2.10. Although the deviation appears smaller the greater the number of steps taken, the accumulative effect is the same.

Forming force influence

From the results obtained it is clear that by increasing forming force, the amount of material springback is reduced. As mentioned in the results section this may be used as a mitigation tool for springback and enable a wider processing window for differing materials. Further investigation is required regarding the material influence, and also the capability of the production machine, and its ability to be upgraded if needed.

Forming effect on material properties

It can be said that the use of hardness as an indicator for formability in this instance is unwise. Even the use of mini tensile specimens taken in the longitudinal direction of the tube gives limited knowledge of the final tubes hydroformability, as hydroforming is essential a plane strain operation. However, it is an indication that can be linked to the formability of the final product.

5.2.4 Conclusion

The conclusions from this investigation are:-

1. 3D profilometer is the preferred choice of profile measurement
2. A rounded micrometer provides improved accuracy compared to a flat face for thickness measurement
3. Blank positioning in the tooling is critical, for more reliable results place the pressing in centre of the tooling below hydraulic ram
4. Sheet orientation has an effect on the degree of springback of the formed component
5. There is no effect on springback K value for same bend radius, greater bend angle

6. An increase in forming pressure increases the springback K value
7. The plastic hinge effect observed during bending, results in areas of high strain
8. The use of hardness as an indicator for a materials loss of formability after forming is unwise in this instance

5.2.5 References

5.2.1 BS EN 10305-3:2002, Steel tubes for precision applications-Technical delivery conditions, Part 3

5.2.2 Baljesh Mehmi, Engineering Doctorate Thesis, the Factors Influencing the Final Shape of Formed Components, University of Wales Swansea, 2002

5.2.3 H. Merkle, High Strength Steel Project, Automotive Applications, Customer Technical Centre, Welsh Technology Centre, Port Talbot, Internal Report

5.2.4 Sheet Steel Forming Handbook, Edition 1, SSAB Internal Document, October 1997

5.2.5 Roger Darlington, Engineering Doctorate Thesis, Tube Hydroforming of Steel for Automotive Applications, University of Wales Swansea, 2002

5.2.6 Figures / Tables

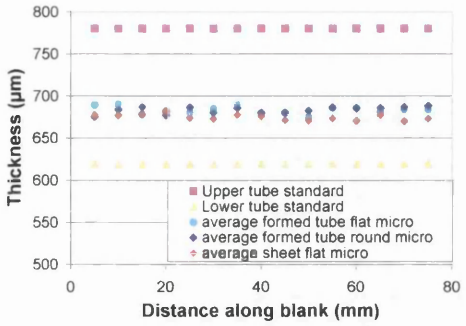

Figure 5.2.1: Thickness measurement comparative plot

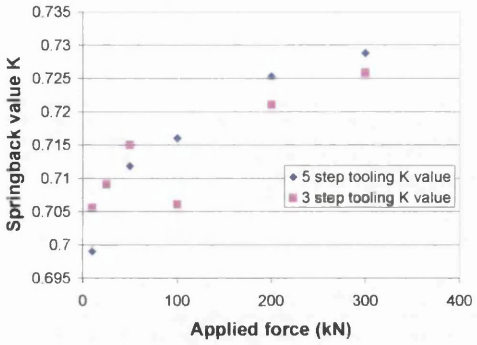

Figure 5.2.2: Differing tool set forming force investigation

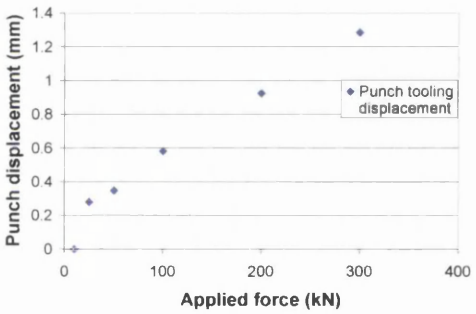

Figure 5.2.3: Punch displacement with increased forming force

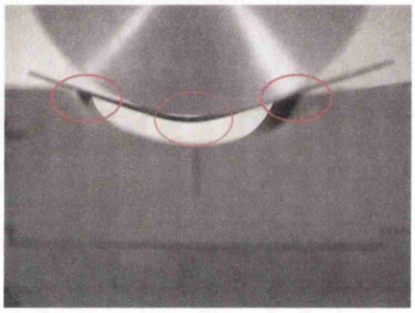

Figure 5.2.4: Areas under investigation during the effects of forming on material properties

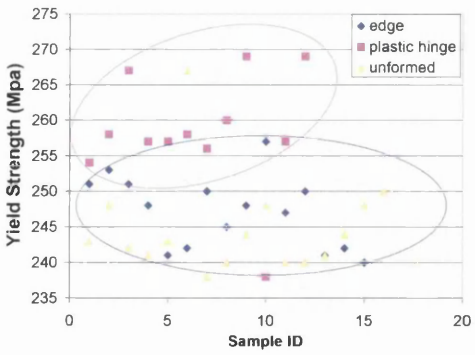

Figure 5.2.5: Mini tensile results from areas around the formed component

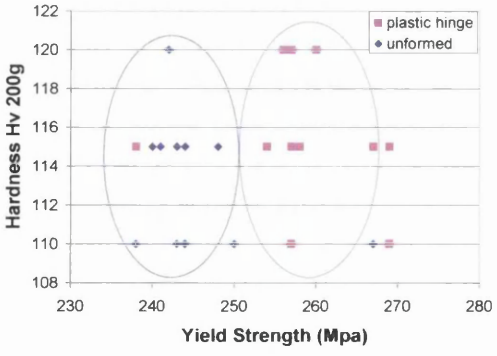

Figure 5.2.6: Hardness vs yield strength for formed samples

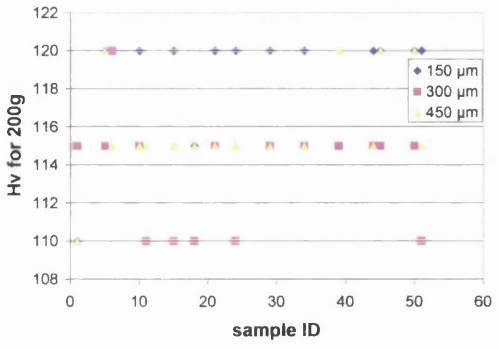

Figure 5.2.7: Hardness profile parent

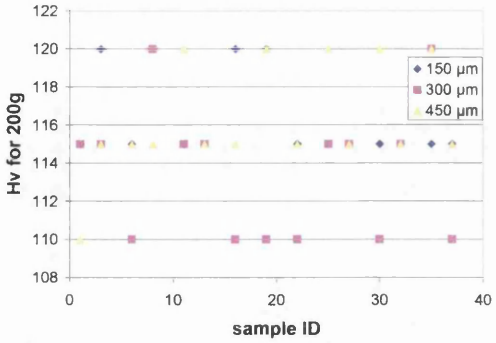

Figure 5.2.8: Hardness profile edge

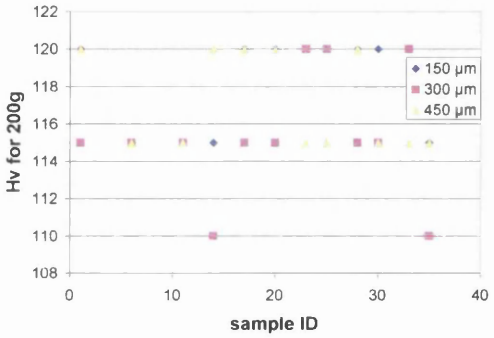

Figure 5.2.9: Hardness profile plastic hinge

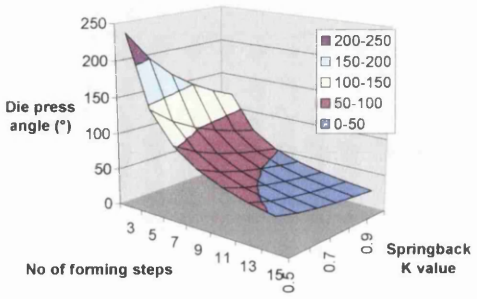

Figure 5.2.10: Influence of springback K value

Sample ID	Repeated 3D profiler	Repeated protractor	Mid point pressing
1	0.6955	0.6913	0.6914
2	0.6951	0.6977	0.7051
3	0.6947	0.7069	0.6951
4	0.6959	0.7192	0.7122
5	0.7045	0.7023	0.6991
6	0.6965	0.6932	0.7255
Average Springback K value	0.6970	0.7018	0.7047
Standard deviation	0.0037	0.0103	0.0126

*Table 5.2.1:*Results of the profile measurement selection trial

Sample ID	Flat faced micrometer thickness (μm)	Rounded face micrometer thickness (μm)
1	698	697
2	698	678
3	666	679
4	669	685
5	682	687
6	688	687
7	676	691
8	674	683
9	676	679
10	666	696
11	693	690
Average thickness (μm)	680.545	686.545
Standard deviation	12.094	6.578

Table 5.2.2: Results of the thickness measurement selection trial

Sample ID	Mid point pressing	5mm overhang
1	0.6914	0.6990
2	0.7051	0.6860
3	0.6951	0.7010
4	0.7122	0.6906
5	0.6991	0.6847
6	0.7255	0.6866
Average Springback K value	0.7047	0.6913

Table 5.2.3: Blank positioning results trial

Sample ID	Springback K value in 0° direction	Springback K value in 90° direction
1	0.6942	0.6914
2	0.6994	0.7051
3	0.7242	0.6951
4	0.7173	0.7122
5	0.7173	0.6991
6	0.7063	0.7255
Average value k	0.7098	0.7047
Standard Deviation	0.0117	0.0126
No. observations	6.0000	6.0000
Standard error of mean	0.0052	0.0056
Standard error of difference between means	0.0077	
t value	0.6617	

For Ttest of 10 degrees of freedom and probability of below 50% and highly likely that they come from the same population

Table 5.2.4: Material orientation results trial

Sample ID	5 step tooling k value	3 step tooling k value
1	0.6942	0.7039
2	0.6994	0.7111
3	0.7242	0.7036
4	0.7173	0.7080
5	0.7173	0.7030
6	0.7063	0.7132
Average value k	0.7098	0.7072
Standard Deviation	0.0117	0.0043
No. of observations	6.0000	6.0000
Standard error of mean	0.0052	0.0019
Standard error of difference between means	0.0056	
t value	0.4722	

For Ttest of 10 degrees of freedom and probability of below 50% and highly likely that they come from the same population

Table 5.2.5: Tooling geometry results trial

5.3 Tool tolerance

5.3.1 Aim

The aim of this investigation was to understand the influence of tooling tolerance, on roundness of tube and the springback K value.

5.3.2 Results / Discussion

The plastic hinge effect was observed in all the forming trials, see fig. 5.3.1
Table 5.3.1 shows the results of the forming trials for differing tool tolerances and the subsequent formed bend angle. Table 5.3.2 shows the calculated springback K value for the differing tool tolerances considered. From the results it can be seen that the 42.5 mm radius die gave the highest springback K values for each of the materials, due to the level of strain induced during forming of the part. With a reduction in tool radius a higher degree of strain is induced, increasing the proportion of plastic deformation in the part, subsequently reducing springback.
When the 0.7mm thick material is considered, it can be seen in Table 5.3.2 that a decrease in springback occurs when tooling designed for thicker materials is used. This is most probably due to the use of ill fitting tooling introducing a highly localised coined area at the centre of the die profile, which results in a reduction in springback. This effect has been used with success in other studies as a form of springback reduction [5.3.1, 5.3.2, 5.3.3]. The resulting decrease in the overall tube formability needs to be investigated further, as this may be a limiting factor on the amount of tool interchange that is permissible before final formability is compromised to an unwanted extent.
From Table 5.3.2 it can be also seen that for materials whose thickness is greater than the designed thickness for the tooling an increase in springback occurs. For the DP 800 steel studied this effect can be attributed to two factors. Firstly the bend radius is larger than the materials designed tooling, giving a decrease in bending strain during forming (increasing the elastic proportion leading to more springback). Secondly, 'lock-out' (observed) on the die walls, see fig. 5.3.2, resulting in poor punch and die closure, such

that the component is not fully formed. For the DP 350YP the observed cause of this effect was entirely attributable to tool lock-out.

This effect would require further investigation, into the point at which the formed component no longer conforms to the tube roundness standard EN 10305-3:2002(E). as this would be the limiting factor in this instance for the amount of tooling interchange which may occur.

5.3.3 Conclusion

From the results obtained during this investigation, several conclusions can be drawn.

1. A general decrease in springback occurs when die radius is kept constant, and punch radius is made smaller than that of the assigned punch radius for that material thickness. The result of this is likely to be a localised coined area at the centre of the die profile reducing the elastic proportion of strain in the material at that point, which leads to a decrease in springback.
2. Provided no tooling lock out occurred, forming of the general shape was noted for the material and tooling combinations investigated.
3. Further investigation is required into the amount of tooling interchange that is permissible whilst still conforming to the EN standard for tube roundness.
4. There is a need to investigate if the true cause of springback reduction is coining. If this is the case then further investigation is also needed to find the permissible level of coining, before a reduction in formability occurs.

5.3.4 References

5.3.1 C. Sudo, M. Kojima and T. Matsuoka, Some investigations on elastic recovery of press formed parts of high strength sheets, IDDRG International deep drawing research group, 23-27 Sept. 1974

5.3.2 H. Livatyali, H. C. Wu, T. Altan, Prediction and elimination of springback in straight flanging using computer-aided design methods. Part1 & Part 2 FEM predictions and tool design, Journal of Materials Processing Technology 66,1997/9/7

5.3.3 A. Forcellese, L. Frantini, F. Gabrielli, F. Micari, The evaluation of springback in 3D stamping and coining process. Journal of Materials Processing Technology 80-81, 1998 pg.108-112

5.3.5 Figures / Tables

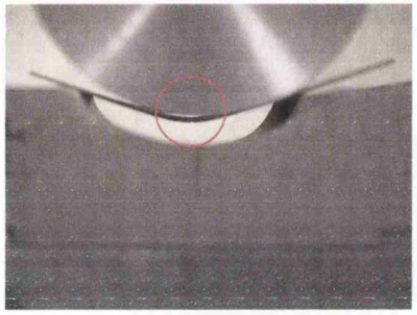

Figure 5.3.1: Plastic hinge effect observed in all the forming trials

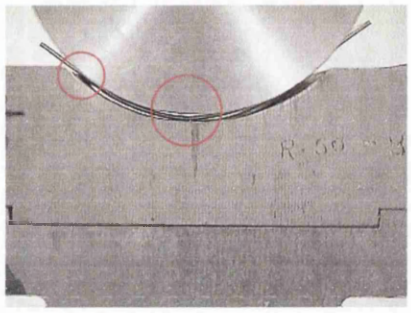

Figure 5.3.2: Material 'lock-out' observed on the die walls

Material	Punch Radius 49.3mm Die Radius 50mm/90°	Punch Radius 42.5mm Die Radius 43.5mm/90°	Punch Radius 48.5mm Die Radius 50mm/90°	Punch Radius 48mm Die Radius 50mm/90°
	Measured Radius of Pressing mm	Measured Radius of Pressing mm	Measured Radius of Pressing mm	Measured Radius of Pressing mm
0.7mm GA 140		48.12	56.17	55.33
0.7mm GI IF 240		56.67	66.85	66.10
0.7mm Nizec 260		56.86	67.78	66.81
1mm DP 800	152.46		144.25	144.26
1.5mm DP 350YP	64.31	52.01		58.26

Table 5.3.1: Results for the roundness and springback investigation using differing tooling

Material	Punch Radius 49.3mm Die Radius 50mm/90°	Punch Radius 42.5mm Die Radius 43.5mm/90°	Punch Radius 48.5mm Die Radius 50mm/90°	Punch Radius 48mm Die Radius 50mm/90°
	Springback K value	Springback K value	Springback K value	Springback K value
0.7mm GA 140	0.86	0.90	0.89	0.90
0.7mm GI IF 240	0.70	0.77	0.75	0.76
0.7mm Nizec 260	0.70	0.76	0.74	0.75
1mm DP 800	0.33	0.38	0.35	0.35
1.5mm DP 350YP	0.78	0.84	0.83	0.86

Table 5.3.2: Results of the springback investigation for the differing tool tolerances

5.4 Initial springback trials

MTS Experimentation

5.4a.1 Aim

The aim of this investigation was to press a range of mild steel, CMn, IF, DP steels using the experimental tooling available, and quantifying general trends from the results.
Tooling was made to fit the materials nominal thickness so that any ill fitting tooling interaction could be neglected.

5.4a.2 Results

The results for the experimental tooling on the MTS machine can be seen in Table 5.4a.1. As differing bend radii and material variations existed, the amount of comparable data for each nominal thickness was restricted to a maximum of 6 data plots, and four for the 1.5mm nominal thickness material.
From the results shown in Table 5.4a.1 it was possible to plot the interaction of yield strength versus springback K value for 2mm nominal material thickness. The results can be seen in fig. 5.4a.1. Both the 0° and 90° direction were measured, and from fig. 5.4a.1 it can be seen that as yield strength increases so the springback K value decreases.
From the results in Table 5.4a.1 it is possible to plot the interaction of material thickness with respect to the springback K value, see fig. 5.4a.2. Although a trend in fig. 5.4a.2 is evident this is not a true reflection of the relationship. The imposed strain level on the material would also affect the relationship (derived from material thickness and bend radius), and secondly the material's yield strength is not exactly the same. Fig. 5.4a.2 shows that as the material thickness reduces so the springback K value decreases, indicating an increase in springback.
Fig. 5.4a.3 shows the effect of strain level on springback, using the 0.7mm GI IF 240 material. The results show that as the level of strain in the material increases so the level of springback K value increases, with a consequential decrease in springback. The amount of strain has been calculated knowing the material thickness and bend radius.

It can been seen from fig. 5.4a.4 that when the yield strength of a material is normalised by considering the thickness (ex. 0.07mm GI IF 240 (90°) = 261/0.7 = 373) then when plotted against springback K value a trend is evident. This is only possible when the bend radius is the same, as a large differential of strain level would give a greater amount of scatter. It is evident from fig. 5.4a.4 that as the thickness normalised yield strength increases so the level of springback K value decreases.

5.4a.3 Discussion

Table 5.4a.2 shows the comparison between material orientation / yield strength / springback K value. Highlighted in yellow are the tests at a 90° to the rolling direction these conform to the general perception that transverse to rolling direction 0° the higher yield occurs, and due to an increase in yield strength also an increase in springback should occur, i.e. a reduction in springback K value. It can be seen from table 5.4a.2 that the majority of the steels tested show this characteristic. Table 5.4a.3, also highlights the materials that do not conform to this perception, which are highlighted in red. This may occur for differing reasons. When tensile tests were carried out an average of three were taken for each direction, for springback an average of six per sample were taken, giving a statistically more reliable value. Disparities in the tensile tests, springback tests, operator error and general result variance could be the cause for the errors, all of which are valid reasons.

Table 5.4a.3 shows the comparison of percentage difference between the yield strength of a material in differing directions when considering the springback K value. A negative value indicates that the 0° direction is greater in value than the 90° direction. The difference in yield strength did not exceed 10%, whilst the greatest differential in springback was 4%, which was noted for the DP 800 steel. From table 5.4a.3 it can be said that the difference between the yield strength in the two directions is not reflected to the same degree in the magnitude of difference noted in the springback K value. This can also be seen in the plot of these variables in fig. 5.4a.5. From these results it is possible also to see the degree of flexibility required by the tubular blank machine for these materials and forming conditions (4%). However, this figure will change with materials

of increased yield strength, anisotropy and bend radii, as these parameters will induce greater degrees of springback and differential directional behaviour. This highlights the need for the present investigation, as the trend for automotive hydroformed tubular blanks is for large diameter to thickness ratio tubes, of high and ultra high strengths [5.4a.1]. The general trend that can be compared to previous results is, an increase in yield strength results in an increase in springback, and decrease in material yield, results in a decrease in springback as noted by other authors. [5.4a.2, 5.4a.3]

5.4a.4 Conclusions

From the results obtained in this investigation it can be said that

1. An increase in yield strength results in a decrease in springback K value noted (increase in actual springback).
2. A decrease in material yield, results in an increase in the springback K value obtained.
3. An increase in the amount of strain in the bend results in an increase in the springback K value.
4. Normalisation of the material thickness is a convenient method of comparison for various materials being bent over the same radius.
5. In general the 90° direction of a cold rolled sheet steel material returns the lower value of springback K value (increase in actual springback).
6. The percentage difference in yield strength from differing directions of a material does not transfer to an equivalent difference in springback K value.

5.4a.5 References

5.4a.1 E. Bollinger, D. W. Jutten, Tubes for Hydroforming, proceedings of the interntional conference on hydroforming, fellbach, germany, October 1999, pg 97-103. ISBN 3-88355-285-2.

5.4a.2 B. Mehmi, Engineering Doctorate Thesis, the Factors Influencing the Final Shape of Formed Components, University of Wales Swansea, 2002

5.4a.3 H. Merkle, High Strength Steel Project, Automotive Applications, Customer Technical Centre, Welsh Technology Centre, Port Talbot, Internal Report

5.4a.6 Figures / Tables

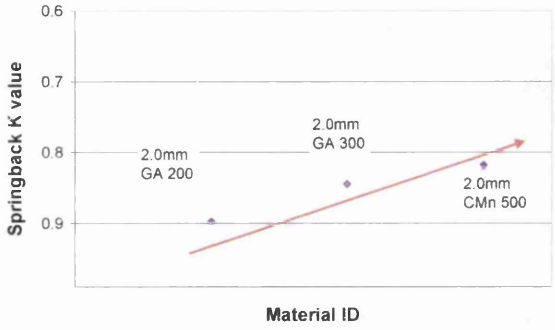

Figure 5.4a.1: MTS experimental results showing the effect of yield strength versus springback

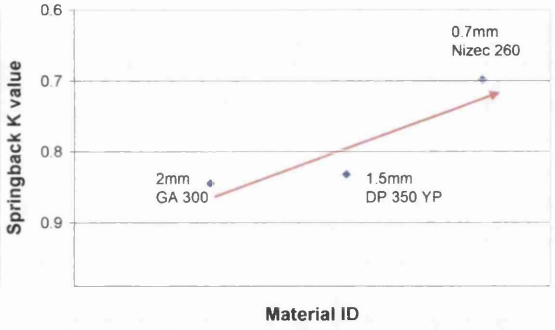

Figure 5.4a.2: MTS experimental results showing the effect of thickness versus springback

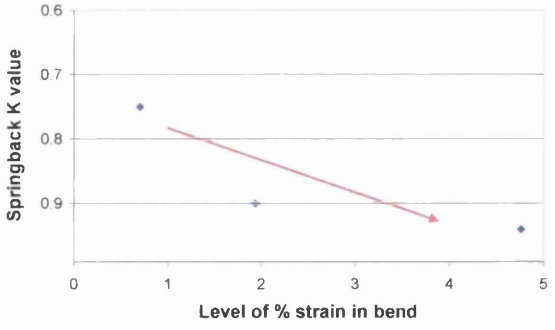

Figure 5.4a.3: MTS experimental results showing the effect of strain on springback using GI IF 240

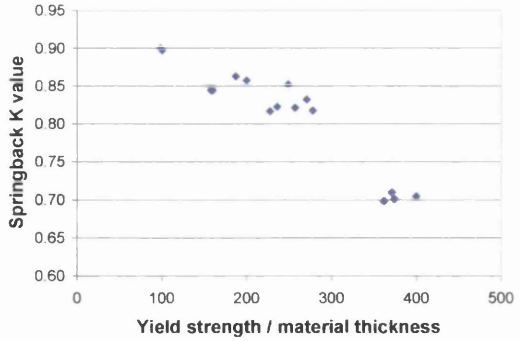

*Figure 5.4a.4:*MTS experimental results showing the effect of material thickness normalised yield strength on springback K value

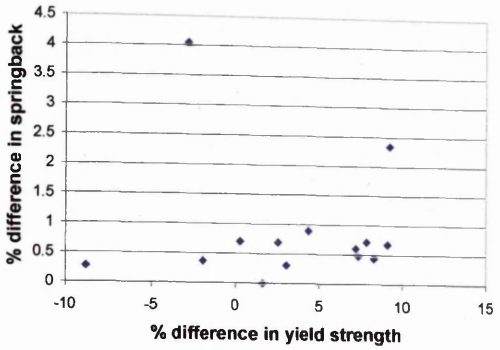

Figure 5.4a.5: Percentage difference between material yield strength and springback K value associated with sheet orientation

Material ID		Thickness (mm)	E (MPa)	Rp (MPa)	Rm (MPa)	r Average	n Average	Tool radius (mm)	Nuetral Radius (mm)	Springback K value
GA140	90°	0.747	194382	149	305	2.322	0.224	50	49.6265	0.8575
GA140	0°	0.744	210802	139	308	1.928	0.232	50	49.6280	0.8627
GI IF 240	90°	0.653	212187	261	373	1.966	0.198	50	49.6735	0.7047
GI IF 240	0°	0.653	206901	242	376	1.532	0.206	50	49.6735	0.7098
Nizec 260	90°	0.703	215713	254	385	1.739	0.16	50	49.6485	0.6984
Nizec 260	0°	0.693	214026	259	395	1.211	0.163	50	49.6535	0.7010
GA 140	90°	0.812	197000	145	303	1.897	0.227	18.5	18.0940	0.9309
GA 140	0°	0.811	201000	159	307	1.526	0.223	18.5	18.0945	0.9335
GA 260	90°	0.813	229000	274	423	1.568	0.178	18.5	18.0935	0.8754
GA 260	0°	0.814	202000	253	417	1.006	0.188	18.5	18.0930	0.8793
GA300	90°	0.838	215000	330	436	1.388	0.157	18.5	18.0810	0.8629
GA300	0°	0.787	204000	322	459	0.972	0.166	18.5	18.1065	0.8690
GA 140	90°	1.007	201000	168	305	2.361	0.229	43.5	42.9965	0.8840
GA 140	0°	1.005	184000	161	308	1.853	0.236	43.5	42.9975	0.8920
GA260	90°	0.991	214000	312	419	1.341	0.155	43.5	43.0045	0.8146
GA260	0°	0.997	199000	286	417	1.042	0.172	43.5	43.0015	0.8202
DP 800	90°	0.991	206000	812	1062	0.99	0.141	43.5	43.0045	0.3762
DP 800	0°	0.998	196000	836	1076	0.99	0.141	43.5	43.0010	0.3921
DP 350	90°	1.594	219000	362	554	0.801	0.15	50	49.2030	0.8167
DP 350	0°	1.532	208000	361	547	0.581	0.151	50	49.2340	0.8225
DP 350YP	90°	1.49	215000	403	443	1.053	0.164	50	49.2550	0.8320
DP 350YP	0°	1.484	202000	369	435	0.725	0.173	50	49.2580	0.8520
GA 200	90°	2.07	194000	207	332	0.876	0.199	50	48.9650	0.8972
GA 200	0°	2.047	184000	201	340	0.769	0.196	50	48.9765	0.9000
GA 300	90°	2.02	198000	322	442	1.052	0.187	50	48.9900	0.8444
GA 300	0°	2.012	192000	317	436	0.867	0.188	50	48.9940	0.8444
CMn 500	90°	2.001	213000	555	624	0.833	0.117	50	48.9995	0.8175
CMn 500	0°	2.015	199000	517	610	0.666	0.125	50	48.9925	0.8214

Table 5.4a.1: Springback results for the MTS experimental tooling

Material ID	Orientation	Yield Strength Rp(MPa)	Springback K value
GA140	90°	149	0.8575
GA140	0°	139	0.8627
GI IF 240	90°	261	0.7047
GI IF 240	0°	242	0.7098
Nizec 260	90°	254	0.6984
Nizec 260	0°	259	0.7010
GA 140	90°	145	0.9309
GA 140	0°	159	0.9335
GA 260	90°	274	0.8754
GA 260	0°	253	0.8793
GA300	90°	330	0.8629
GA300	0°	322	0.8690
GA 140	90°	168	0.8840
GA 140	0°	161	0.8920
GA260	90°	312	0.8146
GA260	0°	286	0.8202
DP 800	90°	812	0.3762
DP 800	0°	836	0.3921
DP 350	90°	362	0.8167
DP 350	0°	361	0.8225
DP 350YP	90°	403	0.8320
DP 350YP	0°	369	0.8520
GA 200	90°	207	0.8972
GA 200	0°	201	0.9000
GA 300	90°	322	0.8444
GA 300	0°	317	0.8444
CMn 500	90°	555	0.8175
CMn 500	0°	517	0.8214

Table 5.4a.2: Springback results for the MTS experimental tooling in conjunction with material orientation and yield strength.

Material ID	% Difference Yield Strength	% Difference Springback K value
GA140	7.1942	0.6063
GI IF 240	7.8512	0.7185
Nizec 260	-1.9305	0.3710
GA 140	-8.8050	0.2759
GA 260	8.3004	0.4403
GA300	2.4845	0.6949
GA 140	4.3478	0.8969
GA260	9.0909	0.6776
DP 800	-2.8708	4.0494
DP 350	0.2770	0.7052
DP 350YP	9.2141	2.3474
GA 200	2.9851	0.3086
GA 300	1.5773	0.0000
CMn 500	7.3501	0.4752

Table 5.4a.3: Percentage difference between material yield strength and springback K value associated with sheet orientation

V bend Investigation

5.4b.1 Aims

The aim of this investigation was to build on the initial characterisation trials which concentrated on large radius bends using the MTS experimental tooling, by using a V bend test rig to enable the study of smaller radii bends.

Four of the primary steel materials were tested, in conjunction with material data obtained from a similar springback trial being carried out at the Corus Automotive Application group by Merkle [5.4b.1].

This was then expanded further so that data from both sets of results were analysed together to see if any further trend other that those previously seen could be extracted.

5.4b.2 Results

Table 5.4b.1 shows the results of both experiments carried out in this investigation and also that of Merkle, the italic text shows the results obtained by Merkle. The plot of yield strength versus springback K value resulting from the experiments can be seen in fig. 5.4b.1. and as seen from previous work, section 5.4a. The trend of increasing yield strength with a decrease in springback K value was observed again. It is possible to further refine these results by normalising the yield strength by the material thickness, this can be seen in fig. 5.4b.2. Fig. 5.4b.2 differs from fig. 5.4b.1 in that the scatter in results is reduced. In comparison to fig. 5.4b.1 it can be seen that the extreme point within the graph (highest yield strength/material thickness) no longer appear to be in line with the other results, and a tailing off appears to be evident.

In fig. 5.4b.3 it can be seen that when a selection of the previous results from the MTS investigation are compared to those gained in the V bend experiment, a differing trend is noted for each set. It can be seen that the results obtained from the V bend test result in a trend which is shallower in gradient than that obtained from the MTS investigation. The difference between the two studies is that the bend radius is smaller, and therefore the level of strain in the material walls during pressing is greater in the V bend experiments.

As stated previously this indicates that as the strain level increases the effect of springback is reduced.

Table 5.4b.2 shows the complete set of data from both the MTS and V bend experiments in addition to that of Merkle's results which are shown in italic print. From these results further interrogation of the material trends seen in the first investigation of material characterisation can take place.

Fig. 5.4b.4 shows the results of the comparison between the yield strength of a material and the r average value. It can be seen that depending on the material type the trend appears to be different. 'Other grade' materials that represent those that have not been designated as DP or CMn show a distinct trend of decreasing r average value with an increase in yield strength. A transition then appears to take place were the steels designated as DP and CMn level off in value, remaining in general below the value of 1. It would not be wise to try and read further into these results unless complete material characterisation has taken place, as it has been shown that material designation by manufacturer is often generalised, and is not a true reflection on the materials properties [5.4b.2]. This was seen in the DP 350 YP material in this investigation, which by tensile test alone showed similar mechanical properties to CMn steels rather than DP as stated in the sales and supply literature [5.4b.3].

From fig. 5.4b.5 it can be seen that steel classification also is reflected in comparison between the yield strength of a material and the average n value. Fig. 5.4b.5 shows that the steels that have been labelled as DP appear to have an increased average n value than steels of CMn and other types.

Fig. 5.4b.6 shows the comparison between the average r value of a material, and the average n value. It can be seen that the higher strength material (DP, CMn) have both smaller n average and r average values. As stated previously in the results section of material characterisation section 5.1 this is likely to be the consequence of the grain size of the materials.

5.4b.3 Discussion

The initial results from this study exhibit the same trends as noted in the general MTS experiment, that of increased yield strength / increased springback, increased material thickness / decreased springback. The latter results discussing the r and n value trends, seen when both results are combined give an insight into the behaviour of differing material types, their classification and possible future areas for research.

5.4b.4 Conclusions

From the results obtained during this investigation the following conclusions can be made: -

1. Increasing yield strength increases the springback of a material.
2. It appears that as the yield strength / material thickness ratio of a material increase springback increases.
3. As strain level increases the effect of springback is reduced.
4. Further investigation is needed for full material characterisation, so that intrinsic properties such as r and n values behaviour can be assigned to differing types of steels.

5.4b.5 References

5.4b.1 H. Merkle, High Strength Steel Project, Automotive Applications, Customer Technical Centre, Welsh Technology Centre, Port Talbot, Internal Report

5.4b.2 N. Beynon, Private Correspondance, Customer Technical Centre, Welsh Technology Centre, Port Talbot

5.4b.3 SSAB Dual Phase Steels Sales Literature

5.4b.6 Figures / Tables

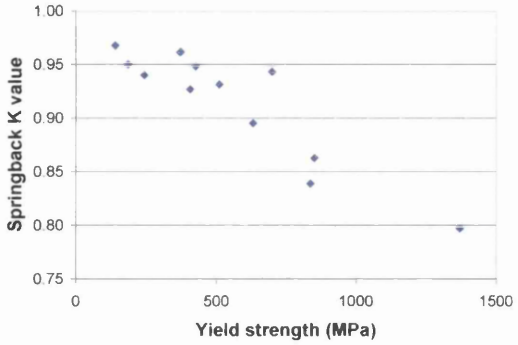

Figure 5.4b.1: V bend experimental results showing the effect of yield strength versus springback incorporating Merkle's work

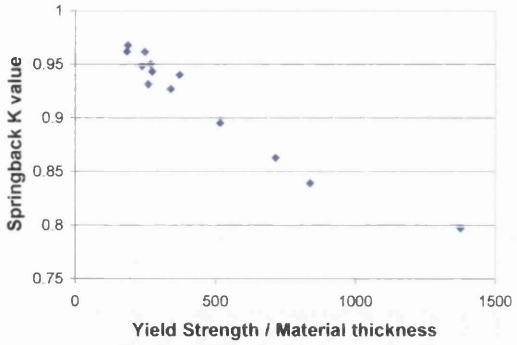

Figure 5.4b.2: V bend experimental results showing the effect of material thickness normalised yield strength on springback K value incorporating Merkle's work

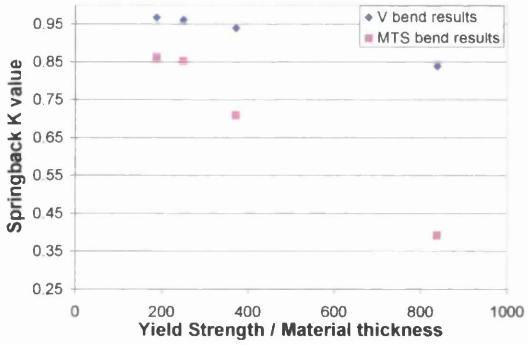

Figure 5.4b.3: Comparison between previously obtained MTS results plotted against results obtained from V bend using same material

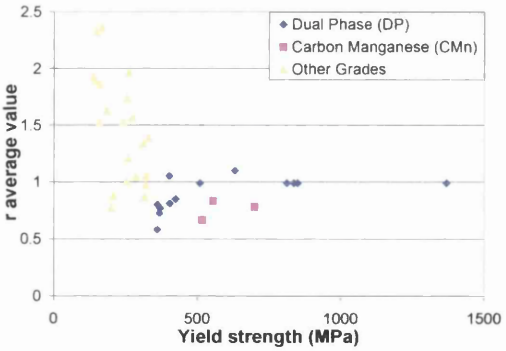

Figure 5.4b.4: Comparison between the yield strength of a material and the r average value

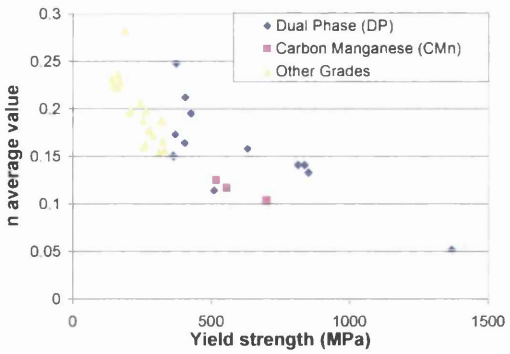

Figure 5.4b.5: Comparison between the yield strength of a material and the n average value

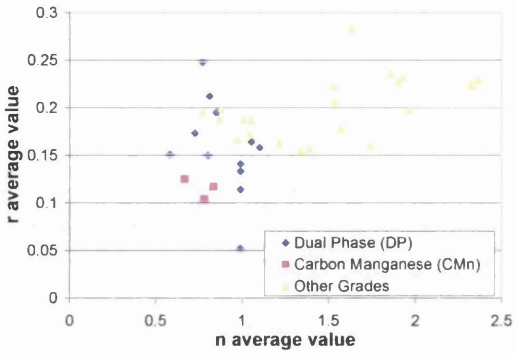

Figure 5.4b.6: Comparison between the r average value of a material and the n average value

Material ID	Orientation	Thickness (mm)	E (MPa)	Rp (MPa)	Rm (MPa)	r Average	n Average	Tool radius	Neutral Radius	Springback K value
GA140	0°	0.744	210802	139	308	1.928	0.232	7	7.3735	0.9680
GI IF240	0°	0.653	206901	242	376	1.532	0.206	7	7.3265	0.9402
DP 800	0°	0.998	196000	836	1076	0.99	0.141	7	7.4955	0.8392
DP 350YP	0°	1.484	202000	369	435	0.725	0.173	7	7.7450	0.9617
DP 400	*45*	*1.191*	*188000*	*405*	*671*	*0.81*	*0.212*	*7*	*7.5955*	*0.9271*
DP 400	*45*	*1.782*	*171000*	*425*	*653*	*0.85*	*0.195*	*7*	*7.891*	*0.9485*
DP 350	*0*	*2.025*	*172000*	*371*	*609*	*0.77*	*0.248*	*7*	*8.0125*	*0.9621*
DP 630	*90*	*1.223*	*184000*	*631*	*836*	*1.1*	*0.158*	*7*	*7.6115*	*0.8954*
DP 500	*90*	*1.956*	*181000*	*509*	*812*	*0.99*	*0.114*	*7*	*7.978*	*0.9315*
DP 850	*45*	*1.191*	*176000*	*850*	*1089*	*0.99*	*0.133*	*7*	*7.5955*	*0.8630*
DP 1300	*90*	*0.996*	*187000*	*1369*	*1489*	*0.99*	*0.052*	*7*	*7.498*	*0.7973*
CMn 700	*90*	*2.545*	*176000*	*699*	*776*	*0.78*	*0.104*	*7*	*8.2725*	*0.9434*
GA 180	*90*	*0.688*	*191000*	*185*	*311*	*1.63*	*0.283*	*7*	*7.344*	*0.9503*

Table 5.4b.1: Springback results for the V bend tooling incorporating Merkle's work

Material ID	Orientation	Thickness (mm)	E (MPa)	Rp (MPa)	Rm (MPa)	r Average	n Average	Tool radius (mm)	Neutral Radius (mm)	Springback K value
GA140	90°	0.747	194382	149	305	2.322	0.224	50	49.6265	0.8575
GA140	0°	0.744	210802	139	308	1.928	0.232	50	49.6280	0.8627
GI IF240	90°	0.653	212187	261	373	1.966	0.198	50	49.6735	0.7047
GI IF240	0°	0.653	206901	242	376	1.532	0.206	50	49.6735	0.7098
Nizec 260	90°	0.703	215713	254	385	1.739	0.16	50	49.6485	0.6984
Nizec 260	0°	0.693	214026	259	395	1.211	0.163	50	49.6535	0.7010
GA 140	90°	0.812	197000	145	303	1.897	0.227	18.5	18.0940	0.9309
GA 140	0°	0.811	201000	159	307	1.526	0.223	18.5	18.0945	0.9335
GA 260	90°	0.813	229000	274	423	1.568	0.178	18.5	18.0935	0.8754
GA 260	0°	0.814	202000	253	417	1.006	0.188	18.5	18.0930	0.8793
GA300	90°	0.838	215000	330	436	1.388	0.157	18.5	18.0810	0.8629
GA300	0°	0.787	204000	322	459	0.972	0.166	18.5	18.1065	0.8690
GA 140	90°	1.007	201000	168	305	2.361	0.229	43.5	42.9965	0.8840
GA 140	0°	1.005	184000	161	308	1.853	0.236	43.5	42.9975	0.8920
GA260	90°	0.991	214000	312	419	1.341	0.155	43.5	43.0045	0.8146
GA260	0°	0.997	199000	286	417	1.042	0.172	43.5	43.0015	0.8202
DP 800	90°	0.991	206000	812	1062	0.99	0.141	43.5	43.0045	0.3762
DP 800	0°	0.998	196000	836	1076	0.99	0.141	43.5	43.0010	0.3921
DP 350	90°	1.594	219000	362	554	0.801	0.15	50	49.2030	0.8167
DP 350	0°	1.532	208000	361	547	0.581	0.151	50	49.2340	0.8225
DP 350YP	90°	1.49	215000	403	443	1.053	0.164	50	49.2550	0.8320
DP 350YP	0°	1.484	202000	369	435	0.725	0.173	50	49.2580	0.8520
GA 200	90°	2.07	194000	207	332	0.876	0.199	50	48.9650	0.8972
GA 200	0°	2.047	184000	201	340	0.769	0.196	50	48.9765	0.9000
GA 300	90°	2.02	198000	322	442	1.052	0.187	50	48.9900	0.8444
GA 300	0°	2.012	192000	317	436	0.867	0.188	50	48.9940	0.8444
CMn 500	90°	2.001	213000	555	624	0.833	0.117	50	48.9995	0.8175
CMn 500	0°	2.015	199000	517	610	0.666	0.125	50	48.9925	0.8214
GA140	0°	0.744	210802	139	308	1.928	0.232	7	7.3735	0.9680
GI IF240	0°	0.653	206901	242	376	1.532	0.206	7	7.3265	0.9402
DP 800	0°	0.998	196000	836	1076	0.99	0.141	7	7.4955	0.8392
DP 350YP	0°	1.484	202000	369	435	0.725	0.173	7	7.7450	0.9617
DP 400	*45*	*1.191*	*188000*	*405*	*671*	*0.81*	*0.212*	*7*	*7.5955*	*0.9271*
DP 400	*45*	*1.782*	*171000*	*425*	*653*	*0.85*	*0.195*	*7*	*7.8910*	*0.9485*
DP 350	*0*	*2.025*	*172000*	*371*	*609*	*0.77*	*0.248*	*7*	*8.0125*	*0.9621*
DP 630	*90*	*1.223*	*184000*	*631*	*836*	*1.1*	*0.158*	*7*	*7.6115*	*0.8954*
DP 500	*90*	*1.956*	*181000*	*509*	*812*	*0.99*	*0.114*	*7*	*7.9780*	*0.9315*
DP 850	*45*	*1.191*	*176000*	*850*	*1089*	*0.99*	*0.133*	*7*	*7.5955*	*0.8630*
DP 1300	*90*	*0.996*	*187000*	*1369*	*1489*	*0.99*	*0.052*	*7*	*7.4980*	*0.7973*
CMn 700	*90*	*2.545*	*176000*	*699*	*776*	*0.78*	*0.104*	*7*	*8.2725*	*0.9434*
GA 180	*90*	*0.688*	*191000*	*185*	*311*	*1.63*	*0.283*	*7*	*7.3440*	*0.9503*

Table 5.4b.2: Springback results for both the MTS experimental tooling and V bend tooling incorporating Merkle's work

5.5 Coining Investigation

5.5.1 Aims

The aim of this investigation is to study the effect of increasing forming pressure on the final formed component profile, and to quantify the loss of formability, noted.
The initial investigation was carried out on the 0.7mm GA IF 240 material. A subsequent investigation included those materials indicated as primary steels.

5.5.2 Results

From Table 5.5.1 it can be seen that as the sample width decreases the forming pressure increased, so the resultant radius of the formed component decreased. Figs. 5.5.1 a and b shows the resultant form of the pressed GI IF 240 samples of varying width as measured by the 3D profilometer.
Fig. 5.5.2a shows a plot of the springback K value against sample width. From fig. 5.5.2a it can be seen that the trend appears to follow a power law fit, this however is not the case as the reduction in strip width and subsequent material area is non linear. It can be said that as the width of the sample increases so the springback K value decreases indicating an increase in springback.
In fig. 5.5.2b the sample width is transformed into the actual forming pressure that is seen by the samples, the trend is that of a reduction in springback (increase in K value) with an increase in forming pressure, as mentioned previously. The resultant trend appears to take the form of a curve with a linear section followed by a non linear section. The two points relating to the 5mm and 10mm samples, are those in the non linear section.
Fig 5.5.2c is a repeated plot of fig. 5.5.2.b showing only the apparent linear section of the data. If a trendline for these data points is plotted, it can be seen that a linear fit exists and that the intercept of this trendline is at springback K value of 0.7231, which is within 2% of the recorded springback K value for this steel in section 5.2, with no purposely induced coining.
Thickness measurements were taken of the 5,10,15, and 20mm wide samples, generated by measuring both the inner and outer profile of the final formed component by using the 3D profilometer. Opposite sides of the formed component

were measured, and the results can be seen in figs. 5.5.3a-d. A positive displacement in the y axis is an indication of material thinning.

From fig 5.5.3a it can be seen that a definite thinning of the material has occurred during the forming operation. It is also evident that this thinning is non symmetrical, as the right and left hand profiles show, not only a difference in the degree of thinning but also the point of initial thinning. In figs. 5.5.3b,c and d it can be said that no thinning has taken place.

Table 5.5.2 shows the substrate thickness of the differing formed samples shown in figs. 5.5.3a-d measured by means of a microscope. From Table 5.5.2 it can be seen that the only sample which shows a reduction in the material substrate thickness is that of the 5mm sample, indicating that compressive yielding has taken place.

Fig. 5.5.4 shows the through thickness hardness profile of the 5mm sample in varying positions. From the results it can be seen that an increase in hardness has occurred in all areas of the material that has been formed. It would also appear that the hardness of the material at 150 microns is higher than from results taken closer to the surface. The general order of hardness is centre, right, left, then unformed, where the centre value is highest.

Figs. 5.5.4a-d show the hardness traverse of the 10-20mm samples, taken at various points along the formed components length.

From fig 5.5.4a it is evident that the material appears to have a slight increase in hardness as the distance from the substrate surface increases.

In fig 5.5.4b this same trend of hardness increasing as distance from substrate increases as seen in fig 5.5.4a is present, and a trend of material hardness increase with respect to increased forming pressure may be evident as it can be seen that the 15mm sample on average shows the largest values.

From fig. 5.5.4c it can be seen that the trend of increasing hardness with distance from substrate surface continues, with a more uniformed trend of forming force against material hardness becoming evident.

Fig 5.5.4d is much like that seen in figure 5.5.4b in that the trend of hardness to substrate depth is evident, but no real evidence of an influence of forming pressure on material hardness is evident. The values for the formed samples are on par with those of the unformed samples seen in fig. 5.5.4.

What can be said from figs. 5.5.4a-d is that the scatter associated with the measurement of hardness at the substrate surface is less than that seen at the other levels through the material thickness.

5.5.3 Discussion

From the results shown in Table 5.5.1 and fig 5.5.2a-c, it can be seen that an increase in forming pressure results in a reduction in final formed radius, indicating a reduction in springback.

It is also evident that a linear relationship between springback and forming pressure exists for the majority of the results. The exact point of transition between linear and non linear behaviour is unclear, but from fig. 5.5.2b and table 5.5.1 it can be seen to fall between 254 and 381 MPa forming pressure. Results shown in table 5.5.2 indicate that material deformation i.e. plastic flow only occurs in the 5mm sample (762 MPa forming pressure). It would therefore be unwise to conclude that the transition point is yielding in compression.

The true cause of the reduction in springback due to the increased forming load could be attributed to differing analogies and may also be the accumulation of these. For example:

Plane Strain Compression after plane strain bending

This analogy has one single factor that may not sit well with forming and material experts, and that is the analogy that the bending plane remains in a state of plane strain throughout the application of increase forming pressure. For this to be possible the fit up of tooling onto material would have to be excellent but also allow plane strain to take place, and also the punch and die set would have to be totally rigid. Work in this field was first carried out by Bridgman and latter carried on by Baranski, then further developed by Hill [5.5.1]. However, this only considered plane strain compression as a single entity and not as an incremental component of forming, therefore the literature on this amalgamation of differing forming conditions is extremely limited.

This analogy would suite the conditions of the experimental procedure well. Proof however is lacking in certain areas. Considering the results in fig. 5.5.2b as

compressive plane strain yielding (neglecting the Bauschinger effect) would occur around 279 MPa, but no plastic deformation is evident until the sample was formed with a pressure of 762 MPa. This may be attributed to material variations, experimental measurement error, but most likely high static friction on the tooling surface creating a hydrostatic stress condition, resulting in a higher compressive load being needed for yielding to occur.

Combined bending and tension of sheet

Once again this type of analogy has factors associated with it that cause concern in its applicability in this scenario. As the analysis of plastic bending is non linear, the order in which the tension and the moment are applied may influence the results. The greatest error factor in this analogy is the ability for a tensile load to be applied on the sample after bending has taken place. This would only occur if the tooling was sufficiently ill fitting to enable material lock out in the die walls while the punch is still able to induce a forming force onto the material creating a tensile load across the material width. The consequence of this type of forming is a reduction in springback as the through thickness stress is transformed into a totally plastic tensile component. This type of forming is often seen in industries where large formed radii are needed as in aircraft skin manufacture. Other factors such as the movement of the neutral axis to the inside of the bend curvature will also take place.

Reverse bending after initial bending

It is unlikely that this type of scenario takes place in a pure form, that is for bending to take place and then bend in the opposite direction to follow in the next step. This is often the case when considering the flow of material over draw beads during the forming of parts associated with deep drawing scenarios. However, the principle of reverse bending may be considered, one in which the stress of a part is formed in on manner i.e. tension and then completed in compression, thus the material will see a tensile plastic forming force followed by a plastic compressive force, most likely to occur in the vicinity of the tooling edge. Towards the end of the forming operation as the material flows into the die cavity, lock out on the outer edges would have to occur, giving a tensile component, then when the tooling has closed the application of the

compressive component would then take place. This would lead to a reduction in the yielding characteristics of the material (Bauschinger effect).

The true cause of the reduction in the amount of springback will only be deduced by further in depth research, but even then caution will need to be taken as any assumptions in the initial outset of the experiments may in fact hinder the ability to find the true cause. Finite element investigation may be the most promising method of investigation. However physical evidence to corroborate the results may be hard to produce as the bending strains are small and physical changes will be very small.

When consideration is given to the results in fig. 5.5.3a-d and Table 5.5.2 it can be seen that the correlation between the two differing measurement methods is relatively good. Where the 3D profilometer showed a material thinning of 0.124mm on the right and 0.084 on the left, microscopic measurement showed a reduction of 0.065mm on the right and 0.05mm on the left. What must be remembered here is that the coating thickness was also included in the 3D profilometer measurement, and that the degree of error in the profilometer measurement would be expected to be higher than that of the microscopic measurement. Tool movement is the likely cause of the difference between the left and right measurements, causing a greater amount of forming pressure on the one surface in comparison to the other. This would therefore be an area of concern when forming at such high pressures, as tool movement would not only result in disparities on the finished component, but also induce bending moments on the punch tooling stem, for which the results could be catastrophic.

From the results obtained in fig. 5.5.4 and 5.5.4a-d it can be said that on thinning the hardness of a material increases. This would be expected as strain hardening would have taken place. However, this increase in hardness appears not to be so evident in none thinned samples even though the material has undergone plastic deformation in the formation of the component. The only one area that appears to conform to published data [5.5.2] is the hardness profile of the centre for the 10,15, and 20mm samples. Here was noted a general trend of increasing hardness level with increasing forming pressure. In general, it would be unwise to use hardness level as a precise indicator of the amount of stress a component has encountered while being formed, due to the large amount of scatter that is apparent from the results obtained. Hardness would be more suitable in this instance as a general trend indicator. A better approach would have been to take mini tensile samples along the sample length. This approach

however was not possible as the testing machine had a limited testing capability of 300kN, and the only other method possible to increase forming pressure was to reduce the sample area.

It is evident from fig. 5.5.4, and 5.5.4a-d that as the distance from the substrate increased so the hardness value increased. From bending theory concerning small bend radii the opposite would be expected, but as this is a situation of large bend radius, and therefore low strain levels, the influence of strain induced hardness is small and the trend would in all likelihood be attributed to the parent material (also evident in unformed sample). As the material is a cold rolled product it is possible that during the annealing process a reduction in substrate hardness occurred. In comparison to the results seen in the initial investigation these are elevated slightly, but only by 7 Hv.

Further material coining trials

Fig. 5.5.5 shows the results for the investigation into coining of the primary steels. As with fig. 5.5.2c only the linear proportion of the springback K value vs forming pressure curve was considered. From the results obtained it can be seen that a trendline fit exists in the various materials, and the intercepts are within a couple of percent of the springback results for samples which have not been coined, see Table 5.5.3. Of the materials tested in fig 5.5.5 the DP 800 has the greatest amount of scatter associated with it. This is likely to be an error associated with the measurement of a material of high inherent springback characteristic. From Table 5.5.3 it is also possible to see that the majority of the springback K values for the trendline intercepts are in fact higher than those of the results for samples which have not been coined suggesting that a degree of coining has taken place in the previous investigations.

Further investigation into the accumulative effects of differing forming conditions was carried out. The effect of coining was investigated on tensile samples for each of the materials. Figs. 5.5.6a-e show the engineering stress/strain curves for tensile samples that have undergone compression out of plane (perpendicular) to the tensile sample. From the results it can be seen that there is no effect of compressing a tensile specimen out of plane before tensile testing.

It is possible to say with a degree of confidence that the effects of coining on all the materials tested in fig 5.5.5 showed that an increase in forming pressure decreases the amount of springback noted for a material. There also exists a linear trend between the springback K value and the forming pressure encountered by the material during coining. It is possible to fit a trendline to the linear section of the curves and find the springback K value of the material when no coining occurs (intercept of trendline). From these results it would be possible to increase the forming window of the tooling (i.e. for differing materials). The capability of the forming machine would have to be sized to a force appropriate for a reduction of springback for the strongest thinnest material.

Out of plane compression on tensile specimens before deformation does not affect the tensile properties of the material. This would be expected as the compressive force has not caused the material to yield. Only elastic stress is induced and this is removed when the sample is taken away from press prior to testing.

5.5.4 Conclusions

1. An increase in forming pressure leads to a decrease in springback.
2. A limited linear trend exists between springback and forming pressure.
3. It is possible to deduce the springback K value of a material prior to the onset of coining from these linear trends.
4. An increase in material hardness was evident in the samples that underwent thinning (compressive yield).
5. Material hardness appears to increase the further away from the substrate surface the measurement is taken. This would appear to be as a consequence of the cold rolling annealling process.
6. The introduction of out of plane compressive forces on tensile specimens before subsequent testing has no effect so long as compressive yielding does not occur.
7. Further investigation is needed to confirm the mechanism by which springback is reduced.
8. Appropriate machine sizing is needed to increase coining capabilities.

5.5.5 References

5.5.1 R. Hill, The mathematical theory of plasticity, The Oxford Engineering Science Series, Oxford University Press, 1989, ISBN 0-19-856162-8

5.5.2 Prof Lange, K, Handbook of Metal Forming McGrall-Hill, Inc, 1985. ISBN 0-87263-457-4

5.5.6 Figures / Tables

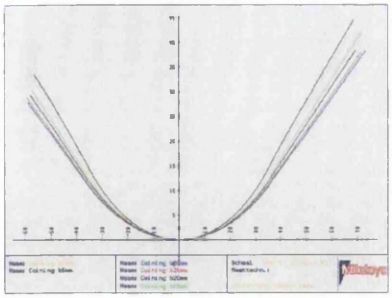

Figure 5.5.1a: Resultant form of the pressed component as measured by the 3D profilometer 5-30mm samples

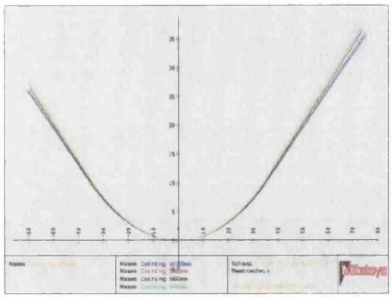

Figure 5.5.1b: Resultant form of the pressed component as measured by the 3D profilometer 30-100mm samples

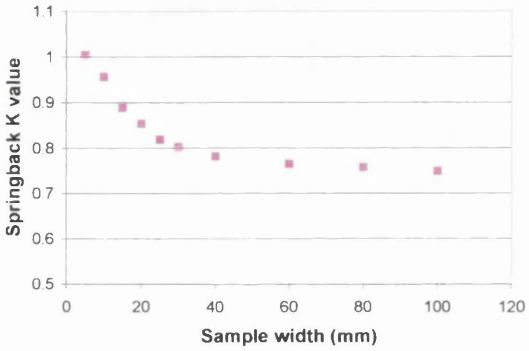

Figure 5.5.2a: Springback K values for GI IF 240 formed using 300kN force and die of 50mm/punch 49.3mm formed angle of 90° with varying sample widths

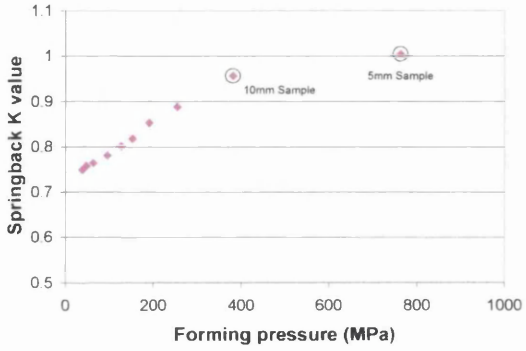

Figure 5.5.2b: Springback K values for GI IF 240 with respect to forming pressure

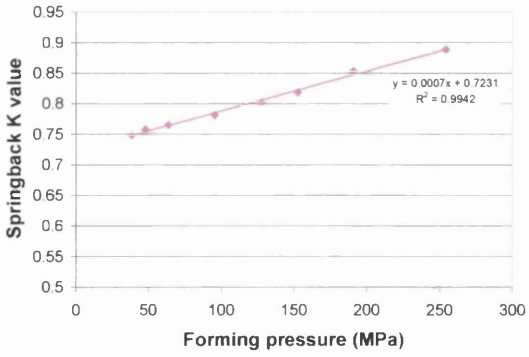

Figure 5.5.2c: Springback K values for GI IF 240 with respect to forming pressure showing linear section and trendline

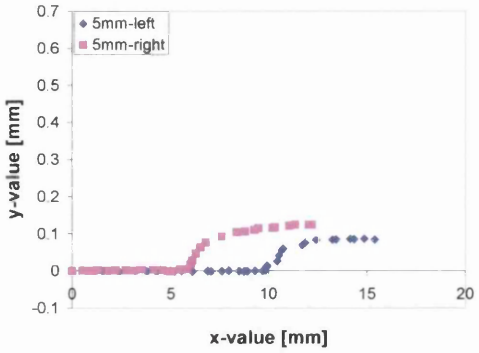

Figure 5.5.3a: 3D profilometer thickness measurement 5mm sample

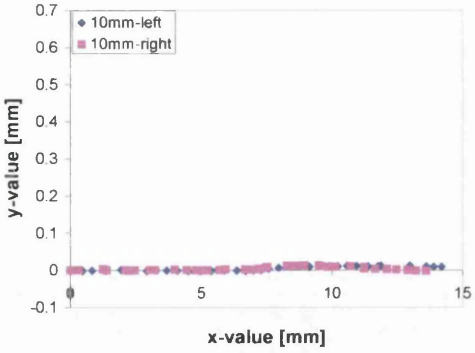

Figure 5.5.3b: 3D profilometer thickness measurement 10mm sample

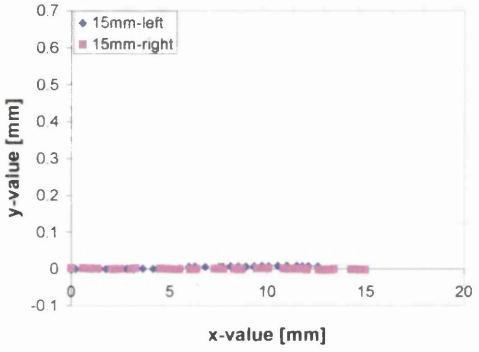

Figure 5.5.3c: 3D profilometer thickness measurement 15mm sample

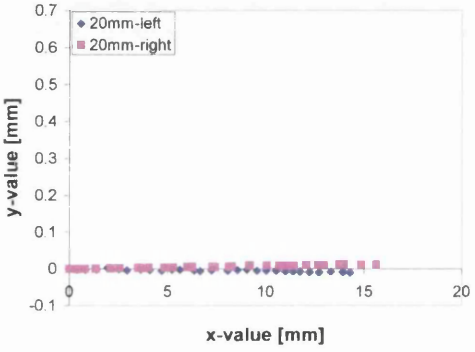

Figure 5.5.3d: 3D profilometer thickness measurement 20mm sample

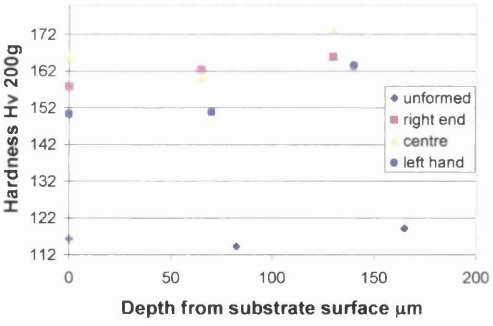

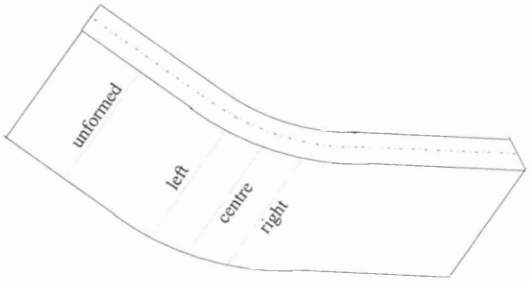

Figure 5.5.4: Through thickness hardness profile of 5mm sample

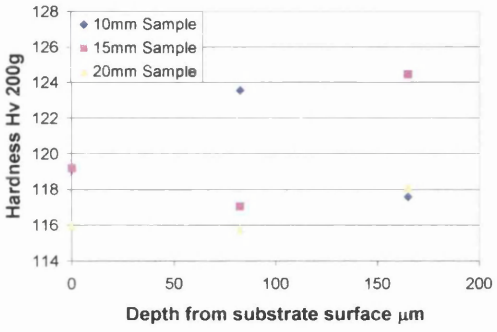

Figure 5.5.4a: Through thickness hardness profile of 10-20mm unformed sample

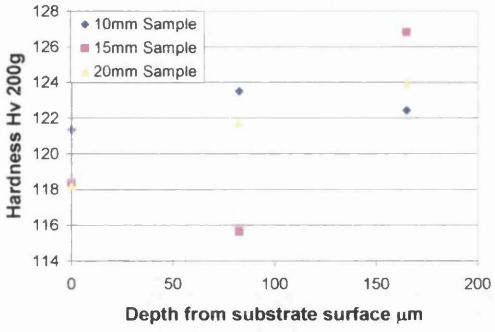

Figure 5.5.4b: Through thickness hardness profile of 10-20mm right hand sample

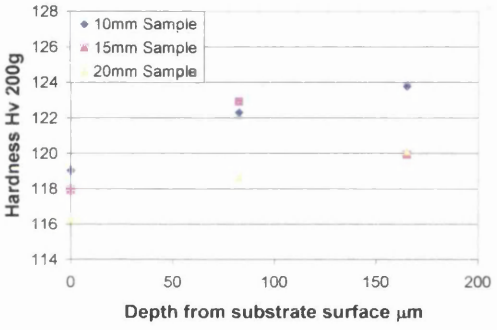

Figure 5.5.4c: Through thickness hardness profile of 10-20mm centre sample

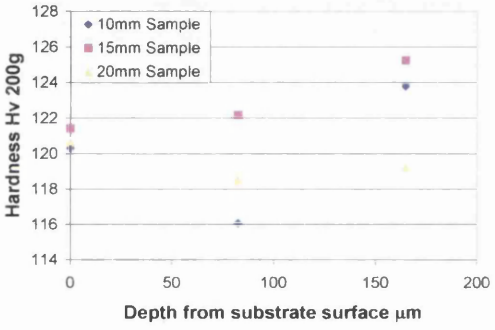

Figure 5.5.4d: Through thickness hardness profile of 10-20mm left hand sample

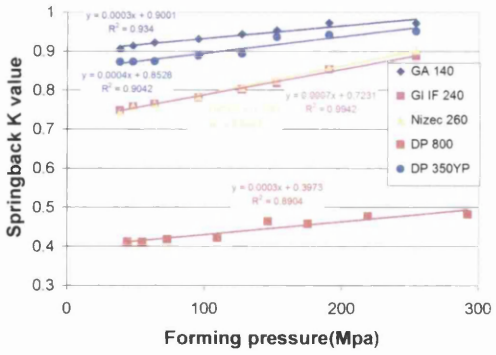

Figure 5.5.5: Springback variation as a consequence of normalised forming pressure for all primary steels

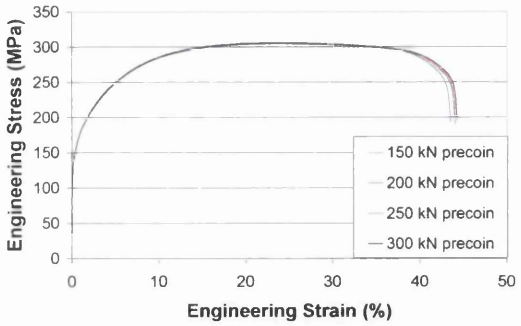

*Figure 5.5.6a:*Precoined GA 140 engineering stress/strain curve

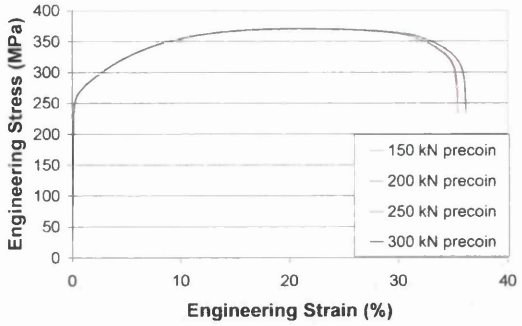

Figure 5.5.6b: Precoined GI IF 240 engineering stress/strain curve

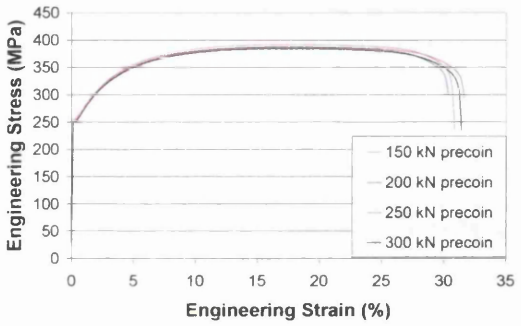

Figure 5.5.6c: Precoined Nizec 260 engineering stress/strain curve

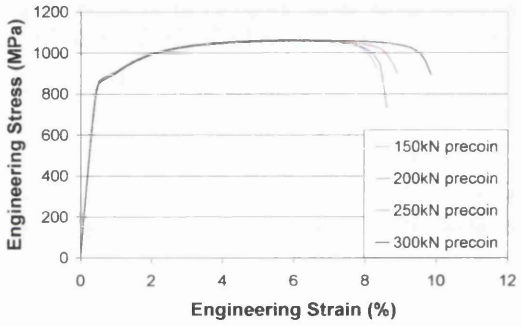

Figure 5.5.6d: Precoined DP 800 engineering stress/strain curve

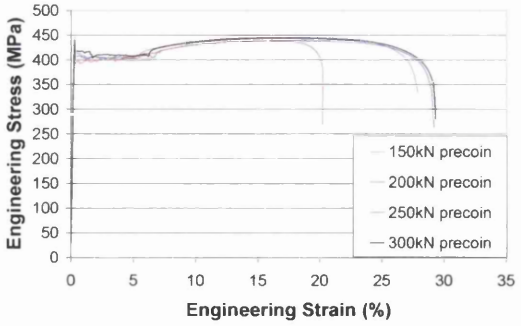

Figure 5.5.6e: Precoined DP 350 YP engineering stress/strain curve

Sample Width	radius	Pressure	
[mm]	[mm]	[kN/mm^2]	Mpa
100	66.782	0.03813	38.1316
80	65.957	0.04766	47.6644
60	65.351	0.06355	63.5526
40	63.993	0.09533	95.3289
30	62.319	0.12711	127.105
25	61.08	0.15253	152.526
20	58.576	0.19066	190.658
15	56.271	0.25421	254.21
10	52.258	0.38132	381.316
5	49.803	0.76263	762.631

Table 5.5.1: Sample width /forming pressure conversion

Sample Width	Substrate Thickness	Sample Width	Substrate Thickness	Sample Width	Substrate Thickness	Sample Width	Substrate Thickness
5mm		10mm		15mm		20mm	
unformed	630µm	unformed	630µm	unformed	630µm	unformed	630µm
right	565µm	right	630µm	right	630µm	right	625µm
centre	565µm	centre	630µm	centre	632,5µm	centre	630µm
left	580µm	left	630µm	left	630µm	left	625µm

sample thickness inclusive of coating 0.64 mm

Table 5.5.2: Substrate thickness measurement of 5-20mm samples by microscope

Material	GA 140	GI IF 240	Nizec 260	DP 800	DP 350YP
Non coining K value	0.8672	0.7098	0.7010	0.3921	0.8520
Coining intercept K value	0.8528	0.7231	0.7191	0.3973	0.9001

Table 5.5.3: Comparison between non coining trials and coining trials intercept values

5.6 Analytical Model Investigation

5.6.1 Aims

The aim of this investigation was to see if a selection of the currently published analytical predictive models were capable of satisfactorily predicting springback, for a range of materials under differing bending and loading conditions.

The level of confidence set for prediction satisfaction was ±5% of the actual measured value.

It is important for the tool designer and machine operator too not only understand springback, but also to be able to predict it. The designer must be able to predict springback so that the tooling can be made to accommodate the phenomenon, and the operator so that he can gauge how well the finished article is being produced such that if any deviations occurs this can be quantify with to the designer.

Data from the results of section 5.4 will be used as the as measured actual results.

The models that were evaluated were: -

Marciniak

$$K = 1 - 3(\rho/t)(\sigma_1/E)$$

Leu

$$K = (T/e^{-n}n^n)(1 + r/\sqrt{1+2r})^{1+n} \times 3(1-\upsilon^2)/2E(1+n)(t/2\rho)^{n-1}$$

Zhang

$$K = 1 - \left(3\sigma_1(1-\upsilon^2)\rho/Et\right)$$

Vegter

$$K = 1 - \left(3S\rho/Et\right) + 4\left(\frac{E}{E_1}\right)^2\left(\frac{S\rho}{Et}\right)^3$$

Klamecki

$$K = -\left(3\sigma_1\rho/Et\right) + 4\left(\frac{\sigma_1\rho}{Et}\right)^3 + 1$$

Modulus modified

$$K = 1 - \left(3S\rho/E_1t\right)$$

5.6.2 Results

Evaluation of Predictive Models using MTS experimental results

Fig. 5.6.1 shows the MTS results grouped with respect to material thickness, indicating the degree of strain (calculated from theory) each material has undergone during bending. From fig. 5.6.1 the actual measured results from the MTS investigation are plotted with the corresponding predicted result for each of the analytical predictive models. It can be said from the results shown in fig. 5.6.1 that none of the predictive models are able to predict exactly the measure springback values for all of the steels. From fig. 5.6.1 it can be seen that no pattern exists to enable the assignment of a model for a given steel grade, most, at one point or another predict the degree of springback. However, none continuously predict correctly for a range of steel grades.

At around 1% strain it is also evident from fig. 5.6.1 that the level of springback by all predictive models is under predicted (springback K value for predicted models is greater than that of the actual measured values).

Comparisons of differing experimental techniques (MTS & V bend)

Fig. 5.6.2 shows results for both the MTS and V bend experimentations. The difference between the two forms of experiments as discussed in section 5.4 is the level of induced strain during the forming operation. Shown also in fig. 5.6.2 are the predicted results for each of the forming operations. It can be said that the predicted results for the V bend tests do satisfactorily predict the amount of springback for each of the forming operations. However, they are unable to do so for the MTS experiments. This indicates that the predictive models cope better with situations of high strain bending than the low strain bending seen in the MTS experiment.

Evaluation of Predictive Models on V bend experimentation (Merkles results)

Fig. 5.6.3 shows the V bend results of Merkle grouped with respect to their material thickness, indicating the degree of strain (calculated from theory) each has undergone during bending. From fig. 5.6.3 it can also be seen that the actual measured results of the V bend investigation are plotted with the corresponding predicted result for each of the analytical predictive models. It can be said from the results shown in fig. 5.6.3 that the predictive models are able to predict satisfactorily the measured springback values for the majority of the steels. The high strength dual phase steels with strain levels around 3% are still outside the 5% satisfaction limit of prediction. However, above a 3% level of strain, prediction falls into the 5% banding of satisfying prediction accuracy. A trend noticed in the results of fig. 5.6.1 and also repeated in fig. 5.6.3 is that the models underestimate springback. This would suggest that within the model a factor has been neglected, or an assumption has been made which has a greater degree of influence than first thought.

Fig. 5.6.4 shows the combination of both the MTS experimental and V bend experimental results. The graph is arranged so that the bends of low strain level are situated to the left hand side and move to the right hand side as strain level increases. From fig. 5.6.4 it can be seen that as strain level increases so the amount of scatter in both the actual and measured results decreases. The transition from general under and over prediction, to continual under prediction by the models is also evident in fig. 5.6.4.

Comparisons of differing predictive models using differing experimental techniques (MTS & V bend)

Fig. 5.6.5a and 5.6.5b show the plots of actual results; against measured results for the MTS experiment and MTS+V bend experiment respectively for the Marciniak model. From fig. 5.6.5a it can be seen that when considering the y=x criterion from the trend line seen on the graph it can be said that the model underpredicts the level of springback in general, this is reaffirmed when considering the intercept value. Which represents the constant predictive error offset. The value of which is -0.6535 indicating a general trend

of underprediction. Prediction begins to improve when this negative value is counter acted by the lines gradient value of 1.7 at lower levels of springback i.e. high values of K. The R^2 value is low and therefore a degree of scatter would be expected from the predicted results about the graph trend line. The range of the results shows an inability to cope with situations where high levels of springback are taking place. Fig. 5.6.5b, which shows the results for both the MTS and V bend experiments, differs little from the plot in fig. 5.6.5a. A slight improvement on the trend line has occurred, a reduction in the constant predictive error offset has occurred, however this is matched in turn with a reduction in the trendline gradient. Overall a small improvement has occurred. The R^2 values of the graph have differed little, showing that the inclusion of the V bend data has not marked ably increased the confidence in predictability, indicating a preference of this model to be used for high strain bend prediction.

Fig. 5.6.6a and 5.6.6b shows the results form the Leu model for the MTS and MTS+V bend experiments respectively. From fig. 5.6.6a it can be seen that the model continually underpredicts the level of springback of the measured results when considering the y=x criterion. This is also reflected in the make up of the trendline equation where the constant predictive error offset which is positive and valued at 0.956 is counter acted by a negative gradient, and therefore massing the predictive models in an area akin to that of low springback. The trend line shows that this model is unsuitable for bend conditions where conditions of high springback are present. The single greatest factor influencing the trend line of this model is the results of the 1.0mm DP 800 steel. Lue's model is unable to cope with the material and bend conditions. This is again reflected in the R^2 value of the graph and also the range. Fig. 5.6.6b shows the results of the combined MTS and V bend experiments. It can be seen that the inclusion of the V bend results has improved the trend line and R^2 value considerably. Once again the single greatest factor influencing the trend line and R^2 value is the 1.0mm DP 800 steel from the MTS experiment. With a gradient value of the trendline equation less than 1, and a low positive value for the constant predictive error offset indicates that at low levels of springback the predictive springback will be higher than that observed. From the results in both fig. 5.6.6a and b it can be said that the Lue model continually under predicts the level of

springback. It is also restricted in its use, since only low strength material and high strain bends appear to be predicted with confidence.

From fig. 5.6.7a and 5.6.7b the results for the Zhang model for the MTS and MTS+V bend experiments respectively can be seen. Fig. 5.6.7a shows the MTS experimental results against those predicted by the Zhang model, it is evident from the trend line that this model under predicts the level of springback in general when considering the y=x criterion. The trendline equation shows a negative value for the constant predictive error offset which would indicate and over prediction of springback K value, therefore an decrease in springback prediction. Fig. 5.6.7a also shows that the scatter of experimental results is relatively small, around the graph trend line.

From fig 5.6.7b it can be seen from the MTS and V bend results that the inclusion of the high strain bend results has improved the trend line equation indicating that at lower levels of springback K value prediction is better. The R^2 value of the trend line has improved little. This indicates that the Zhang model is able to cope with moderate levels of springback, and able to confine experimental scatter to a small range.

Fig 5.6.8a and b show the results from the Vegter model for both the MTS experiment and also the MTS and V bend experiments. From fig 5.6.8a it is possible to see that this model over and underpredict the level of springback, not only from the y=x imaginary line but also the actual graph trend line. When considering the trendline equation it can be seen that at low levels of springback K value an overprediction of springback K value would occur, as the value of K increases so the trendline gradient compensates for the high value of the constant predictive error offset. The level of R^2 about the graph trend line is low in comparison to that seen in fig. 5.6.8a, and the range shows that the model is unable to cope with levels of high springback. The introduction of the V bend experiment into the data, as shown in fig. 5.6.8b improves the graph trend line slightly and also the R^2 value for the graph trend line. It can be seen from the trendline equation that lower levels and upper levels of prediction are improved slightly. For example at a value of x=0 fig. 5.6.8a returns a value of -0.5273 for actual K value, where as fig. 5.6.8b returns a value of -0.3784, at the value of x=1 we see from fig. 5.6.8a a value of 1.0631, fig 5.6.8b returns a value of 1.0215. From the results shown in both fig. 5.6.8a and b it would be unwise to use this model in situations of low strain bending with high strength steels.

Fig. 5.6.9a and 5.6.9b show the plots of actual results; against measured results for the MTS and MTS+V bend experiments respectively for the Klamecki model. From fig. 5.6.9a it can be seen that when considering the y=x criterion and the graph trend line it can be said that the model both under and overpredicts the level of springback in general. The trendline equation also indicates with a low valued constant predictive error offset a better predictability at lower levels of springback. This is enhanced with a gradient which is close to unity. Also the R^2 value is high and therefore only a small degree of scatter would be expected from the predicted results about the trend line. The model range is the best seen so far, indicating the ability to cope with higher degrees of springback than the previous models. The introduction of the V bend data has resulted in a decrease in the graphs trend line equation in both the constant predictive error offset value and gradient, resulting in a better prediction. The R^2 has increased slightly, this can be seen from fig. 5.6.9b.

From fig. 5.6.10a and 5.6.10b the results for the 'modulus modified' model for the MTS and MTS+V bend experiments respectively can be seen. Fig 5.6.10a shows a model that has predictions that both over and under estimate the level of springback in both the y=x criterion and also the graph trend line equation. This is the closest a graph trend line has come to the y=x criterion of the models investigated thus far. The graph R^2 for the trend line is smaller than that seen in the Klamecki model in fig 5.6.9a, and the range is on par. Fig. 5.6.10b shows the results for the combination of the MTS and V bend experiments. It can be seen from fig. 5.6.10b that this introduction of results changes very little in the graph plot, suggesting that the model is the best of the models considered for situations of high and low strain level, involving high and low strength material.

5.6.3 Discussion

From fig. 5.6.1 it is clear that the model postulated by Leu, which allows for rigid plastic strain hardening material consistently underpredicts the degree of springback. This model also seems unable to correctly predict the direction of springback i.e. +ve or –ve e.g. for the dual phase 800 N/mm^2 material, and appears to push the results in the opposite direction to the other models and actual results. In contrast to Leu, the postulated model

'modulus modified' will in general produce the largest springback prediction of all the models considered.

From the majority of the predictive plots a pattern of model order is evident, with the highest level of springback being predicted by 'modulus modified' then descending to Klamecki, Vegter, Zhang, Marciniak and finally the lowest predictor Leu. It would appear that other than Leu, who has used the tensile properties of the material including strain hardening coefficient in its model, the others are in principle alike, using elastic purely plastic material models. The main deviation of these elastic purely plastic material models is the inclusion of plane strain methodology, for which the main factor ignored is a modified Young's modulus. Those models which have inclusions for both plane stress and modified Young's modulus give higher predictions, which in the case of high strain levels and yield strengths gives closer predictions. This would then suggest that the important factors effecting the accuracy of a predictive model is the determination of Young's modulus and yield point.

If the graphs of the analytical predictive models are considered see, fig. 5.6.5a to 5.6.10b, from analysing the trend line equations and R^2 value it can be seen that the best predictors are Zhang, Klamecki and 'modulus modified', but not necessarily in this order. Depending on the level of importance assigned to the trend line or R^2 will indicate a different model. The poorest performing model all round is that of Leu. Zhang's predictive model has a range from 0.5 – 0.98 on the x-axis, showing a good correlation in the area of low springback, and poor correlation in the region of high springback. Zhang however is not the best at this particular indicator. Klamecki and 'modulus modified' model perform better over a wider range, and are better able to deal with high levels of springback.

When the graphs with the imaginary line discussed earlier are considered, the optimum condition would be for predictive plots to straddle the imaginary line, as a continuous underprediction indicates an omission of a key factor in the model. From the analytical predictive graphs it can be said that the majority under predict the level of springback. Vegter, Klamecki and 'modulus modified' model straddle what would be the imaginary line. This may be attributed to the formulation of their models, which have allowed for plastic moment calculations. In general it is possible to say that no one analytical model

is capable of satisfactorily predicting springback in differing scenarios. However, inclusion of modified Young's Modulus values and yield strength to allow for conditions of plane strain improves model prediction. Also elastic perfectly plastic models (the majority of analytical models) preformed better than that of a rigid plastic and strain hardening model (Leu's model).

It is not possible to say which is overall the best analytical model to use as the two main contenders Klamecki and 'modulus modified' perform better than the rest, but neither achieves total accuracy in every criteria.

In view of the results obtained it can be said that the use of analytical models (in their nature limited by assumptions) to predict springback is unwise, especially when dealing with situations of high springback noted as with thin high strength sheet steel during bending. Analytical models do reveal the important parameters associated with a complex material/ forming operation, and are therefore needed at the start point of any investigation.

5.6.4 Conclusions

The conclusions obtained during this investigation have agreed in general with those previously postulated, and also highlighted new restrictions in the use of such models.

The conclusions from this investigation are: -

1. No one predictive model is capable of satisfactorily predicting springback in differing scenarios.
2. For low levels of strain the predictive models are inaccurate, this can deteriorate further by introducing steels of high yield strength.
3. The scatter in results of predictive models is larger for high strength dual phase steels in large bend radius conditions.
4. 2% appears to be the strain level at which predictive models become reliable (reliability being ± 5%).
5. Strains of 7% and above remain reliable (reliability being ± 5%). However, the models begin to continually underpredict the level of springback.

6. The highest level of springback is predicted by the 'modulus modified' model then descending to Klamecki, Vegter, Zhang, Marciniak and finally the lowest predictor Leu
7. The model that best suits high strain levels is the 'modulus modified' model.
8. Inclusion of modified Young's modulus and yield strength to allow for conditions of plane strain improves model prediction.
9. Better definition of Yield strength and Young's modulus may better improve predictions.
10. All predictive models that were based on elastic perfectly plastic materials preformed better than that which used a rigid plastic and strain hardening model.
11. Rigid plastic and strain hardening model consistently give the lowest predictions.
12. As bend strain level increases so the effect of yield strength/ thickness decreases, the reverse is also true.

5.6.5 Figures / Tables

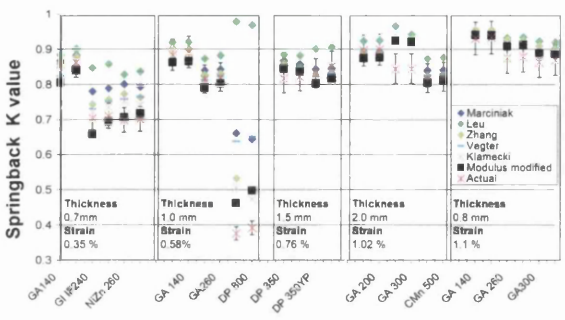

Figure 5.6.1: MTS results grouped into their material thickness, indicating the degree of strain, showing actual and predicted results for various models

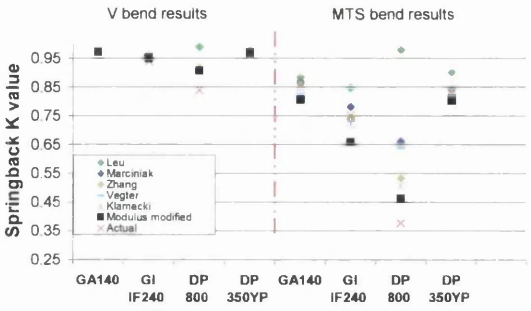

Figure 5.6.2: MTS and V bend results, materials formed from the same steel sheet, showing actual and predicted results for various models

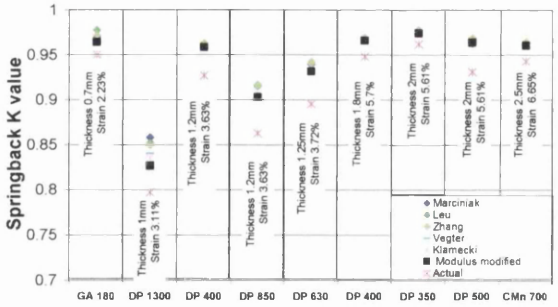

Figure 5.6.3: V bend results grouped into their material thickness, indicating the degree of strain, showing actual and predicted results for various models

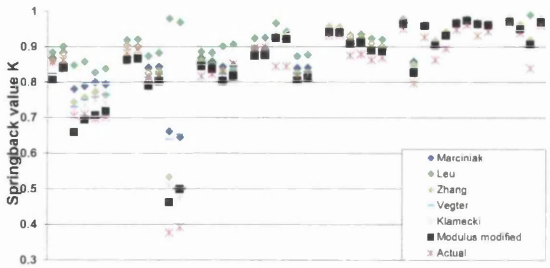

Figure 5.6.4: MTS and V bend results showing actual and predicted results for various models

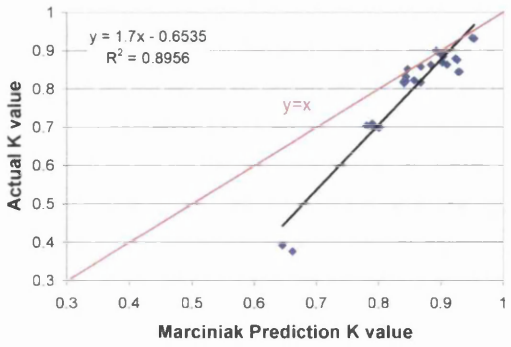

*Figure 5.6.5a:*Marciniak MTS predictive plot

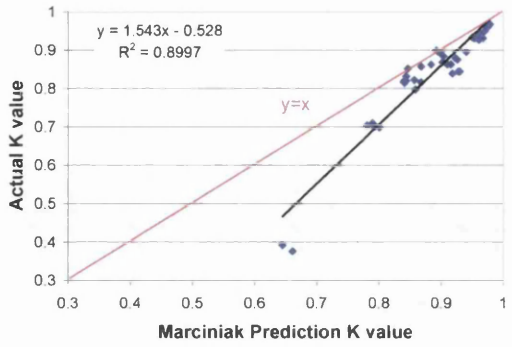

Figure 5.6.5b: Marciniak MTS and V bend predictive plot

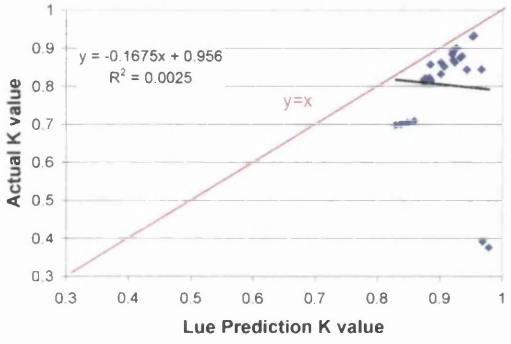

Figure 5.6.6a: Lue MTS predictive plot

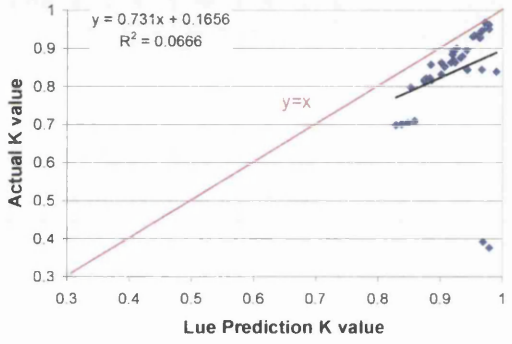

Figure 5.6.6b: Lue MTS and V bend predictive plot

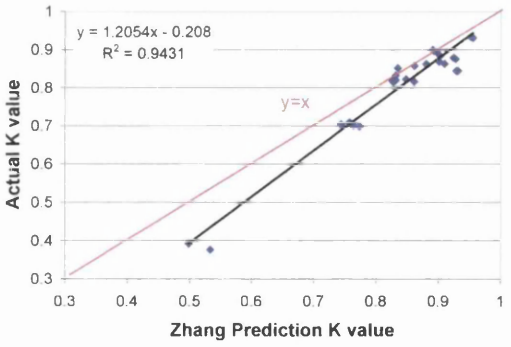

Figure 5.6.7a: Zhang MTS predictive plot

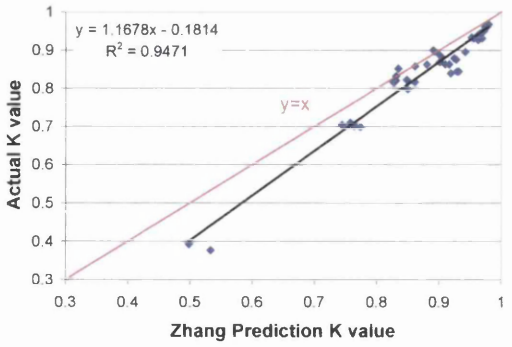

Figure 5.6.7b: Zhang MTS and V bend predictive plot

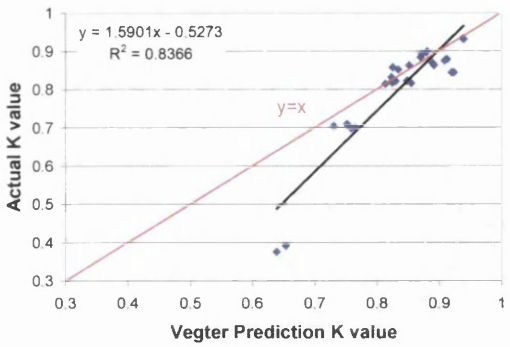

Figure 5.6.8a: Vegter MTS predictive plot

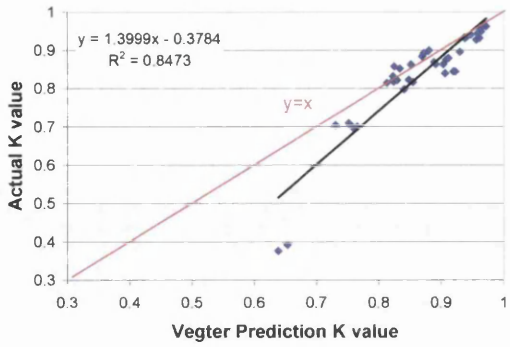

Figure 5.6.8b: Vegter MTS and V bend predictive plot

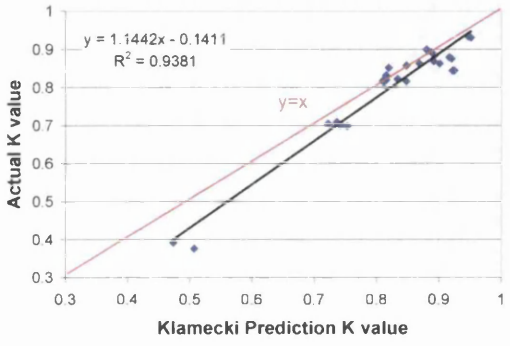

Figure 5.6.9a: Klamecki MTS predictive plot

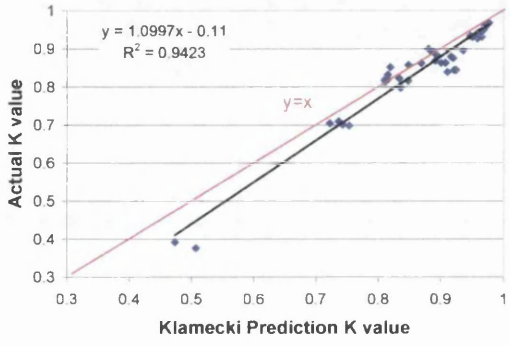

Figure 5.6.9b: Klamecki MTS and V bend predictive plot

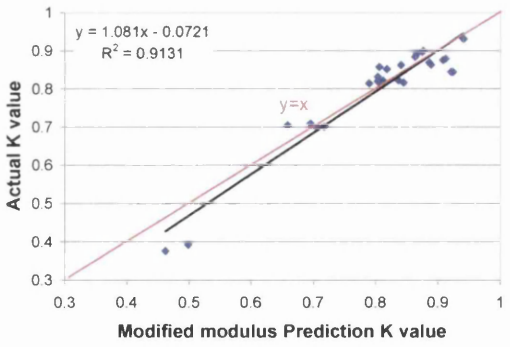

Figure 5.6.10a: Modulus modified MTS predictive plot

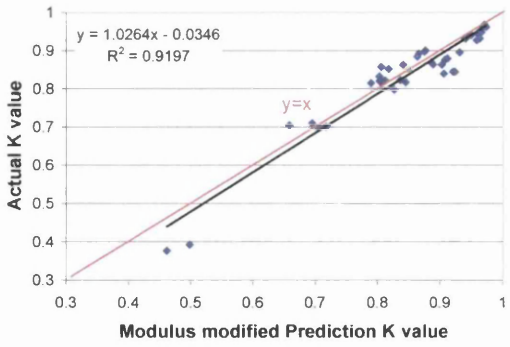

Figure 5.6.10b: Modulus modified MTS and V bend predictive plot

5.7 Numerical algorithm investigation

5.7.1 Aims

The aims of this investigation were firstly to see if it was possible, by the use of a numerical algorithm, to interrogate the mechanical tensile and springback data to highlight the important parameter interactions. Secondly, the objective was to establish if it was possible to use the numerical algorithm as a means of accurately predicting springback.

The analytical models in section 5.6 highlighted the important parameters affecting springback, and also showed the required level of predictability that would be needed to surpass the numerical algorithm, if replacement of analytical models is to be considered.

5.7.2 Results

Fig. 5.7.1 shows the results of the four variable input numerical algorithm. The variables used were material thickness (t), Young's modulus (E), yield strength (Rp), and neutral axis bend radius (ρ), along with the springback K value. All of the data used originated from the results generated from the MTS and V bend trials, including those from Merkle. From fig. 5.7.1 it can be seen that the four variable numerical algorithm performed well in comparison to the analytical predictive models seen in the previous section 5.6. The graph trend line is very close to the y=x criterion, and the R^2 value approaches 1. As would be expected from a graph which meets the first two criterion of y=x trendline and an R^2 value of 1, the range for the graph also show the ability to cope with high and low springback conditions.

By increasing the input variables to five and allowing for an r average value, a closer fitting graph was possible, see fig. 5.7.2. From fig. 5.7.2 it can be seen that the increase in input parameters into the variable make up of the numerical algorithm has slightly increased the graph trend line, and also the R^2 value. Where the graph trend line equation in the four variable input algorithm is $y = 0.9774x + 0.019$, this has been increased to $y = 0.9806x + 0.0163$ for the five variable input algorithm. The change in the constant

predictive error offset has lessened by 0.0027, where as the trendline gradient has changed by 0.036x.

Fig. 5.7.3 shows the results of a six variable input algorithm, where the additional variable added to the five variable input algorithm is the material's n average. As with the previous increase in the number of input variables, the six variable input algorithm has shown an increase in the graph trend line and R^2 value. From the results in fig. 5.7.1 to 5.7.3 it appears as the input variables are increasing so accuracy in the result increases.

Increasing the input variables further to seven, to include tensile strength (Rm), led to further improvements as can be seen in fig. 5.7.4. This graph is closer to the criterion set (y=x) than those graphs seen previously in fig. 5.7.1, 5.7.2, and 5.7.3. It is evident when comparisons are made that as the number of inputs into the numerical algorithm increased so the accuracy of the predicted results has increased. From the series of graphs showing each set of results it can be seen that for each incremental step of variable inclusion the difference in R^2 value has increased.

The mapping of the seven variable input numerical algorithm is not possible as the maximum yield strength is greater than the mid value tensile strength for this range of steels. Therefore the six variable numerical algorithm was selected for the variable data interaction mapping.

From fig. 5.7.5 it can be seen that as the normalized neutral radius increases, and normalised n value remains constant, so the level of springback increases, reflecting the amount of plastic to elastic proportion in the bend (small bend, large plastic portion/ little elastic). The effect of this increase is magnified by the normalised n average value initially. Consider the normalised neutral radius held constant, and the normalised n value increased, for small bend radii this results in no change, but for high bend radii as n value increases so the level of springback increases. It would appear that the maximum value is at $\approx$0.5 normalised n value (at which the n value effect is greatest). Above this value springback is reduced, indicating an inflection in the influence of n value.

It is unclear why this inflection related to n value occurs. The effect is greatest at high bend radii, where a low level of strain is induced into the material. As r value increases from 0 (perfectly plastic solid) to 1(elastic solid) it would be expected that the degree of springback increases, here it does not.

Fig. 5.7.6 shows the plot of normalized Young's modulus versus normalized material thickness. It is evident from fig. 5.7.6 that the relationship between the two factors appear to be banded, i.e. maintaining a constant Young's modulus and normalized material thickness increasing from 0-1, results in a decrease in springback, with an inflection occurring around 0.4 material thickness and a subsequent increase in springback above this value. This inflection appears to be uneven as there is a greater effect on the increase in springback, from 0.6 up to 1 of normalized material thickness, in comparison to the change in springback seen at lower values of normalized material thickness. At low levels of normalized thickness an increase in Young's modulus increases springback, but at higher levels of material thickness this trend is reversed and an increase in Young's modulus sees a minimal decrease in springback. In general the effect of Young's modulus is minimal, and it would appear that all of the behaviour is generated by the change in material thickness. The most likely reason behind this behaviour is the Bauschinger effect, where a differing behaviour from a material in compression to one in tension occurs. This may also be the case if a shift of the neutral axis occurs, where the compression and tension elements are different in magnitude.

Fig. 5.7.7 shows the trends between normalized yield strength and normalized material thickness. At low levels of material thickness an increase in yield strength is accompanied by an increase in springback. This trend appears consistent at the lower half of the graph, i.e. lower levels in material thickness. It is noticeable that a line of inflection running from 0, normalized yield strength, 0.2 normalised material thickness to a point of 0.8 normalised yield strength, 1 material thickness occurs. Trends above this line contradict normal perception of material behaviour during bending, for at these higher levels of material thickness an increase in yield strength results in a decrease in springback. This reversal in roles may be attributed to the Bauschinger effect or neutral axis shift. A notable feature of this graph is that the differing regions of springback depicted in the lower right hand quadrant appear to be uneven or irregular in shape. This may be an indication that the numerical algorithm has returned unstable results.

Shown in fig. 5.7.8 is the plot of normalized r average versus material thickness. Consider a low normalized material thickness, an increase in the normalized r average value results in a limited decrease in springback. This effect is magnified and reversed at

high values of material thickness. If normalized r average is kept constant and material thickness increased an initial decrease in springback occurs, followed by a subsequent increase in springback . Again it is evident from fig. 5.7.8 that a line of inflection exists, which would appear to run from a value of 0 normalised r average ,0.6 normalised material thickness and to a point of 1 normalised r average ,0.4 normalised material thickness. The inflection which occurs in this graph appears to be the result of material thickness behaviour and again may be attributed to the Bauschinger effect or shift of the neutral axis.

If the yield loci of a material is considered, as r value increases so the yield stress in plane stress condition increases, leading to an increase in springback. This contradicts what is depicted on the graph.

Fig. 5.7.9 shows the relationship between normalized n average and material thickness. This graph shows the same behaviour as those previous graphs dealing with normalized material thickness, i.e. an inflection occurs. At low levels of material thickness an increase in n average will result in an increase in springback. At higher levels of normalized material thickness an increase in n average results in a decrease in material springback. An increase in n value for a set level of strain would result in an increase in the yield strength and therefore an increase in elasticity. The inflection due to the thickness effect could not have reversed this, as a purely y axis effect will result in horizontal banding. This is not the case in this instance and for this reason it would appear that an inflection is also at work from the n value variable. One possible cause of the thickness reversal is associated with the Bauschinger effect, where with a higher n average material the difference between the compressive and tensile behaviour may be greater. Couple this with the n value inflection and the areas of high springback at upper and lower thickness are at opposite ends of the x axis.

Fig. 5.7.10 depicts springback behaviour while manipulating normalized neutral radius and normalized material thickness. As with other graphs depicting material thickness this has the same trait, i.e. an inflection occurs within the graph. It can be seen that at low levels of material thickness an increase in neutral radius results in an increase in springback. This is also true at higher levels of material thickness, the effect is greatly reduced. If neutral radius is held at a constant level and an increase in material thickness

occurs, it can be seen that an initial decrease in springback takes place until an imaginary inflection line is met at which point an increase in material thickness yields an increase in springback. From the graph it is possible to see also that effective change in springback is larger where the normalized neutral radius is largest.

A common trait seen with all the graphs associated with material thickness is the presence of an inflection within the graph. As mentioned previously this phenomenon can be associated with the Bauschinger effect, which in layman's terms mean that tensile and compressive properties of material are different, and therefore we see an imbalance when considering the elastic proportion in compressive mode, and the elastic proportion in tensile mode. The result of this disparity is a change in the perceived springback behaviour.

Fig. 5.7.11 depicts the effect of normalized r average and normalized yield strength on springback. It is evident from the graph that the relationship is dominated by yield strength. At lower values of yield strength an increase in r average yields an increase in springback. As yield strength increases so springback increases. It is also evident from the graph that at high yield strength an increase in normalized r average decreases springback. In general the effect of normalised r value is minimal.

Fig. 5.7.12 shows the interaction of normalised n average and normalized yield strength. In fig. 5.7.12 it can been seen that bands of differing levels of springback radiating out from a point of high yield strength and high normalized n average. It can be seen that at low levels of yield strength, an increase in n average results in an initial increase in springback , followed by a decrease. If high normalized yield strength is kept constant and normalized n average is varied between 0 and 1 it can be seen that the percentage difference in springback is greater than that seen when yield strength is low and normalized n average is varied between 0 and 1. This indicates that as yield strength increases the effect of normalised n value increases, and also the inflection seen previously disappears.

Fig. 5.7.13 depicts the interaction between normalized neutral radius and normalized yield strength. A trend described previously in fig. 5.7.12 that of radiating bands of differing springback is also evident in fig. 5.7.13. These bands of differing springback originating at high normalized neutral radius and high normalized yield strength. They

radiate out towards a point of low normalized neutral radius and low normalized yield strength. Consider a low constant value of normalized yield strength, as the normalised neutral radius increases so the level of springback increases, which is magnified when considering higher levels of normalised yield strength. These results would be expected as high neutral radius increases the elastic proportion within the bend. An increase in yield strength further increases this elastic proportion.

Fig. 5.7.14 shows the interaction between normalized n average and normalized r average on springback. It is evident from fig.14 that limited interaction occurs. With respect to normalized n average and normalized r average small areas of differing springback values are evident of which the two main areas occur in the lower normalized n average portion of the graph. In general this could be considered as an interaction were no change in springback occurs.

Fig. 5.7.15 shows the interaction of normalized neutral radius and normalized r average and springback. From fig. 5.7.15 it is evident that an increase in normalized neutral radius results in an increase in springback. This effect is heightened further by an increase in normalized r average.

Fig. 5.7.16 shows the effect that yield strength and Young's modulus has on springback. It can be seen that an increase in yield strength results in an increase in springback. This effect is heightened when considering a material of lower Young's modulus from basic material principles. This result would be expected as high yield strength and low Young's modulus leads to a material which has high elastic recovery.

Fig. 5.7.17 shows the normalized r average and normalized Young's modulus. It can be seen that only consideration of a low Young's modulus and high normalized r value result in a change in springback. In general these two interactions could be neglected.

Fig. 18 shows the effect of normalized n average and normalized Young's modulus has on springback. It is evident from fig. 5.7.18 that little interaction occurs between these two variables on springback. Two isolated areas of change both depicting a lessening of springback are evident. One in the area of high normalized Young's modulus and high normalized n average, and second in the area of low normalized n average and low normalized Young's modulus. These two areas can be attributable to two different mechanisms. One associated with low normalize n average would be predominantly

caused by n average value. The second at high normalised Young's modulus associated to Young's modulus.

From fig. 5.7.19 it can be seen that the interactions of normalized neutral radius and normalized Young's modulus on springback are predominantly affected by normalized neutral radius. It can be seen that as normalized neutral radius increases so the level of springback increases. This effect is heightened with a low normalized Young's modulus value.

Table 5.7.1 shows the results matrix produced by the numerical algorithm for the four variable input parameters. The first row shows the linear terms of the main variables, and the lower rows show the first order interactions terms (including squares of the variables). From Table 5.7.1 it can be seen that the factors expected to increase springback i.e. increase in yield strength and neutral axis bend radius are shown as negative and those associated to a reduction in springback such as thickness and Young's modulus are shown as positive for the linear terms. From the linear terms it can be seen that the variable which has the greatest effect is yield strength. It can also be seen from the table that the first order interactions are stronger in areas other than those of the linear terms. If the first order interaction of yield strength (Rp) is considered with material thickness (t), it is greater in magnitude than the yield strength (Rp), material thickness (t), Young's modulus (E) and neutral bend radius (ρ) linear terms. Table 5.7.1 shows that the first order interactions are in fact greater in magnitude than the linear terms.

The subsequent matrices produced by the 5, 6 and 7 variable numerical algorithms can be seen in Tables 5.7.2, 5.7.3, and 5.7.4 respectively. A factor that emerges from these tables is that in general the first order terms remain the greatest in magnitude when compared to the linear terms. It can be seen from the tables that the first order interaction of yield strength (Rp) and material thickness (t), remains greater in magnitude from the 4 variable algorithm up to the 6 variable algorithm. It is only when the 7 variable algorithm is considered that a change is seen. The title is then passed to the first order interaction between tensile strength (Rm) and strain hardening co efficient (n). the influence of yield strength reduces in the 7 variable numerical algorithm, and is replaced by the tensile strength variable.

Table 5.7.5 shows the initial linear and first order interactions from the 4 variable matrix along with all the subsequent matrix variables for those linear terms and first order interactions. It is evident from Table 5.7.5 that of the linear terms considered only yield strength and the neutral axis bend radius remain the same sign throughout. This shows that the effect on springback does not change, and an increase in these parameters will always lead to an increase in springback for the linear terms. This is also true for the first order interactions of material thickness (t) x material thickness (t). Neutral axis bend radius (ρ) x material thickness (t), yield strength (Rp) x Young's modulus (E), and neutral axis bend radius (ρ) x neutral axis bend radius (ρ). All of the above interactions will lead to a decrease in springback as they increase in magnitude.

5.7.3 Discussion

It must be remembered that the results obtained are a reflection of the input data, and therefore care must be taken when using this method as a predictor for future material springback prediction. From the tabulated results shown in Table 5.7.1-5 it is possible to see the factors that have the greatest influence on springback (dependent on the number of input variables). This can also be used as a guide to the suitability of the results returned by the algorithm for a new material. It is possible to say that a new material that is high in yield strength, in comparison to the algorithm input values will return a value of springback from the algorithm, with a higher degree of error than one with low yield strength. So caution is needed when new materials with high values for high effect variables are considered.

The argument is then why numerical algorithms. For a finite process and materials this method of mapping effects and prediction is highly accurate. Complex interactions are embraced, unlike analytical solution which restrict the number of interactions investigated by placing assumptions on behaviour.

Only the introduction of a new material or parameter will make an algorithm redundant. Its greatest asset is the ability to allow for complex interactions, and the ease at which a new algorithm can be formulated.

The ease of introduction into an FE package also makes the algorithm a powerful tool to enable greater complexity of use, instead of just as a simple bend predictor. An ability exists for a value added product to be marketed with regard to FE packages. Development of a springback add on FE package is feasible. This could be used as a bargaining tool for customers to remain/ join the company supply portfolio with a promise of exclusive rights for the use of the FE package.

From the mapping of variable interactions, a recurring theme is one in which the thickness variable continually introduces an inflection into the graphs. As mentioned previously this may be a result of the Bauschinger effect. Therefore further study into this phenomenon is required. Materials will continually be replaced by more complex types, both in chemical composition and processing. This study alone, has seen the indication of behaviour not usually associated with simple bend forming. It can be foreseen that unless inroads are made into the understanding of the materials and forming methods presently available, then future pressing operations will fall back into the arena of a 'black art'.

The mapping of variable interactions can also be used further for material and process optimisation, indicating variables that could reduce or increase springback.

5.7.4 Conclusions

In general for the six variable numerical algorithm the following conclusions can be drawn:-

1. An increase in strength increases springback
2. An increase in Young's modulus reduces springback
3. An increase in material thickness initially reduces and, then increases springback
4. An increase in n average initially increases and, then reduces springback
5. An increase in r value increases springback
6. An increase in bend radius increases springback
7. Numerical algorithms can be used as maps for material optimisation
8. Numerical algorithms lend themselves readily for inclusion into FE packages
9. Numerical algorithms can cope with complex interactions, but prior knowledge is required into the important parameters to be considered

5.7.5 Figures / Tables

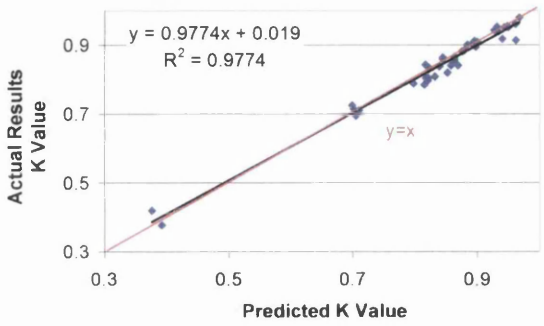

Figure 5.7.1: Four variable numerical algorithm predicted results

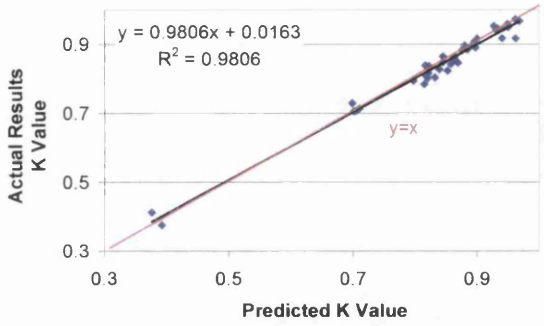

Figure 5.7.2: Five variable numerical algorithm predicted results

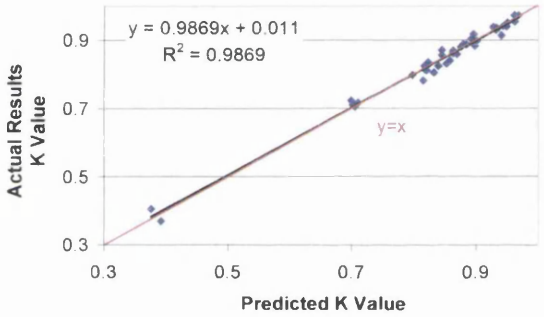

Figure 5.7.3: Six variable numerical algorithm predicted results

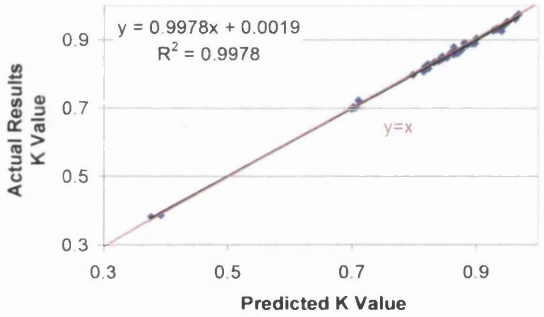

Figure 5.7.4: Seven variable numerical algorithm predicted results

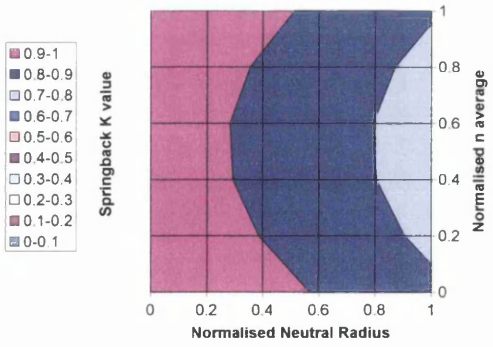

Figure 5.7.5: Six variable numerical algorithm normalised neutral radius vs normalised n average

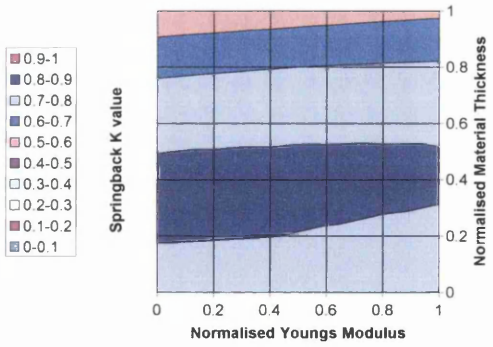

Figure 5.7.6: Six variable numerical algorithm normalised Young's modulus vs normalised material thickness

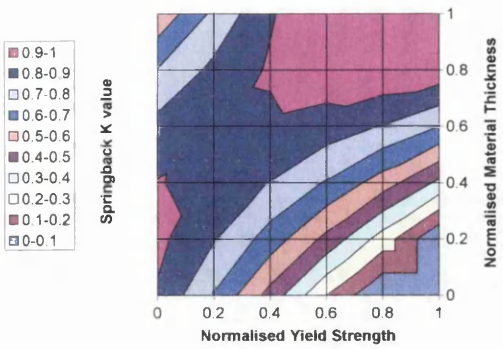

Figure 5.7.7: Six variable numerical algorithm normalised yield strength vs normalised material thickness

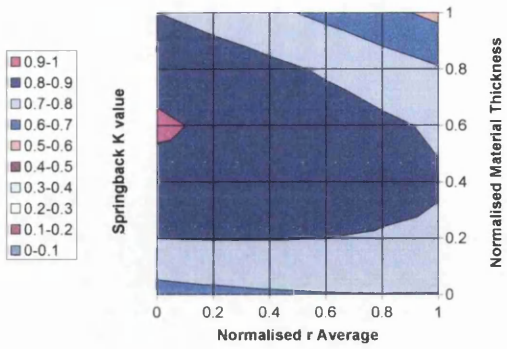

Figure 5.7.8: Six variable numerical algorithm normalised r average vs normalised material thickness

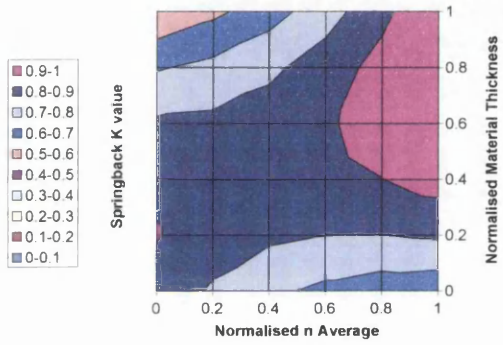

Figure 5.7.9: Six variable numerical algorithm normalised n average vs normalised material thickness

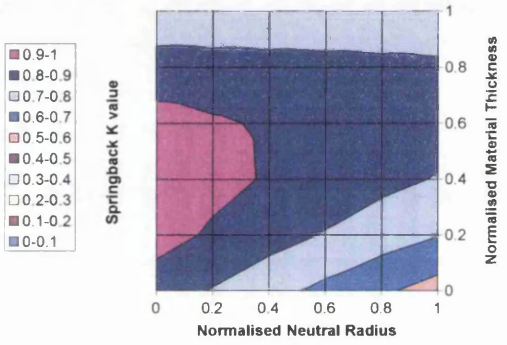

Figure 5.7.10: Six variable numerical algorithm normalised neutral radius vs normalised material thickness

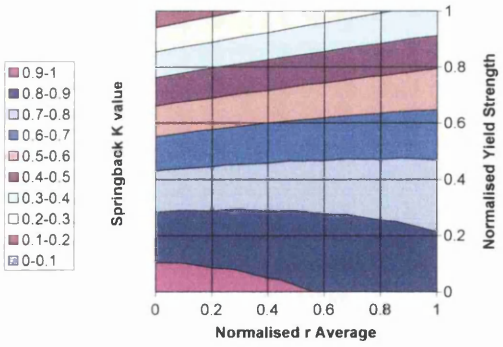

Figure 5.7.11: Six variable numerical algorithm normalised r average vs normalised yield strength

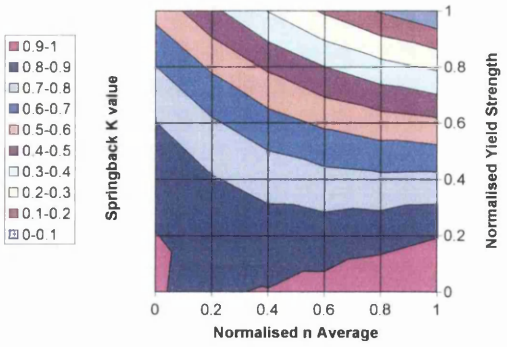

Figure 5.7.12: Six variable numerical algorithm normalised n average vs normalised yield strength

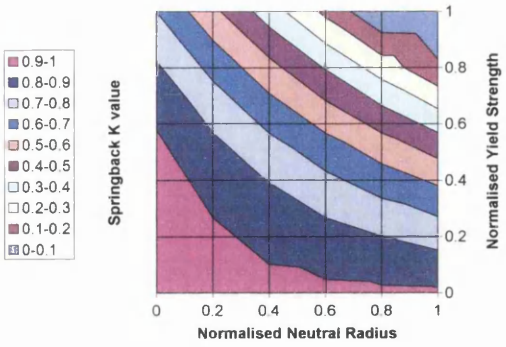

Figure 5.7.13: Six variable numerical algorithm normalised neutral radius vs normalised yield strength

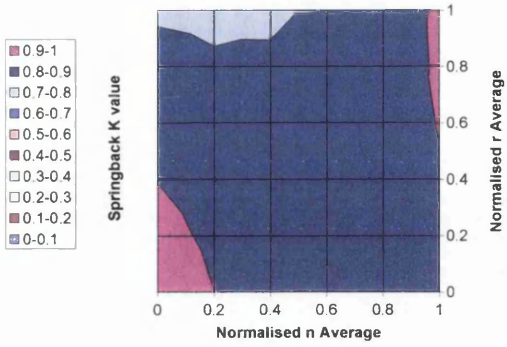

Figure 5.7.14: Six variable numerical algorithm normalised n average vs normalised r average

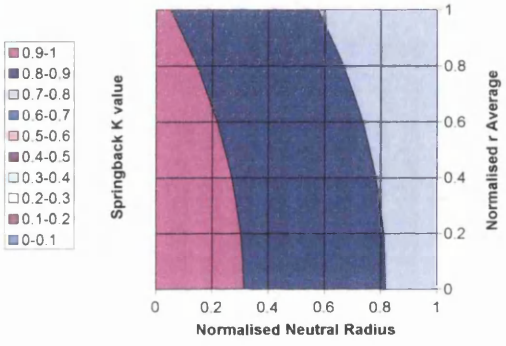

Figure 5.7.15: Six variable numerical algorithm normalised neutral radius vs normalised r average

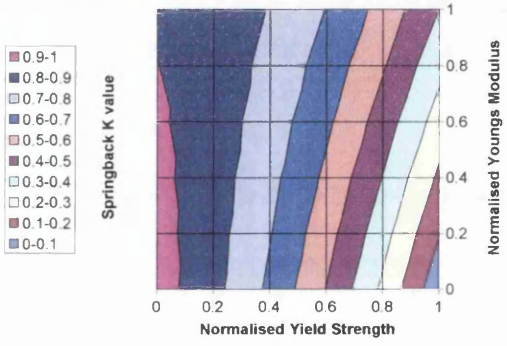

Figure 5.7.16: Six variable numerical algorithm normalised yield strength vs normalised Young's modulus

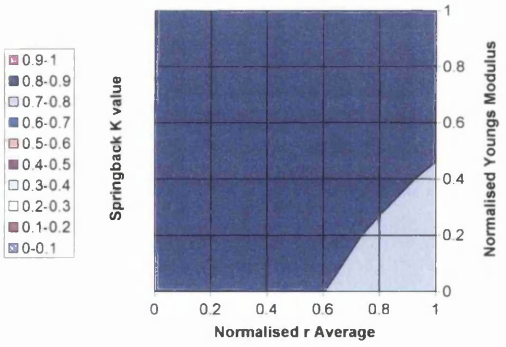

Figure 5.7.17: Six variable numerical algorithm normalised r average vs normalised Young's modulus

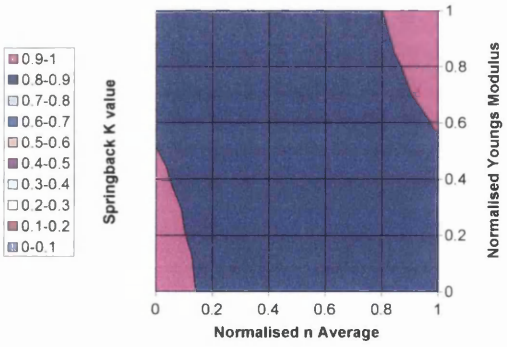

Figure 5.7.18: Six variable numerical algorithm normalised n average vs normalised Young's modulus

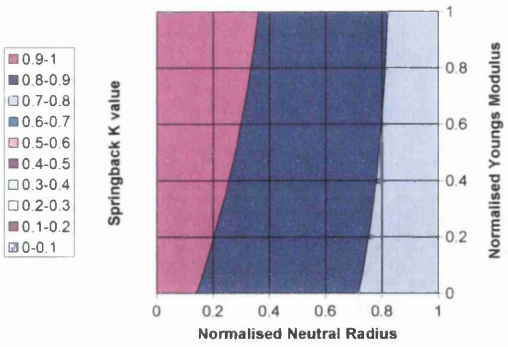

Figure 5.7.19: Six variable numerical algorithm normalised neutral radius vs normalised Young's modulus

		t	*E*	*Rp*	*ρ*
	1	**x1**	**x2**	**x3**	**x4**
1	9.73E-01	3.63E-01	1.30E-03	-8.42E-01	-2.15E-01
x1		-6.87E-01	-1.45E-01	1.39E+00	3.43E-01
x2			-1.14E-02	3.22E-01	4.71E-02
x3				2.85E-01	-8.04E-01
x4					4.53E-02

*Table 5.7.1:*First and second order interactions for four variable numerical algorithm

		t	*E*	*Rp*	*r*	*ρ*
	1	**x1**	**x2**	**x3**	**x4**	**x5**
1	1.03E+00	3.88E-01	-4.19E-02	-1.05E+00	-8.46E-02	-2.03E-01
x1		-7.63E-01	-1.01E-01	1.58E+00	-2.01E-01	3.71E-01
x2			-1.01E-02	3.34E-01	6.93E-02	2.75E-02
x3				3.75E-01	2.71E-01	-7.76E-01
x4					-7.24E-03	6.39E-02
x5						1.28E-02

Table 5.7.2: Linear and first order interactions for five variable numerical algorithm

		t	*E*	*Rp*	*r*	*n*	*ρ*
	1	**x1**	**x2**	**x3**	**x4**	**x5**	**x6**
1	1.22E+00	-2.17E-01	-2.15E-01	-3.79E-01	-1.74E-01	-4.86E-01	-1.14E-01
x1		-6.76E-01	9.86E-02	1.98E+00	-2.59E-01	7.30E-01	3.23E-01
x2			-1.20E-02	4.27E-01	1.41E-01	2.08E-01	-4.76E-02
x3				-4.23E-01	3.04E-01	-6.85E-01	-8.43E-01
x4					-4.79E-02	2.13E-01	1.33E-02
x5						2.08E-01	-6.98E-04
x6							9.89E-03

Table 5.7.3: Linear and first order interactions for six variable numerical algorithm

		t	*E*	*Rp*	*Rm*	*r*	*n*	*ρ*
	1	**x1**	**x2**	**x3**	**x4**	**x5**	**x6**	**x7**
1	3.72E+00	7.74E-01	-1.66E+00	-2.83E+00	-5.62E+00	3.38E-01	-5.91E+00	-9.31E-01
x1		-8.19E-01	1.54E-01	-1.42E+00	2.79E+00	-1.77E-01	-5.70E-01	3.46E-01
x2			3.69E-01	2.35E+00	-6.70E-01	-5.26E-01	2.08E+00	9.10E-02
x3				-1.45E+01	3.38E+01	-1.59E-01	1.51E+00	1.07E+00
x4					-1.42E+01	1.66E-02	6.98E+00	-1.12E+00
x5						9.19E-02	-2.94E-01	2.06E-02
x6							3.03E+00	7.32E-01
x7								1.54E-01

Table 5.7.4: Linear and first order interactions for seven variable numerical algorithm

	1	*t*	*E*	*Rp*	*ρ*
4 variable	9.73E-01	3.63E-01	1.30E-03	-8.42E-01	-2.15E-01
5 variable	1.03E+00	3.88E-01	-4.19E-02	-1.05E+00	-2.03E-01
6 variable	1.22E+00	-2.17E-01	-2.15E-01	-3.79E-01	-1.14E-01
7 variable	3.72E+00	7.74E-01	-1.66E+00	-2.83E+00	-9.31E-01

	t x t	*E x t*	*Rp x t*	*ρx t*
4 variable	-6.87E-01	-1.45E-01	1.39E+00	3.43E-01
5 variable	-7.63E-01	-1.01E-01	1.58E+00	3.71E-01
6 variable	-6.76E-01	9.86E-02	1.98E+00	3.23E-01
7 variable	-8.19E-01	1.54E-01	-1.42E+00	3.46E-01

	E x E	*Rp x E*	*ρx E*
4 variable	-1.14E-02	3.22E-01	4.71E-02
5 variable	-1.01E-02	3.34E-01	2.75E-02
6 variable	-1.20E-02	4.27E-01	-4.76E-02
7 variable	3.69E-01	2.35E+00	9.10E-02

	Rp x Rp	*ρx Rp*
4 variable	2.85E-01	-8.04E-01
5 variable	3.75E-01	-7.76E-01
6 variable	-4.23E-01	-8.43E-01
7 variable	-1.45E+01	1.07E+00

	ρxρ
4 variable	4.53E-02
5 variable	1.28E-02
6 variable	9.89E-03
7 variable	1.54E-01

Table 5.7.5: Selected linear and first order interactions for all numerical algorithms.

5.8 Numerical algorithm analytical model comparison

5.8.1 Aims

The aim of this investigation is to study the areas of differing behaviour for a selection of the models previously interrogated. Zhang was chosen from the group of analytical models, although it was not the best overall performer, it did give relatively good results with a consistent degree of data scatter. The four variable numerical algorithm was also chosen as it used the same input parameters as the Zhang analytical model. In addition to these models the results of the six variable input model was also incorporated into the study to understand why the numerical algorithm was effective as a predictor of springback.
A number of variable interactions were plotted against one another (mapped) to highlight the areas where differing mechanisms were at play.

5.8.2 Results

From fig. 5.8.1a (Zhang predictive model) it can be said that in general as material thickness increases and Young's modulus remains constant springback decreases. Secondly, as Young's modulus decreases and material thickness remains constant, an increase in springback occurs. These two factors in combination result in a graph that has uneven width banding between levels of high and low Young's modulus values. This banding is also not running parallel to any axis, but is sloped in nature.
In contrast, fig. 5.8.1b (4 variable algorithm) depicts a graph that in its lower material thickness region reflects the general trend as depicted in fig 5.8.1a, where as material thickness increase so springback decrease, and as Young's modulus decreases so springback increases. The banded regions appear to be more uniform than those in fig. 5.8.1a, and also less wide. From fig. 5.8.1b it can also be seen that the level of springback encountered is higher than predicted by fig 5.8.1a. At approx. 0.5 of the material thickness the 4 variable algorithmic model depicted in fig. 5.8.1b begins to inflect and an almost symmetric graph is seen along a line running from 0.5 material thickness at high Young's modulus to 0.6 material thickness and low Young's modulus.

In fig 5.8.1c (6 variable algorithm) it can be seen that the inflection point noted in the 4 variable algorithm is still evident. However, the magnitude of effect in thickness has increased, lowering the inflection point, and subsequently altering the balance of the graph, ensuring that high material thickness now results in a greater amount of springback than a thinner material, ex. A value of 0.8 Young's modulus and 1.0 material thickness in the 4 variable model returns a springback K value between 0.7-0.8, where as the 6 variable model returns a value between 0.5-0.6.

From fig. 5.8.2a (Zhang predictive model) it can be seen that, the combination of low thickness and high strength springback is at its highest, and as strength decreases so the effect of springback decreases. A decrease in springback also occurs due to an increase in material thickness. It is noticeable from fig. 5.8.2a that the banded regions are closely packed at lower levels of material thickness, indicating a stronger effect of yield strength at these levels. These effects are then reduced as material thickness is increased. If the results in fig. 5.8.2b (4 variable algorithm) are now compared to the generalized trends mentioned for fig. 5.8.2a it can be seen that these trends are only adhered to at lower levels of material thickness i.e. high strength at low material thickness results in high springback levels, and an increase in the material thickness reduces springback.

It would appear from fig. 5.8.2b that the banding in this lower region of material thickness is far more distinctive than that encountered using the Zhang predictive model as in fig. 5.8.2a and of greater magnitude. The 4 variable numerical algorithmic model depicted in fig. 5.8.2b shows defined banding radiating out from the area of high strength and low material thickness.

This banding appears to be uniform and also less sensitive to material thickness within this region compared to that of fig. 5.8.2a. Secondly, this banding would appear to be from the top quarter of an ellipse, which has a flat major axis. Also a saddle point emerges in fig. 5.8.2b on a line appearing to run from 0 yield strength and 0.4 material thickness to 0.8 yield strength and 1.0 material thickness. From fig. 5.8.2b it would appear that this saddle is symmetric about the line mentioned previously, and it would appear that at high levels of yield strength and material thickness, the 4 variable numerical algorithmic model has reached its outer envelope, and is unable to return a plausible value.

If comparisons are made between fig. 5.8.2c (6 variable algorithm) and fig. 5.8.2b (4 variable algorithm), it can be seen that the essential structures of the graphs are the same. Fig. 5.8.2c appears to show a stronger effect by yield strength, and this has moved the gradient of the inflection point to a stepper angle. The line appears to run from 0 yield strength and 0.3 material thickness to 0.7 yield strength and 1 material thickness.
As shown in fig. 5.8.3a (Zhang predictive model) the effect of high neutral radius bends and low material thickness results in high levels of springback, and as the neutral radius decreases so to does the level of springback. This is also reflected in an increase in material thickness. Fig. 5.8.3a also indicates that as the level of material thickness reduces so the effect of neutral radius becomes greater. In comparison fig. 5.8.3b (4 variable algorithm) shows trends similar to that of fig. 5.8.3a in the lower material thickness region. However, the influence of material thickness would appear to be smaller, as the banded regions are placed at a lower incline than those shown in fig. 5.8.3a. The 4 variable numerical algorithm again introduces an inflection into the graph. A reduction in springback is seen as a consequence of an increase in material thickness and a reduction in neutral radius. Both of these factors are directly related to the amount of induced strain in the material i.e. increasing the strain levels increases the proportion of plastic to elastic deformation. When comparing the levels of springback in fig. 5.8.3a and 5.8.3b it can be seen that the greater amount of springback is shown on fig. 5.8.3b. This indicates that the overall significance level of these two variables in the 4 variable numerical algorithm has less of an effect compared to the same variables using the Zhang model. If comparisons are now made between fig. 5.8.3c (6 variable algorithm) and fig. 5.8.3b (4 variable algorithm), it can be seen that little difference exists between the two plots. It would appear that the 6 variable algorithm adds little to these variable plot.
In fig. 5.8.4a (Zhang predictive model) a well defined linear banding of the behavior between yield strength and Young's modulus is seen. High levels of yield strength in conjunction with low levels of Young's modulus result in high levels of springback. The effect of increasing the Young's modulus is to reduce the impact of yield strength on springback. This is evident at all levels of yield strength and would appear to be constant in magnitude.

When a comparison is made with fig. 5.8.4b (4 variable algorithm), it can be seen that the linear banding remains at low levels of yield strength, but begins to distort as yield strength increases, suggesting that yield strength has less of an effect in the algorithmic model than in Zhang's predictive model. Fig. 5.8.4c (6 variable algorithm) in comparison to fig. 5.8.4b shows an increased effect of yield strength.

Fig. 5.8.4a, 5.8.4b and 5.8.4c follow the general rules that have been published previously. However they differ in direct comparison when levels of high yield strength and low Young's modulus are considered. In respect to this deviation it should be remembered that the numerical algorithm models was derived from actual test data, and Zhang's model was derived by means of mechanical laws and assumptions. It could therefore be argued that the results shown in fig. 5.8.10b and c, as with all the algorithmic plots are a better representation of the interactions taking place.

Fig. 5.8.5a shows the interaction between the neutral radius and the Young's modulus for Zhang's predictive model. It indicates that as the neutral radius increases so the level of springback increases. Increasing the Young's modulus of the material reduces this effect. When a comparison is made with that of the 4 variable algorithmic model as shown in fig. 5.8.5b, it can be seen that the general trend remains, only the effect of Young's modulus is reduced. Evidence of this is in the width of the banding between levels of differing springback (tighter banding larger interaction between variables). If comparisons are now made between fig. 5.8.5c (6 variable algorithm) and fig. 5.8.5b (4 variable algorithm), it can be seen that the effect of neutral radius has decreased slightly, but not to the extent of that seen in fig. 5.8.5a.

Fig. 5.8.6a (Zhang predictive model), 5.8.6b(4 variable algorithm), and 5.8.6c (6 variable algorithm) show the same generalized trends, namely that of high yield strength in conjunction with large neutral radius resulting in high levels of springback. The same radiating bands of differing springback levels are evident. Where the differences lie is in the strength of interaction between the two variables. From fig. 5.8.6b it can be seen that as yield strength decreases along with the neutral radius so the curvature of the bands (leading edge of curvature) begins to reduce indicating a change of interaction value. Whereas the curvature in fig. 5.8.6c shows that the interaction of yield strength has increased. This is evident by the levels of springback within the plot.

5.8.3 Discussion

It has been accepted in general, by both academics and industrialists that an increase in yield strength and neutral radius, along with a decrease in Young's modulus and thickness, results in an increase in springback. This study has shown an agreement with these broad statements in the majority of situations for both the Zhang and algorithmic models. However, a factor repeated throughout the comparative result plots investigated by using the numerical algorithms, is that when material thickness is considered an inflection or saddle is introduced. The cause of these inflections in fig. 5.8.1b/1c, 5.8.2b/2c and 5.8.3b/3c could be an indication of neutral axis shift within the material as the thickness increases. This would seem unlikely as this inflection takes place in a situation where the bend to thickness ratio is approximately 20:1. If this problem is evaluated in simplistic terms the inflection indicates that at some point an increase in material thickness will lead to an increase in the amount of springback noted. An increase in thickness results in an increase in strain and this increase in strain level may trigger a larger reaction from anelastic behaviour or the Bauschinger effect.

The anelastic behaviour of a material is often neglected when considering processes that are carried out in ambient temperature conditions and that are not time dependant. Considering that the majority of these samples were pressed at room temperature (approx. 21°) and measured on the same day, then little if no time dependency occurs and temperature variations would be minimal. However published data [5.8.1, 5.8.2] suggest that errors of up to 20% in high strength sheet steel may occur if no account is made of anelastic effects, under conditions of ambient temperature and no time dependency (effective elastic modulus decreases, therefore springback would increase for high strength steel). Couple this finding with a Bauschinger effect, were a difference of material behaviour in compression and tension takes place we now have a complex interaction which is dependent on strain level encountered and Young's modulus. It could be this interaction that is causing the increase in springback where a decrease is expected.

With regard to the other comparisons made in this experimental study, agreement between the numerical algorithm models and that of Zhang's predictive model were good. Differences arose when consideration was given to the use of Young's modulus as in fig. 5.8.4a and 5.8.5a for Zhangs model, and 5.8.4b/4c, 5.8.5b/5c for numerical algorithms. These comparisons may also be used as indication for the verification to the most suitable definition of elastic modulus to consider when investigating springback.
It has also been evident from this study that the main differences observed between the two numerical algorithms was an increased effect of yield strength, and to a lesser degree Young's modulus.

5.8.4 Conclusion

From the results obtained it has been possible to narrow down the areas that require further research to enable better prediction of springback. Thickness effect appears to be the point at which an analytical model begins to fail, or at least the major factor for it failing. This is a reflection of induced strain in the material, and it is this area of material behaviour during straining and relaxation that requires further investigation. Secondly the level of interaction by yield strength increases as the numerical algorithm input variables increase.
At present, in view of the results obtained it can be said that the use of analytical models (in their nature limited by assumptions) to predict springback is unwise, until such times as a better understanding of the material interactions is gained. The route to a more robust model is through a numerical algorithm, which is better equipped to deal with complex interactions.

5.8.5 References

5.8.1. H. Tsutamori, N. Iwata, N. Suzuki, Springback simulation in sheet metal forming, considering material non-linearity during loading, Proceedings of 22nd Biennial IDDRG Conference Japan, 2002, pg 89-95

5.8.2. R. M. Cleveland, A. K. Ghosh, Inelastic effects on springback in metals, International Journal of Plasticity 18 (2002), pg 769-785

5.8.6 Figures / Tables

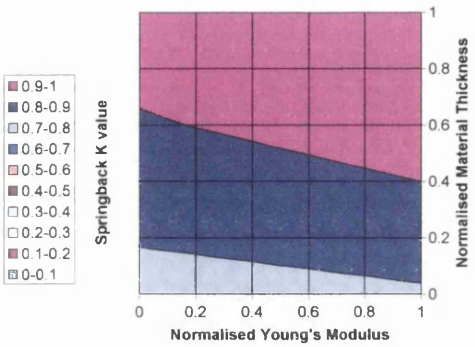

Figure 5.8.1a: Zhang predictive model normalised Young's modulus vs normalised material thickness

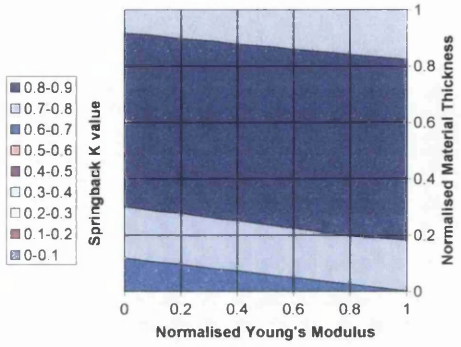

Figure 5.8.1b: Four variable numerical algorithm normalised Young's modulus vs normalised material thickness

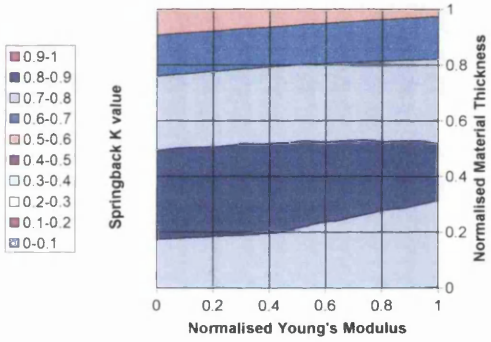

Figure 5.8.1c: Six variable numerical algorithm normalised Young's modulus vs normalised material thickness

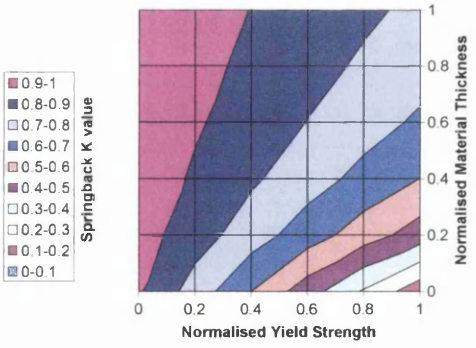

Figure 5.8.2a: Zhang predictive model normalised yield strength vs normalised material thickness

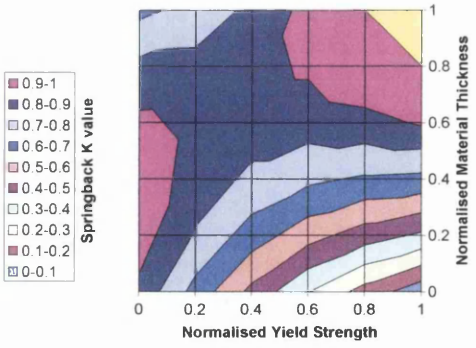

Figure 5.8.2b: Four variable numerical algorithm normalised yield strength vs normalised material thickness

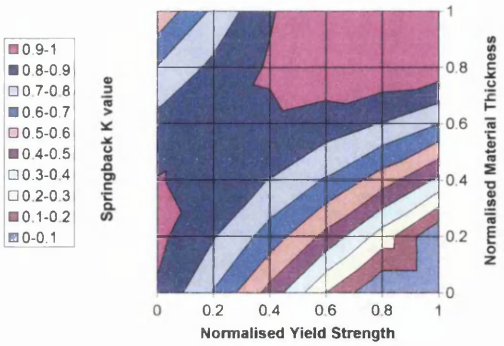

Figure 5.8.2c: Six variable numerical algorithm normalised yield strength vs normalised material thickness

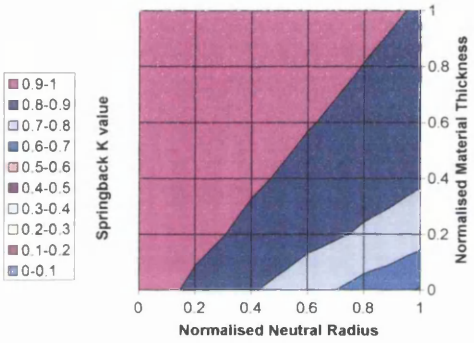

Figure 5.8.3a: Zhang predictive model normalised neutral radius vs normalised material thickness

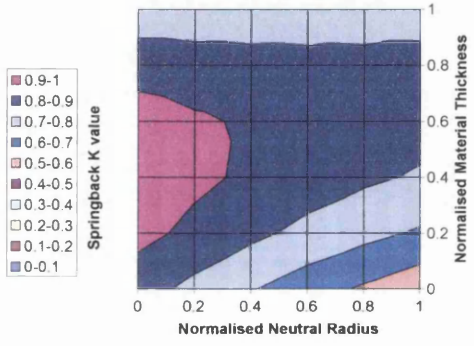

Figure 5.8.3b: Four variable numerical algorithm normalised neutral radius vs normalised material thickness

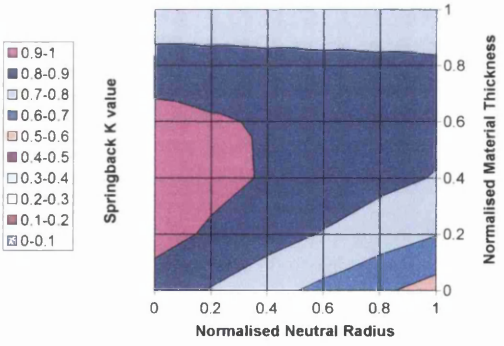

Figure 5.8.3c: Six variable numerical algorithm normalised neutral radius vs normalised material thickness

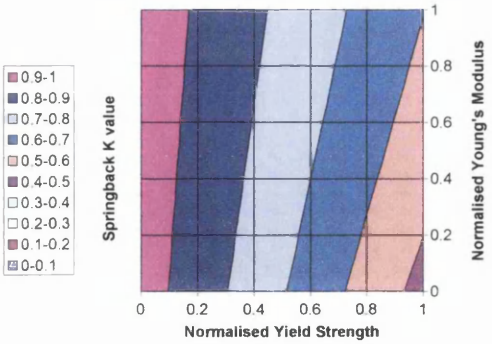

Figure 5.8.4a: Zhang predictive model normalised yield strength vs normalised Young's modulus

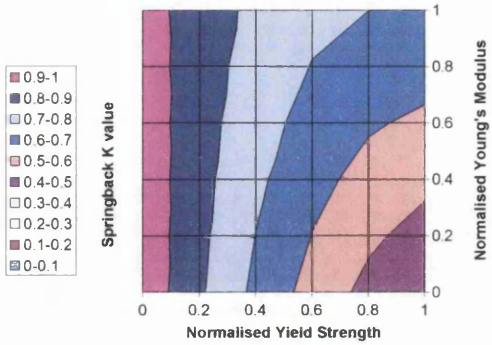

Figure 5.8.4b: Four variable numerical algorithm normalised yield strength vs normalised Young's modulus

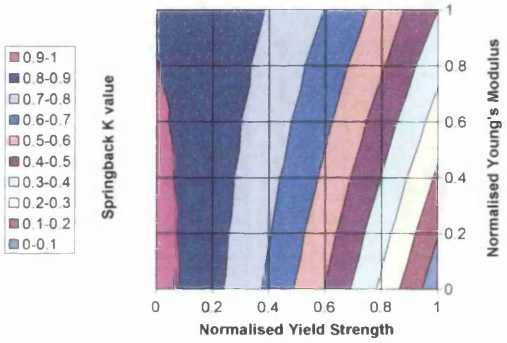

Figure 5.8.4c: Six variable numerical algorithm normalised yield strength vs normalised Young's modulus

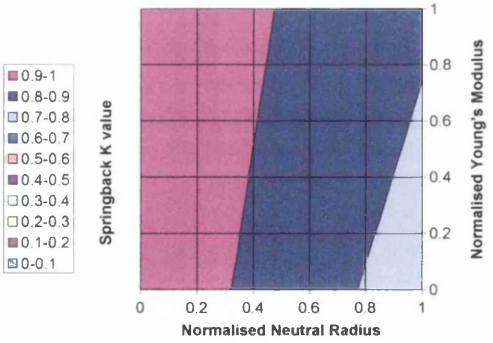

Figure 5.8.5a: Zhang predictive model normalised neutral radius vs normalised Young's modulus

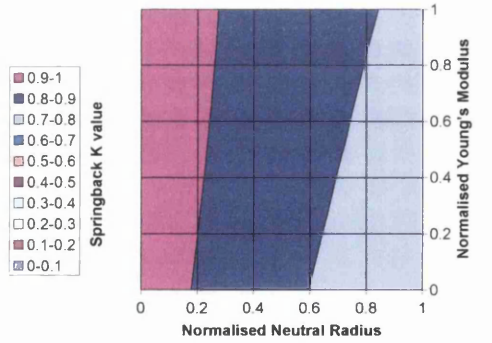

Figure 5.8.5b: Four variable numerical algorithm normalised neutral radius vs normalised Young's modulus

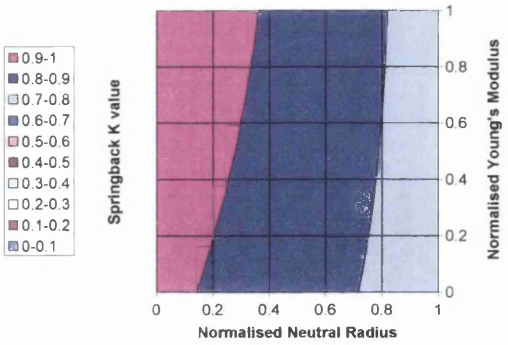

Figure 5.8.5c: Six variable numerical algorithm normalised neutral radius vs normalised Young's modulus

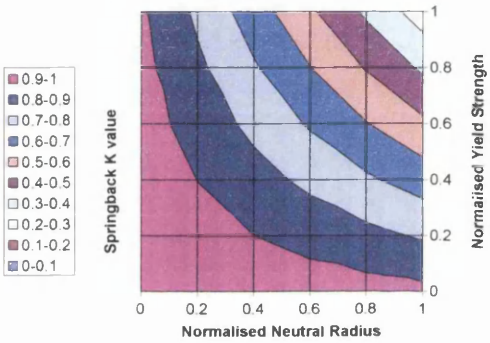

Figure 5.8.6a: Zhang predictive model normalised neutral radius vs normalised yield strength

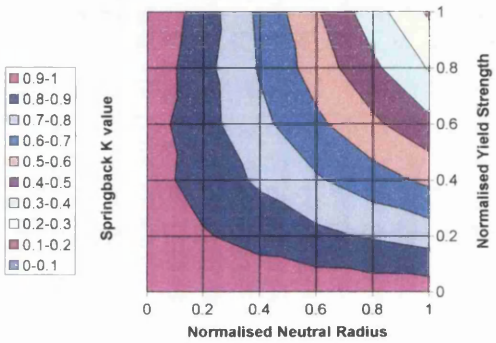

Figure 5.8.6b: Four variable numerical algorithm normalised neutral radius vs normalised yield strength

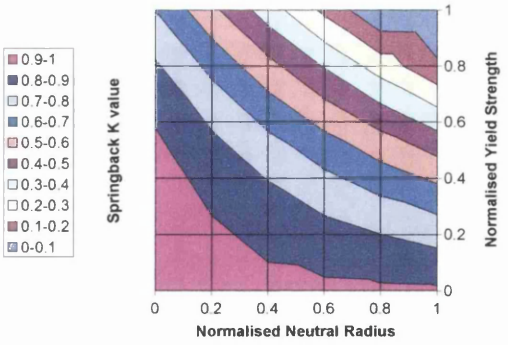

Figure 5.8.6c: Six variable numerical algorithm normalised neutral radius vs normalised yield strength

5.8a Numerical algorithm analytical model comparison

5.8a.1 Aims

The aims of this mini investigation were to identify the areas of difference within the numerical algorithm model, when outlying points were neglected. As with all numerical algorithms this would lead to an effect, the magnitude of which is dependent on the variables considered as inputs.

5.8a.2 Results

From fig. 5.8a.1a and 5.8a.1b it can be seen that the outlying point omission decreases the R^2 value, and also the graph trend line value. From fig. 5.8a.1a-5.8a.4b it is evident the inversing effect of the material thickness is still present. This effect does appear to be lessened when considering the omitted outlying points from the numerical algorithm.
Comparison between fig. 5.8a.5a, and 5.8a.5b show that the effect of yield strength has been reduced when the outlying points are omitted from the numerical algorithm.
Fig. 5.8a.6a and 5.8a.6b show that the effect of omitting the outlying points when developing the numerical algorithm leads to a reduction in the effect of Young's Modulus at higher neutral radii.
As with fig. 5.8a.5b, fig 5.8a.7b shows a reduction in the effect of yield strength when considering the numerical algorithm with the outlying points omitted.

5.8a.3 Discussion

From the results obtained during this investigation it is evident that the major underlying traits shown by the 4 variable numerical algorithm are reflected by the 4 variable numerical algorithm where the outlying points are omitted.
This would suggest that the overall effect of the two outlying points seen in the predictive model plot in fig. 5.8a.1a has little effect on the overall performance of the 4 variable numerical algorithm, other than a nominal lessening of effects of a number of variables.

5.8a.4 Conclusion

1. Omitting the two outlying points from the numerical algorithm make up reduces the models predictive ability
2. The overall effect of the omission of these two data points is minimal in comparison to that seen when considering an analytically derived predictive model

5.8a.5 Figures / Tables

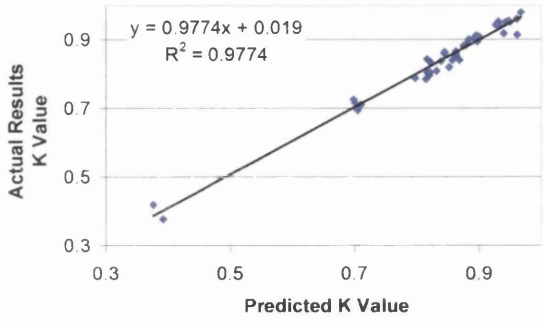

Figure 5.8a.1a: Four variable numerical algorithm predicted results

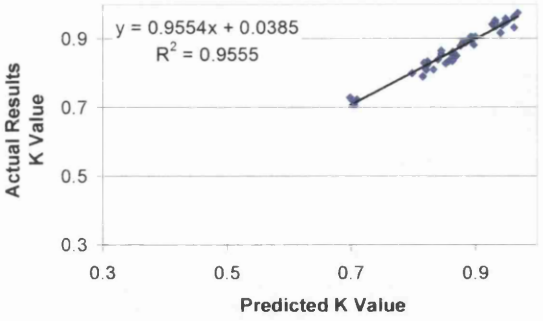

Figure 5.8a.1b: Four variable numerical algorithm predicted results omitting out lying points

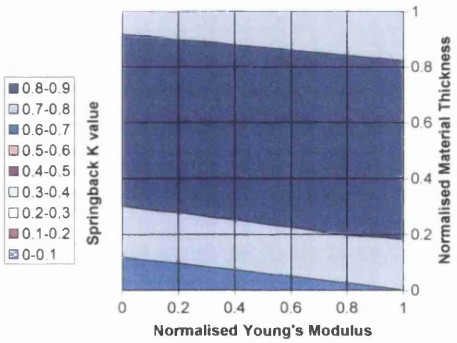

Figure 5.8a.2a: Four variable numerical algorithm normalised Young's modulus vs normalised material thickness

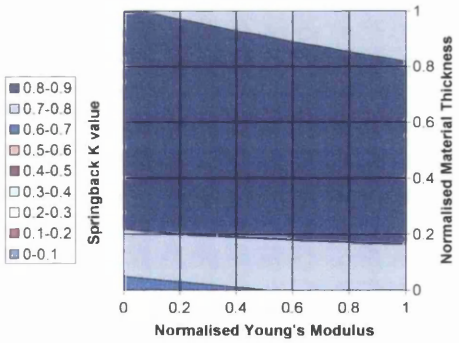

Figure 5.8a.2b: Four variable numerical algorithm normalised Young's modulus vs normalised material thickness omitting out lying points

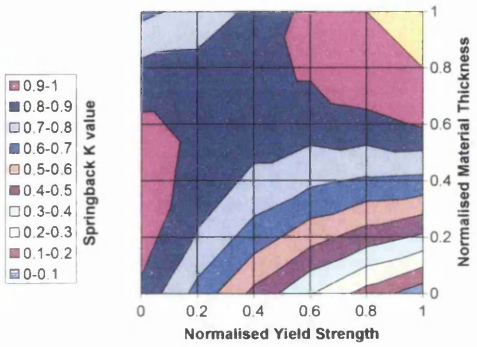

Figure 5.8a.3a: Four variable numerical algorithm normalised yield strength vs normalised material thickness

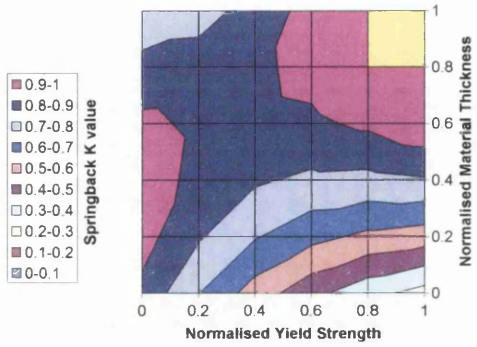

Figure 5.8a.3b: Four variable numerical algorithm normalised yield strength vs normalised material thickness omitting out lying points

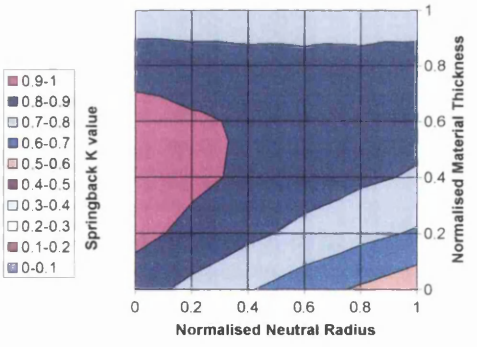

Figure 5.8a 4a: Four variable numerical algorithm normalised neutral radius vs normalised material thickness

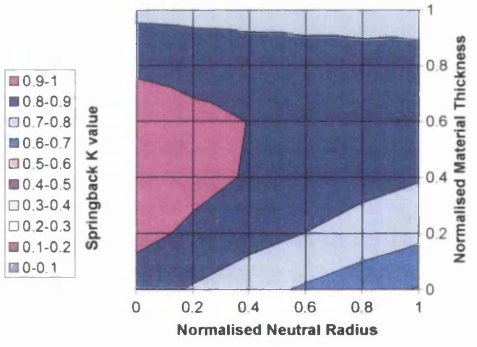

Figure 5.8a.4b: Four variable numerical algorithm normalised neutral radius vs normalised material thickness omitting out lying points

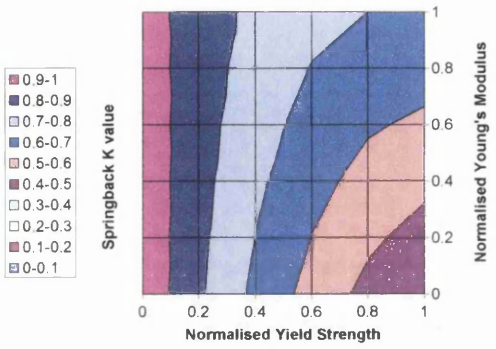

Figure 5.8a.5a: Four variable numerical algorithm normalised yield strength vs normalised Young's modulus

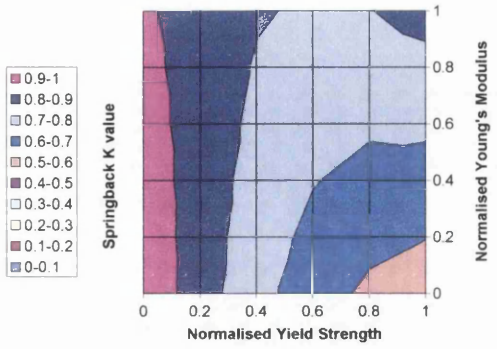

Figure 5.8a.5b: Four variable numerical algorithm normalised yield strength vs normalised Young's modulus omitting out lying points

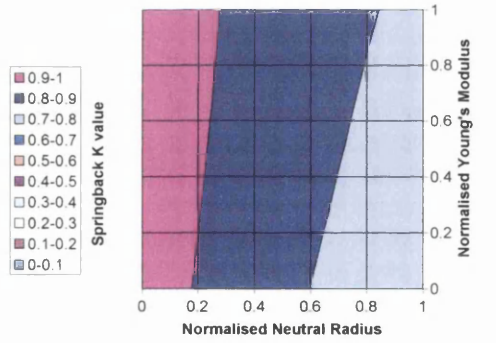

Figure 5.8a.6a: Four variable numerical algorithm normalised neutral radius vs normalised Young's modulus

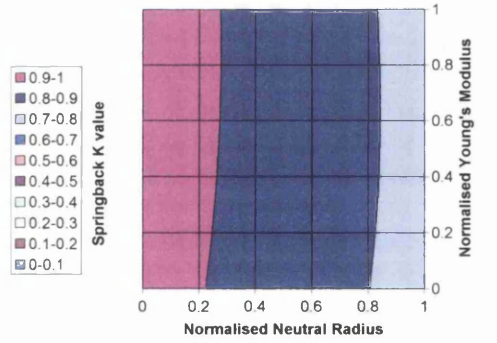

Figure 5.8a.6b: Four variable numerical algorithm normalised neutral radius vs normalised Young's modulus omitting out lying points

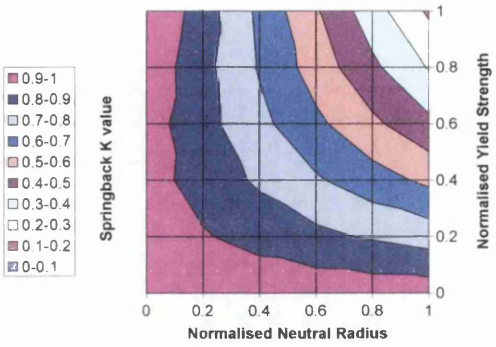

Figure 5.8a.7a: Four variable numerical algorithm normalised neutral radius vs normalised yield strength

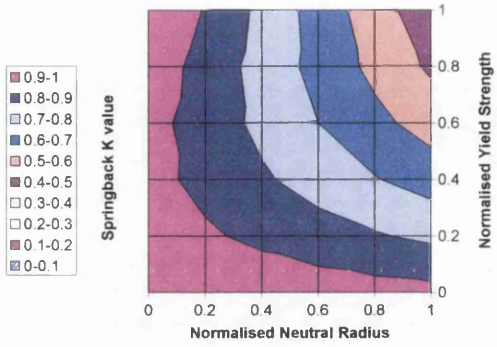

Figure 5.8a.7b: Four variable numerical algorithm normalised neutral radius vs normalised yield strength omitting out lying points

5.9 Initial Tailored Blank Investigation

5.9.1 Aims

The aim of this investigation is to understand the effect of springback on final component geometry in low strain forming modes for tailored blanks.
An understanding of the key material, and loading factors that influence springback is needed to be able to predict springback for a tailored blank produced using a single grade of steel, and also those which are composites of several differing families of sheet steel. Development is needed to accommodate the mismatch in material strength and therefore differing springback behaviour of the wide range of sheet steel used. Thickness changes will produce areas of differing springback, high stress concentration, and limited formability due to weld properties.

5.9.2 Results

The ideal weld conditions for DP 800 and GA 140 LWTB combination was a focal length of 200mm, power set at 6 kW using a helium shielding gas, with a flow rate of 20 l/min. weld speed was set to 8 m/min. The blanks were 120 – 40 mm(width) x 110mm (length), with the weld line situated in the mid point along the length of the blank parallel to the punch centre line.
It was evident when interrogating the profilometer measurement results for the DP 800 and GA 140 LWTB with pressing centre line parallel to the weld line, that two distinct radi measurements existed both emulating from the weld line. From the results shown in fig. 5.9.1 it can be seen that the combination of DP 800 and GA 140 results in the two constituent parts being void of interaction between one another. Fig. 5.9.1 also shows that as the forming pressure increases, so the effects of coining becomes evident (springback is reduced). If a ratio is taken between the two measured springback values for differing forming pressures, and is called K_v as shown if fig. 5.9.2, it can be seen that the springback ratio value K_v increases as the forming pressure increases between the values of 0.005 kN/mm² and 0.0125 kN/mm². From fig. 5.9.2 it would appear that above 0.0125 kN/mm² the value of K_v no longer increases. A point of interest noticed during this investigation was that of a plastic hinge effect. This effect is common when simple bends are performed. It's occurrence is due to single point of contact along the length of the punch at the materials mid span. This load causes a maximum bending moment, and therefore an area of initial yielding. From the observation during this series of experimental pressings it was evident that the plastic hinge would occur in the thinner material. Forming

deformation, to take the die tool geometry, only occured once the thicker material reached the die tool bottom surface.

Fig. 5.9.3 shows the results obtained when GA 140 0.7mm and DP 800 1.0mm are tailored together, then pressed with the weld line traverse to the pressing centre line. The blanks were 100mm x 100mm, with the weld line situated in the mid point along the length of the blank transverse to the punch centre line see fig. 5.9.4. From the results shown in fig. 5.9.3 it appeared that the springback level K flowed from one tailored section to another in a general trend rising from a low value of K in the DP 800 to a high value of K in the GA 140. Results obtained from the samples indicated that an underlying relationship existed, but at this stage it was not obvious as to what relationship existed between the two differing types of material. A further investigation was carried out to see which curve/law best fitted the data. Initial investigations on the samples concentrated on the ability of the results to conform to a linear law, see fig. 5.9.5. From fig. 5.9.5 it can be seen that the pressings resulted in a linear fit, of which the least R^2 value is 0.9485. In most instances this level of R^2 value would suffice to confirm a linear law relationship. However, two areas in the curve raised concerns about the suitability of a linear fit. Firstly, the curve exhibited a poor fit on the extreme DP 800 side of the graph. Secondly when closer interrogation was carried out into the curve it was found that the trend line was also ill fitting around the area of transition between the constituent parts of the LWTB. Due to these discrepancies the overall linear fitting law was neglected. The next approach was still to consider a linear relationship, however, in this case one in which the transition point (weld line) created a point of separation between the two materials. Fig. 5.9.6 shows the results of the sample split into two distinctive linear fitting laws, each having a differing gradient dependent on the material type, the weld line being the common point between the constituent parts of the LWTB. It can be seen from fig. 5.9.6 that the GA 140 springback results fitted well with a linear law, however, this was not reflected on the DP 800 side of the LWTB. From past experience [5.9.1, 5.9.2] in measuring springback, using the same pressing parameters and materials, the R^2 value would be approximately the same for a linear fit in regards to springback in the DP 800, suggesting the suitability of a linear fit up.

Further investigation into the curve of the sample was carried out, and an alternative best fit general curve appeared to be one in which an error function, typically associated with diffusion as a consequence of the interaction between the materials either side of the weld [5.9.3] was used (function of *tanh*[5.9.4, 5.9.5]). Using this in conjunction with the predicted values of springback for each of the constituent parts in the LWTB gave the best fit. The full blank length of 100mm

was normalized between –1 and 1, as it was evident from curve fitting exercise that these values returned a slope similar to that of the curve. The reasoning behind this action was the assumption that the majority of the diffusion i.e. approximately 75%, had taken place within the blank length. It was also evident that the resultant error function curve needed to be adjusted in both the x and y axis directions. To realise this, the error function was initially off-set using a single value or point reference, however this led to an overshoot in comparison to the actual results. The secondary method and the most effective was the use of a linear equation off-set, which brought the error function curve into line with that of the actual results, see fig. 5.9.7.
When a comparison is made between the actual results and those gained by using the diffusion law, with a linear off-set, it can be seen that an R^2 value of 0.9543 is obtained, and an equation of $y = 0.9963x + 0.0073$ see fig. 5.9.8. With the sample a need for linear offset prefix's has meant that the error function curve is no longer an inversed mirror image about the x-axis. The resultant curve is weighted by the differential magnitude of the level of springback of their two constituent parts and the forming method used.

A numerical algorithm was incorporated to try and improve the previous fit, the results of which can be seen in fig. 5.9.9. When a comparison is made between the actual results and those gained by using the numerical algorithm it can be seen that an R^2 value of 0.9836 is obtained, and an equation of $y = 0.9835x + 0.0089$, see fig. 5.9.10.

5.9.3 Discussion

From the results obtained in fig. 5.9.1 it can be said that when the weld line is in parallel to the pressing centre line, the resultant pressing has essentially two distinct formed components. The point of transition from one type to another is the weld line. Each one of the components takes on the form expected from the parent material, with no apparent interaction from the neighbouring material. Also the ability to coin a LWTB enables a manufacturer to increase the K_v value and therefore bring the springback behaviour of differing types of material in line with one another. Further research may be able to quantify to what degree K_v may be increased, thus defining windows of manufacture for LWTB.

From fig. 5.9.3 it has been shown that LWTB that are pressed with the weld line and the punch centre line traverse to each other will result in a blank that has direct interactions between the two constituent parts. The actual mechanism that is at work here is unclear at the present moment, and further research is need in this area. Investigations carried out into curve/law fitting

showed that a numerical algorithm, a diffusion law curve having a secondary linear relationship attached to it (linear off-set), and a linear fit curve separated by the weld line were able to predict accurately the springback behaviour of a LWTB.

It is unclear at this moment as to the preferred methodology to be adopted for prediction of LWTB springback behaviour, as each of the cases has merits. The diffusion law curve returns a low R^2, the linear equation is $y \approx x$ thus suggesting only scatter is the curtailing factor. As for the numerical algorithm the R^2 value is higher however the curtailing factor here is the linear equation, showing that a perfect $y=x$ is unobtainable, and the linear law separated by the weld line is let down by the R^2 associated by the DP 800 constituent part.

The linear off-set in the diffusion law curve may be thought of as the ability to transmit the constituent parts of the adjoining materials springback characteristics. Therefore the relationship would be dependent on the materials mechanical and geometric properties as a function of distance from the weld. The linear off-set can be calculated easily by knowing the final formed results, however further investigation is needed to enable prediction of LWTB final formed shape. This is also true for both the numerical algorithm and linear law separated by the weld line. The result of which would be a larger experimental matrix. From the evidence shown in the results of fig. 5.9.6, 5.9.8 and 5.9.10, the best performer was that of the numerical algorithm, however this does not lead to an easily expressible law. Although the formulation of such predictive equations at this stage is not possible, the underlying principle behind the behaviour is visible.

5.9.4 Conclusion

1. For LWTB pressed with the weld line in parallel to the pressing center line, both constituent parts are void of interaction between one another.
2. As forming pressure increases, so the effects of coining become evident (springback is reduced), enabling differing types of material to exhibit similar springback values.
3. LWTB's that are pressed with the weld line and the punch centre line traverse to each other, result in a blank having interactions between the two constituent parts.
4. Numerical algorithm, diffusion law with linear off-set and linear law separated by the weld line, have proven to be contenders in predicting the springback behaviour of a LWTB pressed with the weld line and the punch centre line traverse to each.

5. More research is needed to indicate preferred methodology for predicting the springback of LWTB pressed with the weld line and the punch centre line traverse to each.
6. Plastic hinge effects seen during pressing occurs in the thinner material.

5.9.5 References

5.9.1 H B Mullan, Influence of springback on final formed component shape of thin high strength sheet steel, Sheet Metal 2003, Proceedings of the International Conference, 14-16 April 2003, University of Ulster Jordanstown, ISBN 1 859231713, pg 447-454

5.9.2 H B Mullan, Improved prediction of springback on final formed components, AMPT 2003, Dublin City University, 8th-11th July 2003, to be presented

5.9.3 D.A. Porter and K.E. Easterling, Phase Transformations in Metals and Alloys, Second edition, Chapman and Hall, ISBN 0 412 45030 5, pg 69-75

5.9.4 K.A. Stroud, Engineering Mathematics, Third edition, Macmillan, ISBN 0 333 4887 1, pg 345-395

5.9.5 G. Stephenson, Mathematical Methods for Science Students, Second edition, Longman Scientific and Technical, ISBN 0 582 44416 0, pg 136-142, 239-240

5.9.6 Figures / Tables

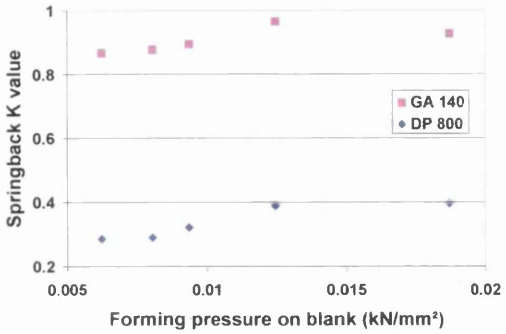

***Figure** 5.9.1:* LWTB of DP 800 and GA 140 Sample width varied from 120mm – 40mm

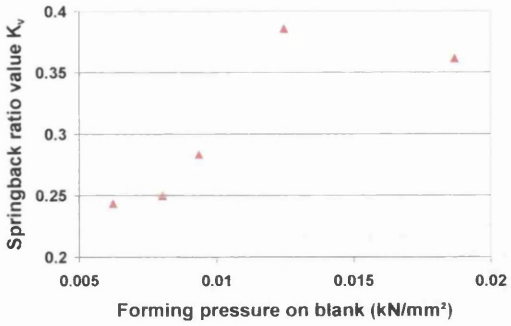

***Figure** 5.9.2:* LWTB of DP 800 and GA 140 showing springback ratio K_v

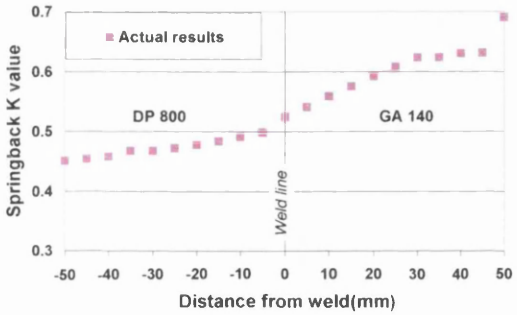

***Figure** 5.9.3:* Pressing LWTB of DP 800 and GA 140, with weld line transverse to pressing centre line

***Figure** 5.9.4:* Pressing LWTB of DP 800 and GA 140

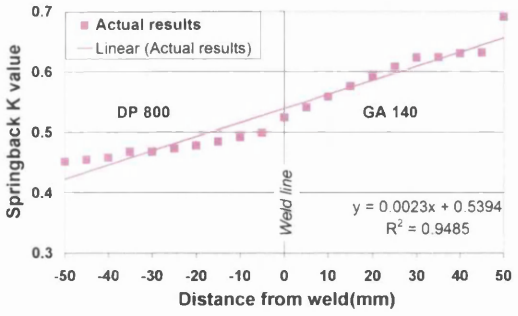

***Figure** 5.9.5:* Overall linear fitting curve for LWTB of DP 800 and GA 140

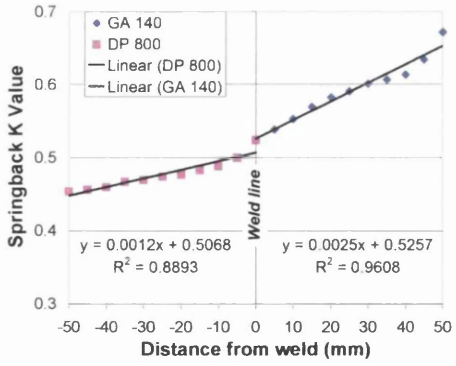

***Figure** 5.9.6:* Separated linear fitting curve for LWTB of DP 800 and GA 140

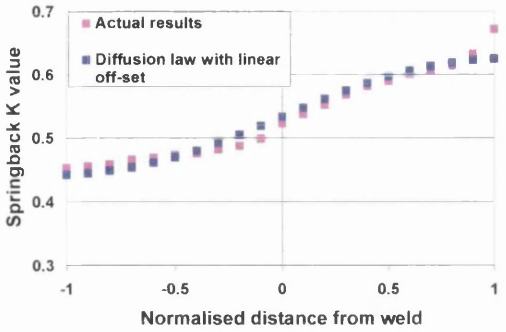

Figure 5.9.7: Pressing LWTB of DP 800 and GA 140, shimmed with weld line transverse to pressing centre line in conjunction with diffusion law incorporating a linear off-set

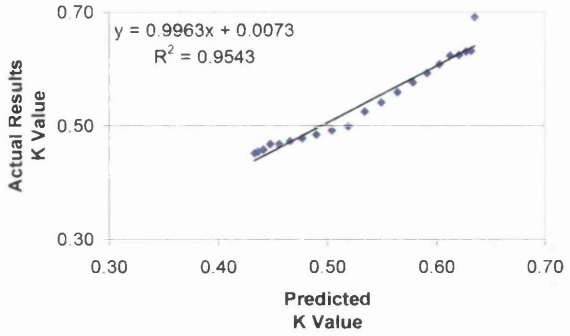

Figure 5.9.8: Comparison of actual verses diffusion law with linear off-set LWTB of DP 800 and GA 140, shimmed with weld line transverse to pressing centre line

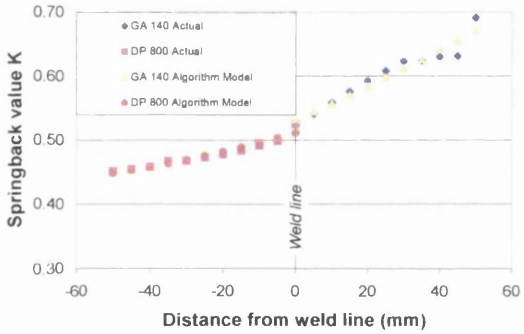

Figure 5.9.9: Algorithm model results for LWTB of DP 800 and GA 140, shimmed with weld line transverse to pressing centre line

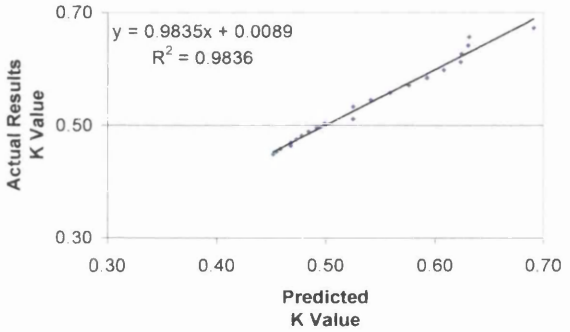

Figure 5.9.10: Comparison of actual verses algorithm model results for LWTB of DP 800 and GA 140, shimmed with weld line transverse to pressing centre line

5.10 Further Tailored Blank Investigation

5.10.1 Aims

The aim of this investigation was to build on the initial LWTB experiments by increasing the material matrix, and adding to the forming conditions previously studied.

5.10.2 Results

The blanks were 100mm x 100mm, with the weld line situated in the mid point along the length of the blank transverse to the punch centre line. Fig. 5.10.1 shows the results of both a shimmed and unshimmed pressed LWTB sample of GA 140 and DP 800 materials. The actual formed unshimmed sample can be seen in fig. 5.10.2. From fig. 5.10.1 it can be seen that two distinct sets of results occur, depending on the inclusion or omission of the shims. It would appear that not only does the DP 800 material have a differing springback K value at –50mm from the weld line, but this disparity increase as the distance to and from the weld line increases. Fig. 5.10.3 depicts a graph in which a linear law is assumed across both materials as previously described in section 5.9. It can be seen that the unshimmed sample in contrast to the shimmed sample has more scatter (R^2 value smaller) than that shown for the shimmed sample, if a linear trend across the two materials is considered, Fig. 5.10.4, depicts the shimmed and unshimmed samples as two distinct linear trends originating at the weld line. It can be seen that the results shown in the previous section 5.9 for the shimmed sample is repeated, in that the linear fit for the GA 140 material is good with an R^2 value of 0.9735. However, the DP 800 linear fit is poorer at 0.876. as mentioned in the previous section. This increase in R^2 value may be a reflection of the materials variability, and this could indeed be a linear fitting law. As with the previous section, 5.9, the results were also investigated using the diffusion law with a linear off-set, the results of which can be seen in fig. 5.10.5. Fig. 5.10.6 shows the linear off-set that was needed on this occasion. From fig. 5.10.7 it can be seen that even with this manipulation the R^2 value is poor, and in fact is poorer than the previous results from section 5.9. Fig. 5.10.8 depicts the unshimmed sample results with those predicted by a numerical algorithm, as described in the previous section. It can be seen that the

predicted results have good correlation with those measured. This can also be seen from fig. 5.10.9 showing the actual results plotted against the measured results, resulting in an R^2 of 0.9566.

Fig. 5.10.10 shows the LWTB of GA 140 and DP 350YP, where the weld line is set at 45° to the pressing centre line, blanks were 50mm (width) x 190mm (length). The results obtained from this sample were identical to those shown in section 5.9 for samples having weld lines in parallel to the pressing line i.e. the differing materials have no effect on the neighbouring material.

Shown in fig. 5.10.11 is the pressing and weld configuration for this forming trial where the weld line is moved in relation to the punch centre line. The blanks were 50 mm(width) x 110mm (length), with the weld line situated in the mid point along the length of the blank parallel to the punch centre line, and then moved away from the punch centre line in 10mm intervals. The formed components of this trial can be seen in fig. 5.10.12, the LWTB consisted of DP 350YP and DP 800. Fig. 5.10.13 shows the behaviour of the tailored blank when the weld line is moved in relation to the centre line of the pressing. From fig. 5.10.13 it can be seen that the springback of the material remains the same so long as the forming pressure remains constant. At the point were the weld line is offset at 30mm to the pressing centreline the springback of both materials is almost identical. This situation however takes place where the weld line is within approx. 5mm of the edge of the tooling, and therefore little if any forming is taking place. As mentioned previously the plastic hinge effect once again appeared to occur in the thinner weaker material.

Fig. 5.10.14 shows the results of the LWTB pressing of GA 140 and DP 350YP shimmed and non shimmed. The samples were 200mm x 80mm with the shortest edge running parallel to the pressing centre line. This meant, that the weld line ran traverse to the weld line, see fig. 5.10.15 for the formed component. From fig. 5.10.14 it can be seen that the springback behaviour of the two materials is similar. This would be expected as in the initial springback trials only a difference of only 1% in the 0° direction and 3% in the 90° direction was recorded. It can be seen that the shimmed sample returned the more consistent readings, where as the non shimmed sample exhibited greater variation. Two

factors may have effected the non shimmed sample, both of which cannot be proven from these results but are conceivable. Firstly, although soft copper was used as a shim material, and no interaction was likely, the cause of the gap differential during the initial stages of the pressing could have increased the affected plastic hinge area, as the thicker material is 'locked' on the edge of the tooling, the thinner is forced to deform more. Secondly, the differential in the thickness will have induced a bending moment in the tooling, resulting in uneven forming of the component.

Fig. 5.10.16 shows the results of a LWTB made from three blanks. Each of the extremities are GA 140, with the centre section being DP 800. It can be seen that all the materials interact, and that the level of springback seen in the materials do not match those seen in fig. 5.10.1. Blanks in fig. 5.10.16 are less in width dimension by approx 25mm, therefore the forming pressure used is 33% greater than that used for fig. 5.10.1. This would explain the disparity in the resultant springback. A linear trend line fit for each of the sections in the LWTB can be seen in fig. 5.10.16. It is evident that the GA 140 fits are good. However, the DP 800 trend lines are less than those accounted for previously, which is unexpected as a higher forming pressure resulting from the reduction in sample area should coin the sample, and reduce the amount of scatter. The final formed component can be seen in fig. 5.10.17.

5.10.3 Discussion

In the previous section it was unclear as to which if any of the methods to predict LWTB springback behaviour was best. The results shown here have highlighted again that several major concerns hang over each of the tested methods. The overall linear trend crossing the weld line performed well, but on both the shimmed and unshimmed samples there does appear to be a curve at the mid points and end of the results. These curves may just be measurement errors, but they are consistent in their location for both samples leading again to the dismissal of the linear trend crossing the weld line.

The linear trend with differing behaviour for the differing materials and forming conditions performs well in the GA 140 region, but was let down in the DP 800 region. As mentioned previously this may be the amount of natural scatter for the DP 800

material. If this was the case, then this trend would still require further investigation, as would all the others considered in this investigation. No method exists presently to predict the value of springback on the weld line.

The use of the diffusion and linear off-set law in the instance of the unshimmed sample performed poorly in comparison to the performance seen for the shimmed sample. This may be due to the two points in fig. 5.10.7 that are higher than would be expected and therefore reducing the R^2 value of the trend line. The major concern with this method again is the fact that the samples need to be formed and measured so that the diffusion law can be set up initially and then compared to the actual results, which in essence is not a truly predictive method. Finally the numerical algorithm method again is not a truly predictive tool as the matrix of differing experiments has to be built upon, to enable a truly robust method.

A practical consideration when considering a LWTB made of differing material thickness is not only the plastic hinge effect but also the orientation of the blank, i.e. material step on the inner surface of the tube, or on the outer surface. For forming purposes there is no ideal. Hydroforming however, would dictate that the step is on the inner surface.

Also whilst the use of shims, in experimental conditions is not an issue, in production it would be uneconomic even to consider. This now raises the question of tooling, and cost effectiveness.

Another point of concern is the setting up of bending moments on the punch tooling when considering LWTB that have a large differential of thickness.

It has been shown that coining may be a method to reduce the disparity between LWTB differing springback characteristics. With the weld line traverse to the pressing line, it is also possible to separate the pressing steps into material type and individualise each of the pressing steps to suite the material being formed during that step.

5.10.4 Conclusion

From the results shown in this investigation, it is possible to say:-

1. That the omission or inclusion of shims in differential thickness LWTB results in two differing formed components. LWTB that use shims are consistent in nature, where as the samples pressed without shims show signs of large fluctuations.
2. The bending methodology must be sympathetic to the future usage of the tube regarding location of the thickness differential step.
3. All the models investigated have their own downfalls, the majority of which is the need to press components before having the ability to predict subsequent springback behaviour.
4. the use of shims in production is uneconomical

5.10.5 Figures / Tables

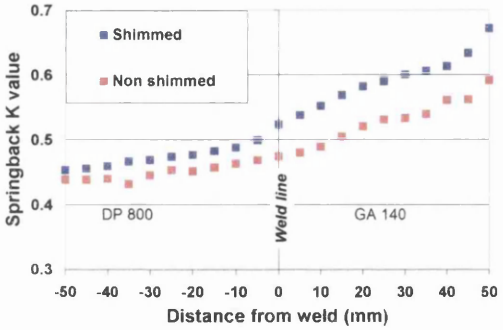

Figure 5.10.1: Pressing LWTB of DP 800 and GA 140 shimmed and unshimmed, with weld line transverse to pressing centre line

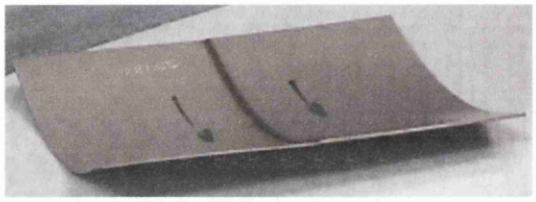

Figure 5.10.2: Picture of pressed LWTB of DP 800 and GA 140 unshimmed, with weld line transverse to pressing centre line

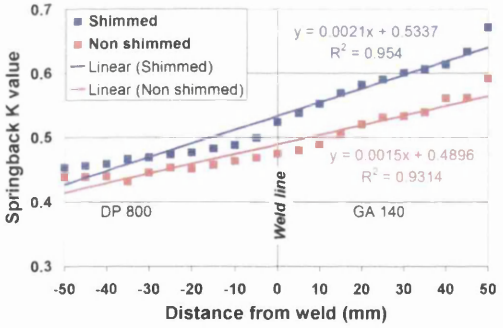

Figure 5.10.3: Overall linear fitting curve for LWTB of DP 800 and GA 140 shimmed and unshimmed

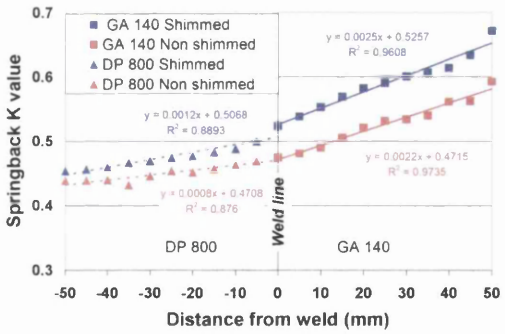

Figure 5.10.4: Separated linear fitting curve for LWTB of DP 800 and GA 140 shimmed and unshimmed,

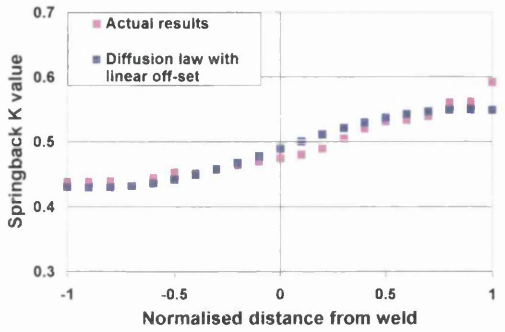

Figure 5.10.5: Pressing LWTB of DP 800 and GA 140, unshimmed with weld line transverse to pressing centre line in conjunction with diffusion law incorporating a linear off-set

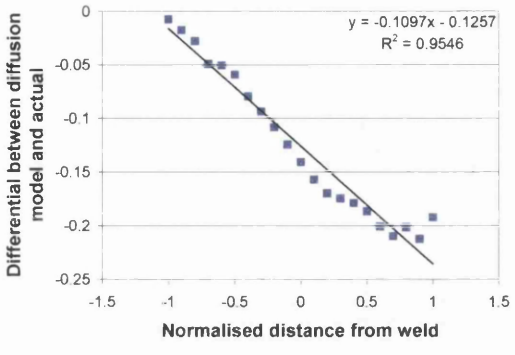

Figure 5.10.6: Comparison of actual verses diffusion law to gauge the linear off-set for LWTB DP 800 and GA 140

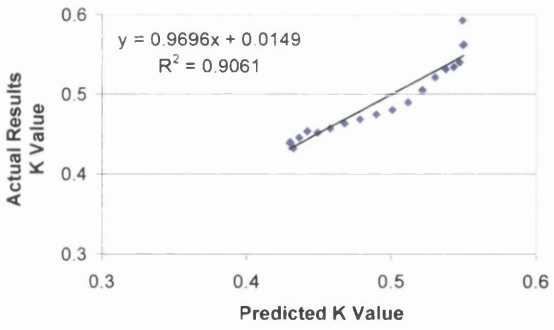

Figure 5.10.7: Comparison of actual verses *diffusion law incorporating a linear off-set* model, for LWTB of DP 800 and GA 140, unshimmed with weld line transverse to pressing centre line

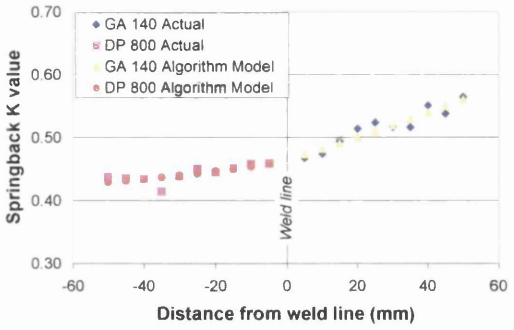

Figure 5.10.8: Comparison of actual verses algorithm model results for LWTB of DP 800 and GA 140, unshimmed with weld line transverse to pressing centre line

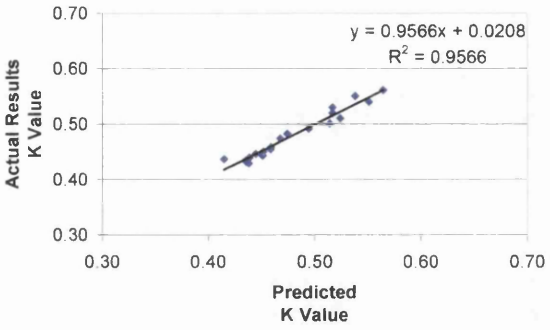

Figure 5.10.9: Comparison of actual verses algorithm model results for LWTB of DP 800 and GA 140, unshimmed with weld line transverse to pressing centre line

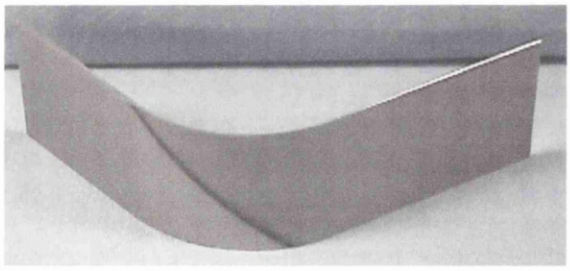

Figure 5.10.10: LWTB of GA 140 and DP 350YP, were the weld line is set at 45°

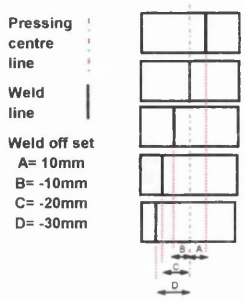

Figure 5.10.11: Schematic of weld line in relation to the punch centre line

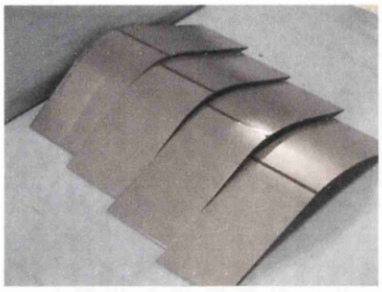

Figure 5.10.12: Punch centre line trial formed components

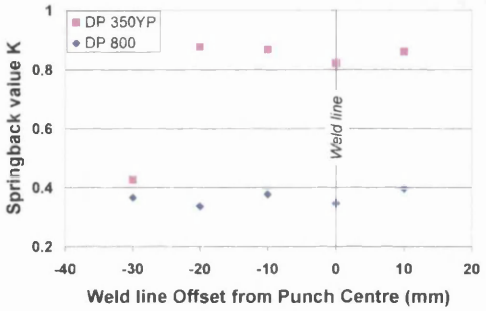

Figure 5.10.13: Punch centre line trial results

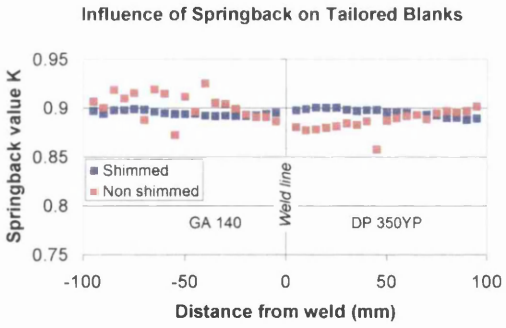

Figure 5.10.14: Pressing LWTB of DP 350 YP and GA 140 shimmed and unshimmed, with weld line transverse to pressing centre line

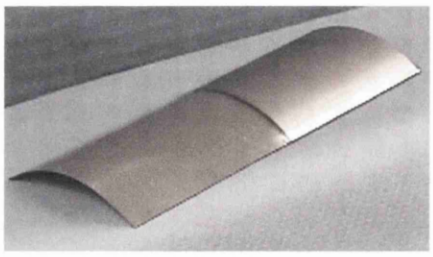

Figure 5.10.15: Picture of pressed LWTB of DP 350 YP and GA 140 shimmed and unshimmed, with weld line transverse to pressing centre

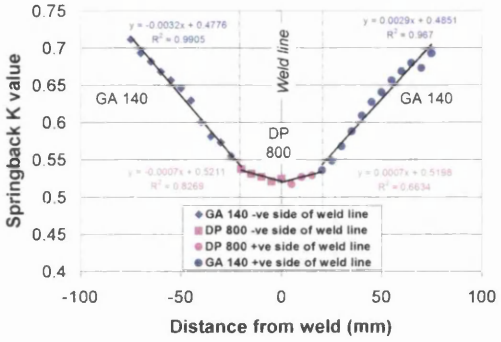

Figure 5.10.16: Pressing LWTB of GA 140,DP 800 and GA 140 shimmed with weld line transverse to pressing centre line

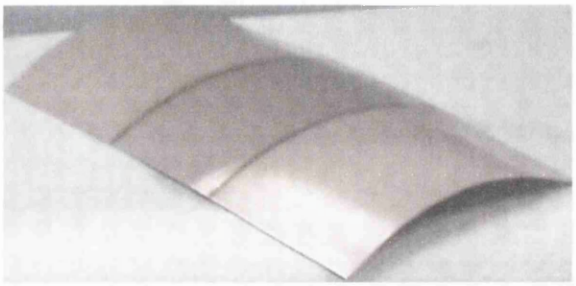

Figure 5.10.17: Picture of pressed LWTB of GA 140,DP 800 and GA 140 shimmed with weld line transverse to pressing centre

6.0 Overall Conclusions

From the results there are several areas of interest that can affect tubular blank formability and also the processability of tubes. It can be seen that the type of material used in the tubular blank processes is anisotropic. Therefore this means that consideration has to be given to the orientation of the sheet being pressed. This does not have to be a limiting factor for the tubular blank process, it could be embraced and used positively.

Noticeable during all of the forming operations was the effect labelled as the plastic hinge effect. As previously described this leaves finger prints along the tube length. One method to mitigate this would be the use of rubber inserts (soft tooling) in the die of the tool. This would therefore be a solid block of rubber that deforms to the shape of the punch when the forming operation occurs. This also would mean that dedicated die tooling would not be required for differing types of material and thickness. Tooling of this type is at present being investigated as to its suitability for large volume production. Caution is needed in this area as the soft tooling would be constantly under wear from the edge of the blanks.

The possibility of a major improvement into the process window expansion comes in the form of coining within the forming process. As described previously, the effect of coining on final tube formability is not yet known. It can be said for definite that should no detrimental effect be seen when coining is employed using steel tooling (hard tooling), the process windows for similar thickness material will become greater as the ability to reduce springback is present.

This however cannot be used in conjunction with soft (rubber) die tooling, as the ability to transfer forming pressure from punch to sheet no longer exists to the same extent as that of hard tooling.

A secondary method to increase the process window of the tooling is the ability to use tooling of greater tolerance levels than the nominal sheet thickness. Although further study is needed to understand the degree of tolerance that still allows tubes to be

formed within recognised standards. From the investigation carried out within this programme it was possible to see that tooling dedicated to 2mm thick material was able to form a tube using 0.7mm thick material to within the EN standard required.

One of the requirements for tool designers and the press operator for tubular blank pressing was the ability to predict the amount of springback that would occur in different types of material. This study shows that the analytical models that were investigated are unable to satisfactorily predict springback. However, the use of numerical algorithms enabled better springback prediction. Even with the shortcomings of numerical algorithm it is not hard to see that a steel producer would be able to create a portfolio of their materials and thus this data could be used within the algorithm. The second advantage is the ability of a numerical algorithm to be latched to a FE program, thus enabling the steel manufacturer to deliver a value added package to their customer, tying the customer more to the company.

With the ever increasing use of LWTB it is necessary that the tubular blank machine is able to cope with demand for this product. It has been shown in this study that springback of an LWTB with the weld line parallel to pressing line can be predicted, however, some work is needed into the prediction of springback for LWTB with weld line traverse to pressing line. No literature has been found regarding the behaviour of LWTB in low strain forming modes, suggesting that this avenue of research is yet unexplored, and advantageous to exploit.

From the coining and tool tolerance results it is not hard to imagine that the differing springback behaviour of the constituent parts of the LWTB can be accommodated by means of coining and tool tolerance. This could be taking one step further and develop programming within the tubular blank machine that could recognise a steel type and adjust the pressing pressure accordingly so that the finished tube shows no dimensional deviation no matter what the material type.

One of the drawbacks seen during the experiments on LWTB was that thickness differentials in the material caused forming irregularities. The inclusion or exclusion of shims in thickness differentiated LWTB's resulted in differing springback behaviour. As shims are an option that is not cost effective for production more effort

would be needed in the investigation of shimless pressings. This may be counteracted by the use of dedicated tooling, however this solution would require a large amount of through put to make the process profitable and possible.

From this investigation it has been possible to highlight areas for improvement of the tubular blank process, but as with many investigations this project has also raised many more questions regarding not only the tubular blank process but also general forming and material characterisation issues.

7.0 Where now

Tube hydroforming has now the potential to produce large structural automotive components as a consequence of the development of the Tubular Blank machine. This was not possible by conventional ERW or CTA methods. Utilisation of this process will enable further weight reduction in future generation vehicles, by replacing stamped and spotwelded steel assemblies, once considered unachievable. However, limited implementation of this technology has taken place for Body-In-White (B-I-W) components, due to the complexity of the process and low levels of confidence and knowledge in the technology. The introduction of the Tubular Blank has eradicated the complexity of the process as the process window for the Tubular Blank is more robust that that of the ERW or CTA tube.

Knowledge of the technology is ever increasing and therefore reducing the lack of confidence in the process. However, within Europe and North America the main stumbling block is an ever decreasing market, with cost as the main driver. Adoption of this technology would require major investment, and the short term loss of market share due to an increase in overheads driving cost up.

The solution could be a combination of steel and machine producers joining forces and delivering a complete package to the automotive manufacturer, limiting their financial investment needed. At present the ideal market place to target is not the well established Europe and North American, but the boom economies and potential growth areas of India and China.

Appendix A

```
      Real*8 a(100,100),b(100),v(100),x(12),r(100)
      Character Text*20
!
! *** [a] is the matrix of least squares coefficients
! *** [b] is the vector of the R.H.S.
! *** v is a dummy variable used in the calculation of [a]
! *** x is the aray of experimental variables
! *** e is the experimental value of the function for any x
!
      write(*,*)'Enter the data file name'
      read(*,11)text
   11 format(a20)
      write(*,*)' Enter the number of variables (Maximum 12)'
      read(*,*)n
      write(*,*)' Enter the number of experimental points'
      read(*,*)m
      open(9,file=text)
      open(10,file='res.dat')
      mm=1+(n*(3+n))/2
!
! *** mm is the number of rows and columns in [a]
!
! *** loop over all the experimental points to calculate [a],[b]
!
      do 5 ii=1,m
           read(9,*)(x(i),i=1,n),e
!
! ***       set up the dummy variables, v
!
           jcount=1
!
! *** jcount refers to column number
!
           v(1)=1.
           do 10 j=1,n
                 jcount=jcount+1
                 v(jcount)=x(j)
   10      continue
           do 20 j=1,n
           do 20 k=j,n
                 jcount=jcount+1
                 v(jcount)=x(j)*x(k)
   20      continue
!
! ***       calculate a(i,j)
!
           icount=1
!
! *** icount refers to row number
!
           do 40 j=1,mm
                 a(1,j)=a(1,j)+v(j)
   40      continue
           do 50 i=1,n
                 icount=icount+1
```

```
                do 55 j=1,mm
                      a(icount,j)=a(icount,j)+v(j)*x(i)
   55           continue
   50      continue
           do 60 i=1,n
           do 60 k=i,n
                 icount=icount+1
                 do 65 j=1,mm
                      a(icount,j)=a(icount,j)+v(j)*x(i)*x(k)
   65            continue
   60      continue
!
! *** calculate R.H.S., b(i)
!
           b(1)=b(1)+e
           icount=1
           do 70 i=1,n
                 icount=icount+1
                 b(icount)=b(icount)+e*x(i)
   70      continue
           do 80 i=1,n
           do 80 k=i,n
                 icount=icount+1
                 b(icount)=b(icount)+e*x(i)*x(k)
   80      continue
    5 continue
!
! *** solve the [a][r]=[b] equation by pivoted gauss elimination
! *** [r] is the vector of roots
!
      call solve(a,b,r,mm)
!
! *** write out [r]
!
      do 83 jj=1,mm
      write(10,1)r(jj)
   83 continue
    1 format(3e15.5)
!
! *** now see how good the fit is by calculating the residuals
!
      close(9)
      open(9,file = text)
      do 85 ii=1,m
           read(9,*)(x(i),i=1,n),e
!
! ***       set up the dummy variables, v
!
           jcount=1
!
! ***       jcount refers to column number
!
           v(1)=1.
           do 110 j=1,n
                 jcount=jcount+1
                 v(jcount)=x(j)
  110      continue
```

```
          do 120 j=1,n
          do 120 k=j,n
                jcount=jcount+1
                v(jcount)=x(j)*x(k)
  120     continue
!
! *** ecal is the calculated value of the experimental variable e
!
           ecal=0.
           do 130 jj=1,mm
                ecal=ecal+v(jj)*r(jj)
  130      continue
           residual=ecal-e
           write(10,1)e,ecal,residual
   85 continue
      end

      SUBROUTINE SOLVE(A,AB,XR,MM)
      REAL*8 A(100,100),AB(100),XR(100)
!
! *** Linear equation solver, pivoted gauss elimination
!
      DO 300 K=1,MM-1
            CALL PIVOT(A,AB,K,MM)
            CALL ELIMINATE(A,AB,K,MM)
  300 CONTINUE
      XR(MM)=AB(MM)/A(MM,MM)
      DO 700 JK=1,MM-1
            CALL BACKSUB(A,AB,XR,MM,JK)
  700 CONTINUE
      RETURN
      end
!
      SUBROUTINE PIVOT(A,AB,K,MM)
      REAL*8 A(100,100),AB(100),TEMP
      L=K
      DO 400 I=K+1,MM
            IF(ABS(A(I,K)).LT.ABS(A(L,K)))GO TO 400
            L=I
  400 CONTINUE
      IF(K.EQ.L)RETURN
      DO 410 J=K,MM
            TEMP=A(K,J)
            A(K,J)=A(L,J)
  410       A(L,J)=TEMP
      TEMP=AB(K)
      AB(K)=AB(L)
      AB(L)=TEMP
      RETURN
!
      ENDSUBROUTINE PIVOT
!
      SUBROUTINE ELIMINATE(A,AB,K,MM)
      REAL*8 A(100,100),AB(100),RM
      DO 300 I=K+1,MM
            RM=A(I,K)/A(K,K)
            A(I,K)=0.
```

```
            DO 301 J=K+1,MM
  301             A(I,J)=A(I,J)-RM*A(K,J)
  300       AB(I)=AB(I)-RM*AB(K)
      RETURN
      ENDSUBROUTINE ELIMINATE
!
      SUBROUTINE BACKSUB(A,AB,XR,MM,JK)
      REAL*8 A(100,100),AB(100),XR(100),S
      I=MM-JK
      S=0.
      DO L=I+1,MM
         S=S+XR(L)*A(I,L)
      ENDDO
      XR(I)=(AB(I)-S)/A(I,I)
      RETURN
      ENDSUBROUTINE BACKSUB
!
```